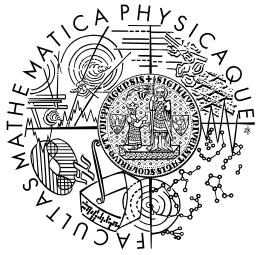

FACULTY
OF MATHEMATICS
AND PHYSICS
Charles University

DOCTORAL THESIS

Zhiqiang Yan

Chemical evolution of galaxies with an environment-dependent stellar initial mass function

Astronomical Institute of Charles University

Supervisor of the doctoral thesis: Pavel Kroupa

Study programme: Astronomy and Astrophysics

Study branch: Theoretical Physics, Astronomy and Astrophysics

Prague 2021

I declare that I carried out this doctoral thesis independently, and only with the cited sources, literature and other professional sources. It has not been used to obtain another or the same degree.

I understand that my work relates to the rights and obligations under the Act No. 121/2000 Sb., the Copyright Act, as amended, in particular the fact that the Charles University has the right to conclude a license agreement on the use of this work as a school work pursuant to Section 60 subsection 1 of the Copyright Act.

In ..... date ....

Author's signature

Dedication

I dedicate this thesis to my wife, parents, son and daughter, who supported my PhD study and accompanied me to foreign countries through unimaginable difficulties. To all the colleagues, friends, and strangers I met in Europe. To my treasured memory in Bonn, Euskirchen, and Prague.

I want to give my special thanks to Prof. Pavel Kroupa and Dr Tereza Jerabkova for being exceedingly supportive and encouraging. They provide not only crucial insight and immense help to the development of this thesis but also unreserved help when I run into trouble.

I also want to thank my supervisor, Prof. Pavel Kroupa, for being critical about the astrophysics mainstream which pushes me to be critical about my own work.

Thank you, China and the Czech Republic, for supporting my PhD study financially. Thank you, Europe, for being such a beautiful place. And thank you, hope we meet again!

Title: Chemical evolution of galaxies with an environment-dependent stellar initial mass function

Author: Zhiqiang Yan

Department: Astronomical Institute of Charles University

Supervisor: Pavel Kroupa, Astronomical Institute of Charles University

Abstract: The presented study gives a comprehensive overview of the theory and the evidence for a systematically varying stellar initial mass function (IMF). Then we focus on the impact of this paradigm change, that is, from the universal invariant IMF to a variable IMF, on galaxy chemical evolution (GCE) studies. For this aim, we developed the first GCE code, GalIMF, that is able to incorporate the empirically calibrated environment-dependent IMF variation theory, the integrated galactic initial mass function (IGIMF) theory. In this theory, the galaxy-wide IMF is calculated by summing all the IMFs in all embedded star clusters which formed throughout the galaxy in 10 Myr time epochs. The GalIMF code recalculates the galaxy-wide IMF at each time step because the integrated galaxy-wide IMF depends on the galactic star formation rate and metallicity. The resulting galaxy-wide IMF and metal abundance evolve with time. Using this code, we examine the chemical evolution of early-type galaxies (ETGs) from dwarf to the most massive. We find that the introduction of the non-canonical IMF affects the best estimation of the galaxy properties such as their mass, star formation history, and star formation efficiency. Moreover, we are able to provide an independent estimation on the stellar formation timescale of galaxies, the type Ia supernova production efficiency, and constrain the IMF variation law of the low-mass stars. This work provides to the community the publicly available GalIMF code with improved constraints on the IMF variation and has, for the first time, resolved the discrepancy between the galaxy formation timescales obtained from stellar population synthesis and chemical enrichment studies.

Keywords: galaxies: stellar population - galaxies: star formation - galaxies: chemical evolution - galaxies: elliptical and lenticular methods: numerical

Contents

Introduction

Modern astrophysics has gone through two major revolutions. One is the Monte Carlo method and Bayes' theorem. The other is the advances in computational power and numerical optimisation routines. As a result, scientific development has become dependent more on pure and parallel computation rather than discursive and linearly ordered reasoning. The conclusions are given more precise and quantitative but not necessarily more helpful when it is buried in implicit assumptions, difficult to compare with inconsistent peer results.

The subject of the present work, that is, the study of galaxy chemical evolution (GCE), has benefited from and, in the meantime, is a victim of modern astrophysics development. The numerical GCE study depends heavily on complicated galaxy models with many parameters describing physical processes not independently well constrained but only justified by the fact that the model as a whole can reproduce the observed feature of galaxies. The GCE study aims to find the most likely formation and evolution history of galaxies that reproduce the chemical abundances we observe today, and by doing so, achieves a better understanding of how galaxies form. However, this methodology is greatly weakened by our capability to accurately measure the chemical abundances of the real galaxies and the limitations of our galaxy model.

On one hand, the measured galaxy abundance that a GCE code aims to reproduce is not certain at all. The galaxy chemical abundance given by a stellar population synthesis (SPS) code depends on the assumed spectrum of single stars and the distribution of the stellar masses, ages, and element abundances. There is a limited number of spectrum models with different stellar initial element abundances, evolving to different phases in the lifetime of a star, and affected by different degrees of dust attenuation. These spectrum models are either calibrated by local stars close to our Sun, which have similar abundances and do not cover every stellar evolution phase or are predicted by theoretical models that are difficult to validate. It is true that different stellar spectrum libraries provide spectra similar enough to not cause a significant difference in the results of the SPS but systematic errors and confirmation bias cannot be excluded.

On the other hand, there are large uncertainties in a GCE model. When and how stars form and what elements do they eject during their final explosion are under debate. The simulation of the hydrodynamic evolution of the gas in a galaxy is not accurate. The physical processes such as gas mixing, cooling, accretion, and stellar feedback in GCE models are still represented by parameters that are not well constrained, let along with the gas with different temperatures and abundances of different elements. In fact, it is not a surprise that we can find more degrees of freedom in a GCE model than the number of observational constraints because we observe only the present-day snapshot of a galaxy while the GCE model simulates its evolution. The more complex a model becomes and the more free parameters (or not well-constrained parameters) it includes to explain a given set of observations, the less predictive power it has.

In particular, the standard GCE model has originally been developed to explain and, therefore, being calibrated by the observation of stars in the MW galaxy. The complex formation history of our disc galaxy results in multiple

stellar populations with significantly different abundance features that require an equally complex GCE model to explain. However, for the extra-galactic galaxies, the information we have accumulated is much less and they form in environments nothing like the MW. The consequence is that the complex GCE model developed over the years with parameters fine-tuned to fit the MW observations is not directly applicable to the extra-galactic galaxies. The value of the many free parameters has not been validated in a different environment nor do we have enough independent observational constraints to do so. The solution to the current situation is to apply a much more simplified GCE model, a basic version that balances the number of free parameters and observational constraints, and starts from the beginning to first explain the global properties of the extra-galactic galaxies. Basically, we need to climb the ladder again from a different starting point to reach a different roof. We need to first adjust the most influential zero-order parameters before we trying to fit the higher-order details.

For example, it has been a long-standing problem to understand the fast formation and early enrichment of the massive elliptical galaxies applying the standard GCE models. Their stellar population appears to be too metal-rich and α-element[1] enhanced (Thomas et al., 2005; Yan et al., 2019a). The X-ray observation of the gas surrounding the galaxy clusters supports this picture – far more metal exists than the amount a standard GCE model can produce (Renzini and Andreon, 2014; Urban et al., 2017; Ghizzardi et al., 2021). Complex galactic feedback models have been developed in order to solve this mystery but failed (De Lucia et al., 2017; Okamoto et al., 2017) because people are trying to reach a different roof without climbing down their current ladder. Problems exist also on the lower end of the galaxy mass distribution. The ultra-faint dwarf galaxies appear to have an abnormally low star formation efficiency (Vincenzo et al., 2014; Romano et al., 2015) and abundance ratios difficult to understand within the standard GCE model (Fernández-Alvar et al., 2018; Theler et al., 2020; Minelli et al., 2021). It is shown in Pflamm-Altenburg and Kroupa (2009) and one of my studies below (Chapter 3.1) that these abnormal features are only apparent when one applies the standard GCE model overfitted by MW observations. Then the only question is, what is the most important component of a GCE that we need to reconsider when studying the extra-galactic galaxies?

Unarguably, the stellar initial mass function (IMF) in the GCE model needs to be examined with caution, that is, how many low-mass stars and how many massive stars form in a stellar population. It has been studied in detail through observation and computational models on how stars evolve differently due to the difference in their initial masses. Low mass stars with a mass of less than about eight solar masses (denoted by $M_\odot$ throughout this thesis) end up as white dwarfs which then have a chance to ignite as a thermonuclear supernova if they obtain enough additional mass from a companion star. The best-known object in this class, the Type Ia supernova (SNIa, we use this term interchangeably with thermonuclear supernova throughout this thesis), produces most of the iron peak elements in the universe over a Gyr to 10 Gyr timescale after the formation of their progenitor stellar population (cf. Eq. 2.10 below). Massive stars above about 8 $M_\odot$, on the other hand, are likely to explode as a core-collapse supernovae

[1] α-elements, including O, Mg, Si, S, and Ca, are synthesised by core-collapse supernovae through α-particle capture.

(CCSN) within 40 Myr, a blink of an eye in galaxy evolution. CCSN distribute most of the α elements to the galaxy and may leave a neutron star or black hole stellar remnant. Therefore, the GCE involving the abundance of different elements in a galaxy depends strongly on the mass distribution of the stars, that is, IMF. This is indeed the standing ground of our ladder for any GCE research.

The standard GCE model has been assuming that the IMF for all stellar populations is the same – the universal and invariant IMF. This idea is supported by the observation of the local universe, where it is found that stellar populations in vastly different environments across several orders of magnitude of temperature and density have indistinguishable IMFs (Kroupa, 2002; Bastian et al., 2010). This is partially due to the fact that the measurement of the IMF is difficult and has large uncertainties. With new IMF indicators and better telescopes for observing extra-galactic galaxies that live in more extreme environments, a systematic variation of the IMF has been discovered (see the overwhelming evidence listed in Chapter 1) and is consistently described by the integrated-galactic IMF (IGIMF) theory (Yan et al., 2017, and references therein). This recent development of the IGIMF theory needs to be convolved with the GCE studies.

The IMF variation in GCE is the theme of my doctoral study where a new GCE model with an environment-dependent IMF and a high temporal resolution is developed particularly for this purpose. The implications of this important model paradigm shift are discussed. For example, how the constraints are changed regarding the physics of stellar evolution and formation, the yield and frequency of core-collapse and Type Ia supernovae, the formation history of galaxies and the recycling of gas. We explore a vast parameter space of SFH, gas supplies, different IMF variation models and SNIa models to demonstrate their effects, utilizing the SIRRAH computer cluster of the Astronomical Institute of the Faculty of Mathematics and Physics of Charles University. The GCE results with the variable galaxy-wide IMF (gwIMF, calculated with the IGIMF theory) are compared side by side with the same model assuming an invariant canonical IMF.

In Chapter 1, we explore the literature on the IMF variation indicators and the pattern of how the IMF varies with the physical properties of the star-forming region. The mathematical formula of the IGIMF theory is developed and programmed, with which we are able to confront the theoretical description with observation. The IGIMF theory is implemented in the galaxy chemical evolution model in Chapter 2 to further test the IGIMF theory. A publicly available python code, GalIMF, is developed to allow for the environment-depended IMF variation and custom applications. In a first study, the GCE model is simplified to a closed-box model and applied to early-type galaxies (ETGs) to study the potential effects of the IGIMF theory. Two realistic applications of the GalIMF are further explored in Chapter 3. In Section 3.1, a case study to reproduce the observed property of a dwarf galaxy, Boötes I, demonstrates that the IGIMF theory explains the observation better than an invariant canonical IMF. The introduction of the new IMF formulation changes our understanding of the star formation efficiency of this ultra-faint dwarf galaxy (UFD). Similarly, when we apply the IGIMF theory to ETGs with different masses in Section 3.2, the estimation of their star formation timescales (SFTs) is different from the canonical model. The canonical model tends to result in extremely short SFT estimations for the massive ETGs, which are difficult to reconcile with hydrodynamical mod-

elling of galaxy formation. This long-standing problem can be solved naturally with the IGIMF theory. Finally, a summary of these studies and the conclusion is given.

This thesis is based on five refereed publications of which the author of this thesis is the first author (see attached list of publications). This series of publications are merged, restructured, and modified to give a linearly ordered reasoning.

1. IMF variation

This chapter is partially based on the publication Yan, Jeřábková, and Kroupa (2017) with the title "The optimally sampled galaxy-wide stellar initial mass function - Observational tests and the publicly available GalIMF code" and Yan, Jeřábková, and Kroupa (2021) with the title "Downsizing revised: Longer star formation timescales for elliptical galaxies with an environment-dependent IMF and number of SNIa". Modifications were made in order to present it as a chapter in the thesis.

1.1 Introduction: What is the IMF?

The birth mass distribution of stars determines the observed properties of stellar populations and is critical to a wide range of astrophysical applications including star formation, stellar populations, galaxy evolution and more (Kennicutt, 1998). This mass distribution of stars is described by their initial mass function (IMF), which is the function for the number of stars per stellar mass bin. Since it is of crucial importance to achieve the correct IMF for the stellar population being studied, a huge amount of effort has been devoted to measuring the IMF since about a century ago with a growing number of review articles dedicated to it (see Section 1.2 below). Using the observed luminosity distribution of stars and an approximated stellar mass-luminosity relation, Salpeter (1955) was able to first measure the IMF of field stars in the solar neighbourhood with a mass between 0.4 and 10 $M_{\odot}$. The result shows that the IMF can be described by a power law. Miller and Scalo (1979) updated the Salpeter IMF for a larger mass range. Then Scalo (1986) gave a much more detailed discussion and discovered subtle features of the IMF. After that, Kroupa et al. (1993) recovers a smooth two-part power-law IMF by showing that the subtle features are due to changes in the stellar mass-luminosity relation and they also, for the first time, applied corrections for unresolved multiple stars. See Fig. 1.1 for a comparison of these IMF measurements for the local field stars and Kroupa and Jerabkova (2019) for more historical details.

As emphasised by Kroupa et al. (2013), in contradiction with the local measurements, a variable stellar initial mass function (IMF) has been expected by theoretical studies for a long time since the star-forming environment should in principle affect the masses of stars that form, for example, through an ambient gas temperature, metallicity, density, and pressure dependences, as argued by Adams and Fatuzzo (1996), Larson (1998), Elmegreen (2004), Dib et al. (2007), and Papadopoulos (2010). Although much effort has been invested in constraining the shape and possible variation of the IMF (Hopkins, 2013, 2018), a comprehensive theory, supported by observational evidence, has not been fully developed. The successful theory describing star formation and IMF must be consistent with the observations both on star cluster and galaxy scales and also needs to be able to

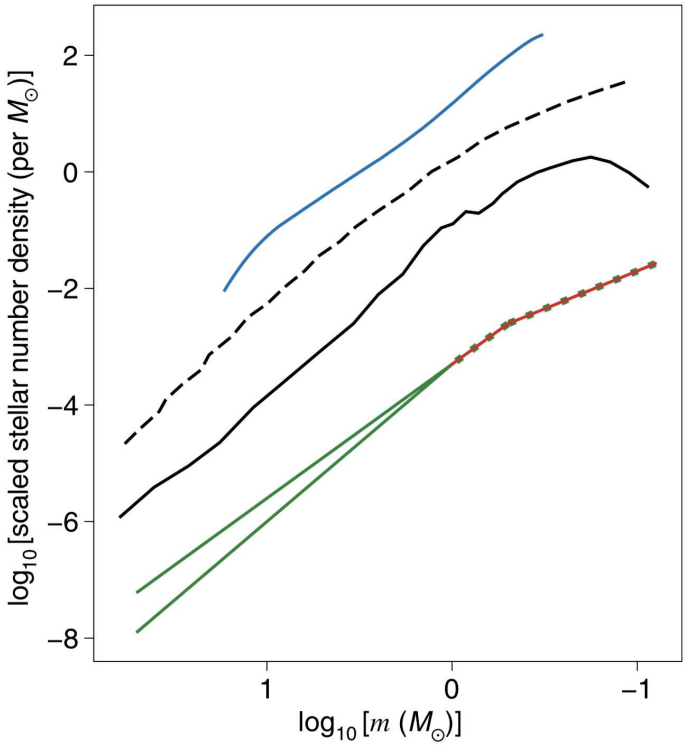

Figure 1.1: Figure taken from Kroupa and Jerabkova 2019. It shows the development history of IMF measurements. From top to bottom, the IMF determined by Salpeter (1955) (blue), Miller and Scalo (1979) (dashed black), Scalo (1986) (solid black), and the present-day generally accepted Kroupa IMF (Kroupa et al. 1993 and Kroupa 2001, green and red, respectively, in near-exact agreement with the Chabrier 2003 IMF). The IMFs are shifted vertically arbitrarily to demonstrate their differences.

make predictions of new phenomena.

A top-heavy IMF in high redshift starburst galaxies is well physically motivated. The early universe has a lower metallicity and a higher ambient temperature, yielding higher stellar masses after accretion (Larson, 1998; Adams and Laughlin, 1996). The extremely metal-poor Population III stars are predicted to have an IMF shifted to higher masses, which results in a top-heavy IMF when combined with other stellar populations. The higher ISM temperature in the early universe leads to a higher Jean's mass, also suggesting a top-heavy IMF (Narayanan and Davé, 2013). Distinct physical processes like collapse, accretion, and dynamical processes are considered as possible origins for the observed relative variations of the IMF in Elmegreen (2004). The model of Elmegreen (2004) suggests a top-heavy IMF in starburst clusters and a bottom-heavy IMF in low surface brightness galaxies. A model considering pre-stellar condensations also suggests a top-heavy IMF in some starburst clusters (Shadmehri, 2004).

This chapter describes the evidence for a systematically varying IMF on different scales in Section 1.2 then it introduces the up-to-date formulation of the IGIMF theory in Section 1.3, which accounts for the IMF variation as a function of star formation environment. Finally, we compare the IMF properties calculated by the IGIMF theory with observations in Section 1.4.

1.2 Observation

1.2.1 Historical consensus of a universal IMF

Star-formation has a complex multi-scale physical nature occurring in sub-parsec regions of molecular clouds, at the same time being coupled to the galactic gravitational potential affected by tides and shears. This poses a computational challenge pushing technical feasibility in terms of computational time and the required spatial resolution. On the other hand, detailed observations of star-forming regions nearby are limited by the near-uniformity of environments, such as the cloud density and metallicity. The investigation of a large variety of different environments in galaxies near and far is limited by observational resolution and it is difficult to break the degeneracy between different physical effects (IMF, star formation history, dust reddening, metallicity, etc.) on the integrated light of a galaxy. Thus, despite a large and fruitful community effort in this field, we are still lacking the full picture of how stars and star clusters form and what are the true IMFs for those extragalactic stellar systems where single stars cannot be resolved. Using resolved stellar populations in the local universe, different functional forms have been proposed to describe the IMF (Salpeter 1955; Scalo 1986; Kroupa 2001; Chabrier 2003, among the most popular). Since 2000, a consensus has emerged for the massive end of the IMF that it is a power-law function. Kroupa (2001, 2002) demonstrated that the observed IMF power-law index above a few solar masses shows a scatter that is smaller than random sampling would give (see Kroupa et al. 2013, their Fig. 27) being consistent with the assumption that the IMF is universal and invariant. Therefore, it is generally accepted that the stellar IMF in star clusters is the universal canonical IMF, for example, the two-part power-law Kroupa IMF (Kroupa, 2001, 2002; Bastian et al., 2010; Kroupa et al., 2013). The lack of scatter and the existence of the $m_{\rm max}$–$M_{\rm ecl}$ relation (see

Section 1.3.2 below) are interpreted by Kroupa et al. (2013) to imply the IMF to be an optimal distribution function (and not a probability density) which is consistent with star formation being highly self-regulated.

1.2.2 IMF variation on different scales

For the IMF in star clusters, many teams are focusing on detailed hydrodynamical simulations studying the initial fragmentation of molecular clouds and trying to reach as high a resolution as possible (e.g. Klessen and Hennebelle 2010, Federrath 2016, Vázquez-Semadeni et al. 2018, Bate 2019, and Guszejnov et al. 2021) in order to be able to capture the complex filamentary structure of molecular clouds (e.g. Hacar et al. 2017, 2018). Marks et al. (2012), applying N-body simulations, demonstrated that the IMF of globular clusters within the Milky Way is a function of their metallicity and mass (cf. Banerjee and Kroupa 2018). From an observational point of view, one can use sub-mm facilities such as APEX or ALMA to investigate the structure of molecular clouds finding more evidence pointing to star-formation happening in thin dense filaments ((Hacar et al., 2017, 2018)). Researching the later stages of star-formation is now becoming possible thanks to the Gaia satellite (e.g. Zari et al. 2018, 2019). The ultra-compact dwarf galaxies, some considered as very massive star clusters, also show evidence of having a top-heavy IMF (Dabringhausen et al. 2009 and Dabringhausen et al. 2012).

On the galaxy scale, Matteucci and Brocato (1990); Vazdekis et al. (2003); Hoversten and Glazebrook (2008); Lee et al. (2009); Meurer et al. (2009); Gunawardhana et al. (2011), and Zhang et al. (2018) have shown with independent methods that galaxy-wide IMFs (gwIMFs) appear to have a systematic variation, being different in star-forming regions with a more extreme environment (revealed by the galaxy-wide star formation rate). In recent years, pioneering studies using spatially resolved spectroscopy (e.g. Martín-Navarro et al. 2015; La Barbera et al. 2017, 2019) are now starting a new branch of research, e.g. Martín-Navarro et al. 2019; Fensch et al. 2019; Emsellem et al. 2019. These studies of stellar populations are also being combined with dynamical modelling (Poci et al., 2019, 2021) presenting powerful tools that can identify different stellar populations in a galaxy in a more reliable way and also getting a better understanding of the formation assembly.

Galaxy clusters appear to form more metal elements than expected assuming a canonical IMF, suggesting a top-heavy IMF. More massive galaxy clusters have smaller stellar-mass fraction but a similar intracluster medium (ICM) metallicity, thus generating a major tension with the nucleosynthesis expectation and inflating the ratio of metal mass in ICM and stars to extremely high values (up to $\approx$6, Renzini and Andreon 2014).

1.2.3 IMF variation at different redshifts

In terms of the redshift and at redshift $z \approx 0$, evidence has suggested a clear correlation between the mass of nearby massive elliptical galaxies and their IMF slope, supporting a more bottom-heavy IMF for more massive galaxies. Many such studies are based on spectral synthesis of the galaxy. For example, Conroy

and van Dokkum (2012) studied the spectral absorption lines in 34 nearby ETGs and suggest that the most plausible explanation is that the IMF becomes increasingly bottom-heavy with increasing velocity dispersion. Similarly, Lagattuta et al. (2017) studied the near-infrared spectroscopy of nearby massive ETGs and conclude that higher mass galaxies are better described with a steeper (dwarf-star rich) IMF slope. A consistent result according to investigations of SDSS galaxies is given by Spiniello et al. (2012); Ferreras et al. (2013); Tortora et al. (2013); La Barbera et al. (2013); Spiniello et al. (2014); Clauwens et al. (2016), suggesting a significantly bottom-heavy IMF which correlates strongly with the galaxy velocity dispersion. Smith et al. (2015a) report that the Na I doublet at 1.14 μm of massive passive galaxies suggests a steeper IMF with increasing velocity dispersion. Then La Barbera et al. (2017) confirmed this study by analyzing four Na features in the optical and near-infrared spectral ranges of two nearby massive ETGs which matched a bottom-heavy IMF. In addition, Spiniello et al. (2015) show that the non-universality of the low-mass end of the IMF is robust against the choice of the SSP model.

Higher redshift galaxies seem to show the same character. Martín-Navarro et al. (2015) suggest that the IMF of a sample of 49 massive quiescent galaxies at $0.9 < z < 1.5$ is bottom-heavier for more massive galaxies and has remained unchanged in the last ≈ 8 Gyr. Cañameras et al. (2017) provide the first direct constraints on the IMF at $z = 1.5$ in a lens, deducing a bottom-heavy IMF. At redshift about 4 to 7, González et al. (2011) find a steep low-mass IMF slope using FAST spectral energy distribution (SED) fitting with a constant SFR and a Salpeter-like (single slope) IMF assumption. Duncan et al. (2014), using a similar method on the galaxies in the same redshift range but with an exponentially decreasing SFR and a Chabrier IMF (Chabrier, 2003), find a significantly steeper low-mass IMF slope and the slope is steeper at higher redshift (see Duncan et al. 2014 their figure 10).

However, the canonical invariant or bottom-heavy IMF cannot account for the Solar or even super-Solar metallicities of massive galaxies at high redshift as is explained by Weidner et al. (2013a). The metal enrichment of the massive galaxies is too early and too fast (Urban et al., 2017).

1.2.4 Scaling relations

Efforts have been made to understand the relation found between IMF slope and galaxy mass as a combination of the mass–metallicity and the metallicity–IMF slope relations. The radial gradients of IMF sensitive features in a sample of 24 ETGs observed by the CALIFA survey in Martín-Navarro et al. (2015) find that the IMF is tightly related to metallicity, becoming more bottom-heavy toward metal-rich populations. The most recent study assessing the diversity of IMF and stellar population maps within the Fornax Cluster confirms the strong metallicity–IMF slope correlation (Martín-Navarro et al., 2021) with metal-rich galaxies forming more low-mass stars than expected by the canonical IMF.

Concerning the abundance ratio of α elements, the IMF correlation with, for instance, the $[Mg/Fe]$ value seems not to be settled. La Barbera et al. (2013, 2015) find that there is no obvious correlation while Smith et al. (2012); Conroy and van Dokkum (2012); Conroy et al. (2014) find that the IMF becomes increas-

ingly bottom-heavy with increasing $[Mg/Fe]$. Under the conventional assumption that these ratios reflect the star-formation timescale, with higher $[Mg/Fe]$ values corresponding to shorter timescales, these studies suggest that galaxies harbouring α-enhanced stellar populations formed in rapid and intense starbursts tend to generate a larger population of low-mass stars than galaxies with extended star-formation histories. Chabrier et al. (2014) then state that such a variation can be caused by the turbulence in high SFR regions which fragment the cloud into smaller pieces. However, not discussed by the authors, the assumption that reflects the star-formation time scale is itself based on the assumption that IMF is invariant. Once applying a bottom-heavy IMF, the $[Mg/Fe]$ ratio naturally becomes larger and thus counterweights the relation because, although the ratio of the number of potential progenitors for CCSN and SNIa keeps the same when the top-part of the IMF (for stars with a mass above 1 $M_{\odot}$) is unchanged, the number of SNIa depends on the square of the number of its potential progenitors (i.e. stars with initial mass between about 3 and 8 $M_{\odot}$ see Eq. 2.11 below) while the number of CCSN changes linearly with the number of stars above 8 $M_{\odot}$. In addition, the assumption that the trends of $[\alpha/Fe]$ ratios can be simply converted into relative time-scale indicators is not valid according to De Lucia et al. (2017). Thus the interpretation of a relation between SFR and low-mass IMF slope may not be reliable, requiring a more robust analysis (for example, Recchi et al. (2009)). Even if the progenitor-SFR–IMF-slope relation is real, it is not a current-SFR–IMF-slope relation and the causation of this correlation is unclear. Moreover, the low-mass IMF studies certainly do not give information on the high-mass IMF behaviour as shown by some X-ray studies mentioned below. Saying all this, Smith et al. (2012); Conroy and van Dokkum (2012); Conroy et al. (2014)'s conjecture is consistent with the more direct constraints summarised in Duncan et al. (2014) as mentioned above, and the conjecture is physically motivated as suggested by Chabrier et al. (2014). Together, they indicate a low-mass IMF slope–SFR relation and the IMF is more bottom-heavy for higher SFR.

The strong lensing studies lead to different deductions concerning the bottom-heavy IMF than suggested by the above studies on dwarf-star-sensitive spectral features. Auger et al. (2010); Barnabè et al. (2013) use stellar dynamics, strong lensing, stellar population synthesis models, and weak lensing shear measurements to constrain the dark matter profile and stellar mass in nearby massive ETGs. These studies prefer a Salpeter-like IMF over a Chabrier or Kroupa IMF[1] being consistent with spectral studies. On the other hand, Smith and Lucey (2013); Smith et al. (2015b); Newman et al. (2017) show that some nearby ETGs are only consistent with a Kroupa IMF while a "heavyweight" IMF, with a mass twice as large as the Kroupa case, is firmly excluded, suggesting tension between dwarf-star indicators and lensing-mass constraints. They conclude that current models struggle to reconcile this feature in the most massive galaxies without breaking other constraints, and caution against over-reliance on the sodium lines in spectroscopic IMF studies. Finally, Leier et al. (2016) reveal a large range of allowed IMF slopes, which may explain the above disagreement, but they need to invoke a significant dark matter component which may be stellar remnants from a top-heavy IMF (see below) rather than a dark matter component (Kroupa,

[1]The Chabrier IMF (Chabrier, 2003) is indistinguishable from the previously constrained canonical Kroupa IMF (Kroupa, 2001) as shown in Fig.8 in Dabringhausen et al. (2008).

2015).

1.2.5 Towards an environment-dependent IMF

The above observations for the bottom-part of the IMF, that is, the observed massive low-redshift galaxies with a bottom-heavy IMF, do not suggest that the IMF in the star-forming progenitors of these massive galaxies in the early Universe have lack of massive stars because the massive stars have a short lifetime and are not observed. Many astronomical facts suggest a top-heavy IMF for massive galaxies. Matteucci (1994) was the first to deduce that massive elliptical galaxies should have had a top-heavy IMF given their chemical abundances. It is also suspected that a top-heavy IMF could help to account for the energetics and chemical enrichment of the early Universe (Larson, 1998). In addition, semi-analytic models of galaxy formation demonstrate that a top-heavy IMF in starbursts can adequately account for the chemical abundances of sub-millimetre galaxies (SMG) at high redshifts while previous models with an invariant IMF can not (Muñoz et al., 2011; Lacey et al., 2016). Likewise, dust produced only by low-to-intermediate-mass stars falls a factor 240 short of the observed dust masses of SMGs in the semi-analytic model, supporting the need for higher supernova yields, substantial grain growth in the interstellar medium or a top-heavy IMF if dust is produced by both low-mass stars and supernovae and is not efficiently destroyed by supernova shocks (Rowlands et al., 2014). Haghi et al. (2017) applied the top-heavy IMF derived by Marks et al. (2012) and signify that the combination of the density- and metallicity-dependent top-heavy IMF, the anti-correlation between age and metallicity, stellar evolution, and standard dynamical evolution yields the best possible agreement with the observed trend of M/L-[Fe/H] for M31 globular clusters (GCs). Finally, Romano et al. (2017); Zhang et al. (2018) constrain the stellar IMF in galaxies using C, O and N isotope abundance ratios and find compelling evidence for a top-heavy stellar IMF in starburst galaxies.

We argue that galaxies cannot be described by a single age single metallicity SSP model as is assumed in van Dokkum and Conroy (2010). However, van Dokkum notes this potential threat and point out that their result is not consistent with the observed colour and M/L evolution of massive cluster galaxies. Indeed, Weidner et al. (2013a); Ferreras et al. (2015) show that no time-independent IMF is capable to reproduce the full set of constraints on the stellar populations of massive ETGs. So the apparant excess of low-mass stars in the present massive ellipticals do not necessarily imply a bottom-heavy IMF of their star-forming progenitors. Indeed, Gunawardhana et al. (2011) study the different evolutionary paths a galaxy would take in the Hα equivalent width and g–r colour plane with a sample of about 33000 galaxies from the Galaxy And Mass Assembly (GAMA) survey and find that the stellar IMF within galaxies has a strong variation with the galaxy SFR by becoming increasingly top-heavy with increasing SFR.

As mentioned above, the low-redshift low-mass IMF studies do not tell us much about the high-mass IMF behaviour. If we assume that the low-mass IMF shape can be extrapolated to the high-mass range, one finds that a top-light IMF can not account for the high metal abundance of massive galaxies (Weidner et al., 2013a). X-ray observations sensitive to the high-mass IMF also

show disagreements with the low-mass IMF trend. Coulter et al. (2017) count the low-mass X-ray binaries per unit near-IR luminosity in seven nearby low-mass ellipticals and conclude that the slope for low-mass stars in the suggested bottom-heavy IMF must not extrapolate to high-mass stars if the IMF is time-invariant. Similarly, Peacock et al. (2017) studied the low-mass X-ray binary populations of nine local ETGs and found that an increasingly top-heavy IMF with increasing velocity dispersion or an invariant IMF are both consistent with these observations while IMFs which become increasingly top-light with velocity dispersion are rejected. Thus the IMF seems to have to be both bottom- and top-heavy.

By comparing models assuming an increasing bottom- or top-heavy IMF at increasing galaxy-wide stellar mass or SFR, Fontanot (2014) suggested that the high stellar mass range is the most promising for breaking the degeneracies between the different proposed IMF variations. But the observations may not be completely against each other if one gives up either the time invariance of the IMF shape or the assumption that an excess of low-mass stars must indicate fewer massive stars (and vice versa) or both.

Combining the above information, one finds that the IMF is more bottom-heavy for higher mass galaxies at low redshift and more top-heavy for higher SFR galaxies at high redshift. Thus the only possible scenario, assuming the observational conclusions are correct, is that the IMF was top- and bottom-heavy for starburst galaxies in the early universe and top-light bottom-heavy at lower redshifts where SFR is low while metallicity is high. As pointed out by Weidner et al. (2013a) in their toy model, a scenario in which the IMF is top-heavy in the early universe and bottom-heavy at late times is in good agreement with various observational constraints on massive elliptical galaxies, such as age, metallicity, α-enhancement, mass-to-light ratio or the mass fraction of the stellar component in low-mass stars.

We note that either a top-heavy or a bottom-heavy IMF, where there is an excess of high or low mass stars, suggests a larger mass-to-light ratio of the galaxy than an invariant IMF. The scenario that the gwIMF changes from top-heavy to bottom-heavy is consistent with a study of 260 nearby ETGs by Cappellari et al. (2011) showing that the mass-to-light ratios for ETGs increase with increasing stellar velocity dispersion, that is, a more massive galaxy was formed with a more top- or bottom-heavy IMF.

But what is the physical reason for the IMF variation and how can this variation be consistent with the IMF on the star cluster scale? Knowing that the star formation duration is generally inversely correlated with the mass of the galaxy (Thomas et al. 2005, 2010 and Recchi et al. 2009), more massive galaxies having a larger SFR in early cosmological times but exhausting their gas reservoir on shorter time scales, one possible solution is to associate the high-mass IMF with the galaxy-wide SFR, and the low-mass IMF with both the galaxy-wide metallicity and SFR. The early universe, with a high SFR, results in both a bottom-heavy and top-heavy IMF. From the downsizing relation (star formation duration inversely correlates with the mass of the galaxy) we know that the early-time SFR of a galaxy positively correlates with its mass. The high-SFR galaxies with a top-heavy and bottom-heavy IMF naturally become the massive galaxies at lower redshifts, which have been suggested to have similar IMF features. At

lower redshifts, the metallicity growth, while the SFR drops, results in a bottom-heavy top-light IMF when the earlier formed massive stars have already died out. Thus the IMF shape varies at different redshifts. A self-consistent formulation between the gwIMF and the IMF on star cluster scales can be achieved by the IGIMF theory where the galaxy-wide stellar population is the combination of all star clusters, each of these having a different IMF in dependence of their metallicity and mass. The mass-to-light ratios of ETGs with different masses calculated by the IGIMF theory has been discussed and calculated in Dabringhausen (2019) and Yan et al. (2021), resulting in a good agreement with observations without the need to add exotic dark matter. In the following section, we introduce the IGIMF theory and demonstrate the key observational tests of it.

1.3 Theory

1.3.1 Overview

The evident IMF variation on small scales (i.e. individual star-forming regions) and in galaxies needs to be consistently explained by a unified IMF theory. A promising proposal, the integrated galactic initial mass function (IGIMF) theory, was developed over the years for this purpose. Originally formulated in Kroupa and Weidner (2003), in which it was called the "field-star IMF", the IGIMF theory predicted and explains the gwIMF variation. The fundamental insight underlying the IGIMF theory is that the empirical systematic variation of the gwIMF, which appears to correlate with galactic SFR and metallicity, has its origin from the variation of the IMF on a molecular-cloud core and embedded star cluster scale where a correlated star formation event (i.e. a gravitationally driven collective process of transformation of the interstellar gaseous matter into stars in molecular-cloud overdensities on a spatial scale of about one pc and within about one Myr Lada and Lada 2003; Kroupa et al. 2013; Megeath et al. 2016) happens. In other words, there exists a universal law of the star-cluster-scale IMF shape which leads to the various IMF shapes of different composite systems.

The IGIMF theory was originally based on a universal IMF on the star-cluster scale (i.e. in Kroupa and Weidner 2003) and embedded cluster mass function (ECMF) with later adoption of a systematically varying IMF given by Marks et al. 2012 and a varying ECMF formulation suggested by Weidner et al. (2013c), leading to a good description in explaining observations. There are three central axioms of the IGIMF theory which are formulated based on observational constraints (cf. Yan et al. 2017). These axioms are:

- All stars form in embedded star clusters. Therefore, all the stars in a galaxy are accounted for by adding all the embedded star clusters formed in that galaxy. This leads to the so-called IGIMF equation (Eq. 1.11 below). This is reasonable because stars form in molecular cloud overdensities that contain much more mass than the mass of the least massive star. Observations indeed suggest that most and perhaps all the observed stars were formed in embedded clusters (Lada and Lada, 2003; Kroupa, 2005; Megeath et al., 2016).

- How the stellar IMF and the ECMF change with physical conditions: These

include not only how the slope of the mass functions changes (Eq. 1.4 and 1.10 below) but also how the upper mass limit of the mass function changes according to the calculation given by the optimal sampling theory (Eq. 1.3 and 1.9 below). As a side note, it is important to differentiate the random sampling with a provided variable upper stellar mass limit from the optimal sampling resulting in the variable upper stellar mass limit. The relation between the stellar mass upper limit and the embedded cluster mass and the relation between the galactic SFR and the most massive just formed star cluster mass in that galaxy is never plugged into the IGIMF formulation as a known input. They are both observations applied to test the natural outcome of the optimal sampling theory and support the theory.

- There is a typical timescale, $\delta t = 10\,\mathrm{Myr}$, for the optimally-sampled galactic stellar population to form. The embedded star clusters formed within this timescale are correlated and optimally populate the ECMF of this formation epoch. Outside this timescale, the embedded star clusters are independent, that is, not populating the same ECMF. The time-scale $\delta t = 10\,\mathrm{Myr}$, discussed in Schulz et al. (2015), is essentially the lifetime of molecular clouds and is also the time-scale in which the inter-stellar-medium of a galaxy churns out an optimal or full population of freshly formed embedded clusters, each of which dissolves into the galactic field through gas expulsion, stellar evolution mass loss and two-body relaxation-driven evaporation.

The detailed mathematical formulation of these axioms and the calculation of the galaxy-wide initial mass function (gwIMF) are given in Section 1.3.3 below.

The IGIMF theory has solved a number of previously outstanding extra-galactic problems such as explaining the UV extended galactic disks (Pflamm-Altenburg and Kroupa, 2008) and naturally accounting for the time-scale problem for building up a sufficient stellar population in dwarf galaxies given their low SFRs (Pflamm-Altenburg and Kroupa, 2009). The theory made the prediction that dwarf galaxies must show a deficit of Hα emission relative to UV emission; see Pflamm-Altenburg et al. (2007, 2009). This was verified to be the case by Lee et al. (2009). The adoption of the IGIMF theory to the galaxy chemical evolution model also leads to good reproduction of what we observe which has previously been unachievable (Gargiulo et al., 2015; Fontanot et al., 2017; Romano et al., 2017; Palla et al., 2020). Thus, the IGIMF theory, based on an empirical relation of the small-scale IMF variation, is able to account for the IMF of galaxies and explain their special features self-consistently thereby also allowing prediction and is capable of incorporating different empirical constraints on the star-cluster scale if they are well constrained by observations (see Section 1.5). With this semi-empirical approach, we can constrain the star-cluster-scale IMF and gwIMF and potentially understand the variations of the IMF in different stellar systems.

1.3.2 Optimal sampling

Before introducing the mathematical formulation of the IGIMF theory in Section 1.3.3, we clarify the stellar sampling method that goes into the presented formulation. It is one question to abstract the mass distribution function from a set of observed discrete stellar masses, which we detail in Section 1.3.3, yet a

different question to simulate a set of stars given the correct IMF (i.e. to draw a set of stellar masses from an IMF). In the simulation of single dwarf galaxies (and in recent years, the cosmological galaxy simulations that are pushing to higher and higher resolutions to study the ultra-faint stellar populations), the number of stars in a galaxy or a "star particle"[2] becomes low enough that the IMF can no longer be considered as a continuous function. A fraction of a supernova explosion in a time step is yielded when the IMF integrated number of stars between two mass limits (given by the stellar mass–lifetime relation, cf. Fig. 2.2) is less than one (Revaz et al., 2016). It has been demonstrated that the more realistic description of a stellar population with a list of sampled stellar masses alter the property and the evolution of the simulated galaxy compared to a model with a continuous energy injection given by the smooth IMF. Both the SFR (Su et al., 2018) and the strength of photoionization (Smith, 2021) are affected. Therefore, the sampling of stellar masses from an IMF has been discussed and applied in an increasing number of recent studies doing simulations for low-mass stellar populations, low-SFR systems, and/or with a high time and mass resolution[3]. The question that remains is how to perform the sampling of stellar masses assuming a known IMF.

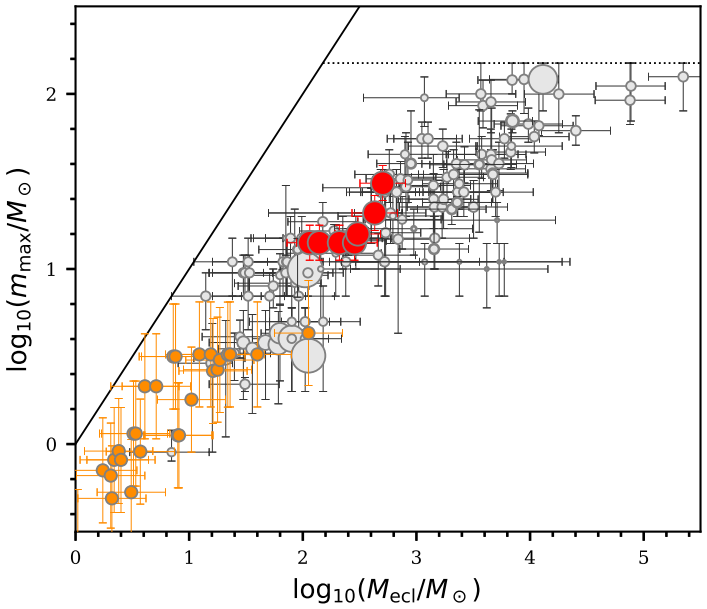

Figure 1.2: The observed relation between the most massive stellar mass and the stellar mass of the embedded cluster (the $m_{\rm max}$–$M_{\rm ecl}$ relation). Data come from Kirk and Myers (2012) (orange circles), Stephens et al. (2017) (red circles), and Weidner et al. (2013b) (gray circles), where Weidner et al. (2013b) is an inhomogeneous set of data culled from the literature for very young clusters without supernova remnants. Larger circles are more accurate measurements. The thin solid line is the $M_{\rm ecl} = m_{\rm max}$ limit and the horizontal thin dotted line represents the physical stellar mass upper limit of 150 $M_\odot$.

[2]The dynamical simulations of galaxies rarely track individual stars (exceptions include Hu et al. 2017 and Emerick et al. 2019 studying dwarf galaxies) but an ensemble of stars called a "star particle" with a mass resolution much higher than single stars (e.g., 10^5 $M_\odot$).

[3]Here we refer to actually sampling the stellar masses, which is different from post-processing the discrete behaviour of a stellar population assuming a continuous IMF as is explained in Applebaum et al. (2020, their section 2.3).

There are two extreme methods to sample stars from an IMF – stochastic sampling and optimal sampling. The stochastic sampling method assumes that the formation of each single star is purely an independent event and a random process. Therefore, it would be reasonable to treat the IMF as a probability distribution function and sample stellar masses randomly from the IMF[4]. On the other end, optimal sampling assumes that the formation of any stellar population is a perfectly self-regulated process and, therefore, that a deterministic relationship exists between the mass of a star cluster and the mass of each single star within that cluster. This is formulated by Eqs. 1 to 7 and 9 in Schulz et al. 2015 and updated in Yan et al. 2017, their section 2.2. We note that the deterministic nature of the optimal sampling makes the sorted sampling process practically more flexible and feasible as the method can give directly the total number of stars in a given mass range while the random sampling has to sample all the stars, including the low-mass stars, to know this information. This is particularly useful when only the sampling of the massive stars is required (e.g. the situation discussed in Applebaum et al. 2020, their section 2.2).

In most cases, sampling only matters for low-mass stellar populations (with masses below about 10^5 $M_\odot$ as is shown by Carigi and Hernandez 2008 and Applebaum et al. 2020 when discussing the number of CCSN) unless one aims to discuss the rare events only triggered by extremely massive stars (e.g. pair-instability supernovae). Low-mass stellar populations not only show discrete stellar feedback behaviour but also a systematic lack of massive stars (Fig. 1.2, Weidner et al. 2010, Weidner et al. 2013b, Yan et al. 2017, and Oh and Kroupa 2018) and, as a consequence, a systematic depletion of Hα line strength relative to the far-ultraviolet (FUV) luminosity (Meurer et al. 2009 and Lee et al. 2009). Both sampling methods can, in principle, account for these depletions. In optimal sampling, the lack of massive stars results from Eqs. 1.3 and 1.9, assuming that the integrated number of stars between the stellar-mass upper limit of a star cluster and the physical stellar-mass upper limit of 150 $M_\odot$ (see references in Yan et al. 2017) is exactly one (detailed in Section 1.3.3 below). In the random sampling theory, the lack of massive stars in low-mass stellar system is accounted for, *on average*, due to the restriction that stars cannot form when the mass of the available gas reservoir is lower than the sampled mass (demonstrated in Cerviño et al. 2013), mimicking, *on average*, the optimally sampled results but with a large scatter.

The observational feature that discriminates the two sampling theories and favours the optimal sampling is the low intrinsic scatter of the relation shown in Fig. 1.2. The small scatter of the data points compared to the uncertainty of the measurements indicates a low or even no intrinsic scatter of the underlying relation between the two quantities (given in Section 1.3.3 below), that is, there exists a deterministic relationship between the mass of a very young star cluster and the mass of the most massive star in that cluster. A Bayesian analysis is preformed (to be published), where the random sampling is rejected with a 4σ confidence level because the model gives a much larger scatter than the observed relation. On the other hand, the number of observed data points outside the stan-

[4]However, there are a variety of treatments regarding when to stop the random drawing of stars in order to match the sampled total stellar mass with the desired value (e.g. the total stellar mass of the star cluster or "star particle" known as a priori).

dard deviation region given by the optimal sampling model (see the solid curve in Fig. 1.3 below) is exactly what is expected for a Gaussian error distribution – around 1/3 of the data points (to be published). We conclude from these tests that the star formation process appears to behave in a highly-self regulated manner and optimal sampling is a better description of nature compared to random sampling.

Finally, we note that optimal sampling is the foundation of the IGIMF theory. The IGIMF theory is formulated (below) such that low-SFR galaxies cannot form massive star clusters. This is a consequence of optimally sampling the cluster masses from an ECMF, which would not be the case when random sampling is applied. With random sampling, the sampled cluster mass distribution for high-SFR and low-SFR galaxies would not have any difference (cf. the sampling procedure in da Silva et al. 2012). Therefore, the integration formulation introduced in the following section for the IGIMF theory serves as a close approximation of the optimally sampled stellar mass distribution (see Yan et al. 2017, their fig. 4). The integrated gwIMF shall not be taken as a distribution function independent from optimal sampling (e.g. Fumagalli et al. 2011 and da Silva et al. 2012).

1.3.3 IGIMF theory

In the following, we specify the exact formula for calculating the gwIMF that is applied for this work. The IMF follows the prescription in Yan et al. (2017) (see α_3 in Eq. 1.4 below), and equation 9 of Yan et al. (2020) (i.e. α_1 and α_2 in Eq. 1.1). In most cases, the most massive star is heavier than 1 $M_\odot$ and we have the following stellar IMF:

$$\xi_\star(m) = \mathrm{d}N_\star/\mathrm{d}m = \begin{cases} 2k_\star m^{-\alpha_1}, & 0.08 \leq m/M_\odot < 0.50\,, \\ k_\star m^{-\alpha_2}, & 0.50 \leq m/M_\odot < 1.00\,, \\ k_\star m^{-\alpha_3}, & 1.00 \leq m/M_\odot < m_{\max}\,. \end{cases} \tag{1.1}$$

$dN_\star$ is the number of stars in the mass interval m to $m+dm$. The IMF upper mass limit, $m_{\max}$, depends on the mass of the embedded cluster (see Oh and Kroupa 2018 and Section 1.4.2 below). The normalization parameter, $k_\star$, is determined by simultaneously solving for the stellar mass in the embedded cluster,

$$M_{\rm ecl} = \int_{0.08\ \mathrm{M}_\odot}^{m_{\max}} m\ \xi_\star(m)\,\mathrm{d}m, \tag{1.2}$$

and $m_{\max}$ according the optimal sampling theory (Kroupa et al., 2013; Schulz et al., 2015; Yan et al., 2017),

$$1 = \int_{m_{\max}}^{m_{\max *}} k_\star m^{-\alpha_3}\,\mathrm{d}m. \tag{1.3}$$

$m_{\max *}$ is the physical stellar upper mass limit. We adopt $m_{\max}(M_{\rm ecl}) \leq m_{\max *} = 150\,M_\odot$ (Yan et al., 2017). We note that Eq. 1.3 is only valid when $m_{\max} > 1\ M_\odot$, which is the case for all clusters more massive than 5 $M_\odot$ and has a sub-Solar metallicity[5]. For cases where $m_{\max} < 1\ M_\odot$, Eq. 1.1 and 1.3 need to be changed

[5]The metallicity enters here because of Eq. 1.4 below. Super-Solar metallicity leads to a bottom-heavy IMF, therefore, reduce the $m_{\max}$ for a given cluster mass.

accordingly involving α_2 and α_1. See the supplementary document of the GalIMF code[6], their section 2.2 and 2.3.

Optimal sampling describes a highly-self regulated star formation process and samples the mass of each star in a stellar population (Kroupa et al., 2013; Schulz et al., 2015; Yan et al., 2017). It does not give a stellar upper mass limit in a statistical sense but directly gives the mass of the most massive star. The optimally sampled stars are consistent with observations. One shall not sample stars again from the mass distribution of the optimally sampled stars or the integrated gwIMF which is an approximation of the optimal sampling procedure, as was wrongly done in Fumagalli et al. (2011) and in the SLUG program (da Silva et al., 2012, their fig. 12). The sampled maximum stellar mass would be lower than the mass of the most massive optimally sampled star and therefore lower than the observed most massive star.

The power-law indices of the IMF have been constrained by Marks et al. (2012) and Yan et al. (2020) (which is supported by the recent studies of Villaume et al. 2017 and Martín-Navarro et al. 2019) as

$$\begin{aligned} \alpha_1 &= 1.3 + \Delta\alpha \cdot (Z - Z_\odot), \\ \alpha_2 &= 2.3 + \Delta\alpha \cdot (Z - Z_\odot), \\ \alpha_3 &= \begin{cases} 2.3, & x < -0.87, \\ -0.41x + 1.94, & x > -0.87, \end{cases} \end{aligned} \tag{1.4}$$

where, Z and $Z_\odot = 0.0142$ are the metal mass fraction of the target star cluster and the Sun, respectively. The value $\Delta\alpha = 63$ is estimated by Yan et al. (2020, their equation 9) and updated by Yan et al. (2021). The parameter x in Eq. 1.4 depends on the metallicity, $[Z/X] \approx [Z] = \log_{10}(Z/Z_\odot)$, and on the core density, $\rho_{\rm cl}$, of the embedded star cluster,

$$x = -0.14[Z] + 0.99 \log_{10}(\rho_{\rm cl}\ [M_\odot/{\rm pc}^3]/10^6), \tag{1.5}$$

with the core density correlated with the mass of the embedded star cluster

$$\log_{10}(\rho_{\rm cl}\ [M_\odot/{\rm pc}^3]) = 0.61 \log_{10}(M_{\rm ecl}\ [M_\odot]) + 2.85, \tag{1.6}$$

as is detailed in Yan et al. (2017, their eq. 7).

The ECMF for a star cluster population formed within a $\delta t = 10^7$ yr star-formation epoch is approximated by a power-law (Gieles et al., 2006; Lieberz and Kroupa, 2017):

$$\xi_{\rm ecl} = {\rm d}N_{\rm ecl}/{\rm d}M_{\rm ecl} = k_{\rm ecl} M_{\rm ecl}^{-\beta}, \quad 5M_\odot \leq M_{\rm ecl} < M_{\rm ecl,max}. \tag{1.7}$$

The total stellar mass is given by

$$M_{\rm tot} = \int_{M_{\rm ecl,min}}^{M_{\rm ecl,max}} M_{\rm ecl}\, \xi_{\rm ecl}(M_{\rm ecl})\, {\rm d}M_{\rm ecl} = \bar{\psi}_{\delta t}\, \delta t, \tag{1.8}$$

[6]https://github.com/Azeret/galIMF/blob/master/supplementary-document-galimf.pdf

where $\bar{\psi}_{\delta t}$ is the average SFR over the $\delta t = 10^7$ yr in units of $M_\odot$/yr.

The upper mass limit of the ECMF, $M_{\rm ecl,max}$, is given by the optimal sampling theory:

$$1 = \int_{M_{\rm ecl,max}}^{10^9\ {\rm M}_\odot} k_{\rm ecl} M_{\rm ecl}^{-\beta}\, {\rm d}M_{\rm ecl}, \tag{1.9}$$

where $10^9 M_\odot$ approximately corresponds to the mass of the most massive known star-cluster-type system, that is, the most massive ultra-compact dwarf (UCD, Dabringhausen et al. 2008). Solving the above two equations yields $k_{\rm ecl}$ and $M_{\rm ecl,max}$.

The power-law index, β, is a function of the mean galaxy-wide SFR over the δt time period, $\bar{\psi}_{\delta t}$, according to Weidner et al. (2013c),

$$\beta = -0.106 \log_{10} \bar{\psi}_{\delta t} + 2. \tag{1.10}$$

This variation is supported by observation (see Weidner et al. 2004 and Yan et al. 2017, their Fig.6 and Appendix B) and also the galactic cluster formation simulation study (Li et al., 2021).

The time-dependent gwIMF follows by adding-up all the stars formed in all embedded clusters,

$$\xi(t) = {\rm d}N_\star/{\rm d}m = \int_{5M_\odot}^{M_{\rm ecl,max}} \xi_\star(m, M_{\rm ecl}, [Z/X])\, \xi_{\rm ecl}(M_{\rm ecl}, \bar{\psi}_{\delta t})\, {\rm d}M_{\rm ecl}. \tag{1.11}$$

Therefore, the gwIMF varies through time according to the galactic metal evolution and SFR fluctuation. Eq. 1.11 is the "IGIMF equation".

The above formulation is empirically determined. They are consistent with the observational constraints from the resolved star clusters and the galaxies as we will demonstrate below.

1.4 Comparing the IGIMF theory with observation

1.4.1 Overview

The IGIMF theory asserts that the time and space integrated IMF of a galaxy can be calculated from the IMFs in all star clusters ever formed in that galaxy. That is, there are three levels of complexity to compare the theoretical and observational IMF:

1. The applied IMF variation law in single star clusters needs to be consistent with the observed stellar populations in different environments. This is not easy since the star clusters form on a timescale that is similar to the lifetime of the most massive star. The dynamical evolution of the star clusters can only be accounted by N-body simulations which can be significantly affected by the assumption of the initial distribution of the stars (e.g. initial mass segregation) and the accuracy of the code that is hard to verify observationally.

2. Within a single star formation epoch of about 10 Myr (see the third axiom in Section 1.3.1), the applied embedded cluster mass distribution and its possible variation needs to be consistent with the observation. Using the IGIMF theory (Eq. 1.11) the gwIMF for this single 10 Myr star formation epoch can be calculated and compared with the observation. Since the massive stars certainly dominate the luminosity of a 10 Myr old stellar population, it is currently only possible to compare the theory and observation for massive stars as is shown in Section 1.4.4 below.

3. The present-day galactic IMF is a composition of multiple simple stellar populations formed with an extended SFH, that is, a time-integrated gwIMF (TIgwIMF). Since the gwIMFs are different for each 10 Myr star formation epoch depending on the instantaneous galactic environment, such as SFR and metallicity, we need to apply a galaxy evolution model (chemical or even chemo-hydrodynamical models) to calculate the TIgwIMF. This can then be compared with galaxies that have stopped their star formation for a certain time which allows observational tests for lower-mass stars. The TIgwIMF also determines the mass-to-light ratio of a galaxy which can be constrained by the dynamical properties or lensing studies of galaxies.

1.4.2 The IMF

Assuming that the IMF for the massive stars ($m > 1M_{\odot}$) follows a single power-law description and that, if the IMF of low-mass stars varies, the IMF slopes of different mass ranges (from 0.08 to $0.5M_{\odot}$ and from 0.5 to $1M_{\odot}$) vary by the same amount (i.e. following Eq. 1.4), then we can test the IMF variation separately for low and high mass stars without measuring the IMF shape for each different mass bins. The constraint on massive-star IMF was derived from the dynamical simulation of GCs (Marks et al., 2012) and can be tested independently by observation of young stellar objects (YSOs) in different star clusters.

For the low-mass stars in a star cluster, the dynamical evolution would preferentially reduce the number of lower-mass stars and therefore change the shape of the IMF. A detailed dynamical simulation is required (e.g. Baumgardt and Makino 2003; Baumgardt and Kroupa 2007).

For massive stars of the young stellar regions, the challenge to measure their IMF would be the poor statistics. Unlike for low-mass stars, there is a very limited number of massive stars in each of the young star clusters on the main sequence. Hence a meaningful statistical analysis is challenging. However, it is possible to test an alternative quantity, namely the mass of the most (and second, etc) massive stars. The optimal sampling theory, assuming a highly self-regulated star formation activity, predicts that there is a correlation between the IMF shape and the mass of the most massive star that would form in a star cluster as discussed next.

The $m_{\rm max}$–$M_{\rm ecl}$ relation

The $m_{\rm max}$–$M_{\rm ecl}$ relation calculated with optimal sampling can be verified by observation. The result is shown in Fig. 1.3. See Yan et al. (2017) for more details regarding the data points in this figure.

The $m_{\rm max}$–$M_{\rm ecl}$ relation agrees well with the observation and is not a fit but is calculated from the assumed IMF variation and optimal sampling. The observational data points in Fig. 1.3 show no evidence for an intrinsic scatter (cf. Weidner et al. 2013b their figure 1). It is not the mean $m_{\rm max}$–$M_{\rm ecl}$ relation but the small scatter of the observations differentiate optimal sampling from random sampling. The observation does not show a scatter as large as the result given by the random sampling procedure. Considering the measurement error of the stellar mass and star cluster mass, the observed correlation between them is consistent with no intrinsic correlation at all.

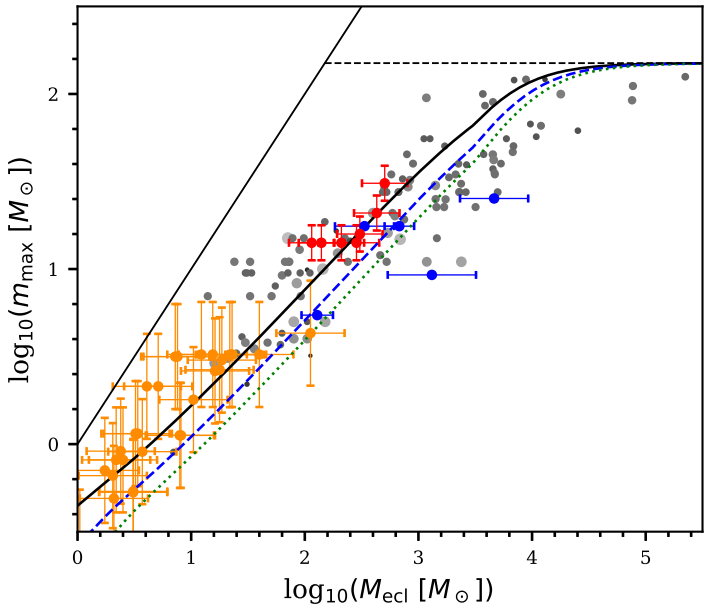

Figure 1.3: Figure taken from Yan et al. 2017. The relation between most massive stellar mass and embedded cluster mass ($m_{\rm max}$–$M_{\rm ecl}$). The optimally sampled results for the most, second, and third massive star mass as a function of embedded cluster mass are shown as a solid curve, blue dashed curve, and green dotted curve, respectively. Observational data come from Kirk and Myers (2012) (orange dots), Stephens et al. (2017) (red dots), Weidner et al. (2013b) (gray dots), and Ramírez Alegría et al. (2016) (blue dots), where Weidner et al. (2013b) is an inhomogeneous set of data culled from the literature for very young clusters without supernova remnants. The average $M_{\rm ecl}$ uncertainty is 0.34 dex, the average $m_{\rm max}$ uncertainty is 0.16 dex, being indicated by gray dots, and light gray dots indicate data points with larger uncertainties. The thin solid line indicates the $M_{\rm ecl} = m_{\rm max}$ limit and the horizontal thin dashed line indicates the $m_{\rm max*} = 150\,M_\odot$ limit (see Eq. 1.3). The light grey data points are slightly larger for better visibility.

1.4.3 The ECMF

Similar to the $m_{\rm max}$–$M_{\rm ecl}$ relation, the distribution of embedded star cluster masses in a galaxy is related to the galaxy-wide SFR. Observations have suggested that low-SFR galaxies do not form massive star clusters. This is expected

by optimal sampling formulated above in Section 1.3.3. Here we compare the observed and calculated $M_{\rm ecl,max}$–$\bar{\psi}_{10^7{\rm yr}}$ relation in Fig. 1.4. The data points provided by Weidner et al. (2004) comprise a homogeneous data set of galaxies with young star clusters. Randriamanakoto et al. (2013) extend these observations to higher SFRs and note that the small scatter of their data is inconsistent with random sampling. These results support our assumed β–$\bar{\psi}_{10^7{\rm yr}}$ relation in Eq. 1.10.

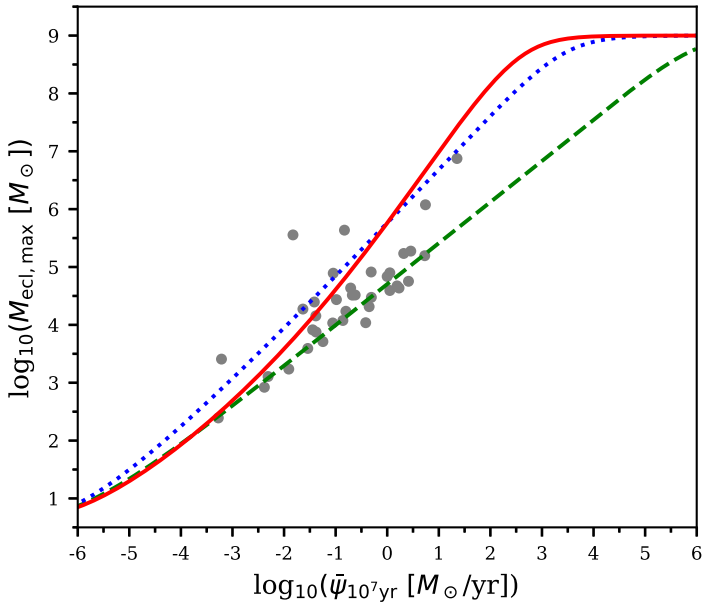

Figure 1.4: Figure taken from Yan et al. 2017. Most massive young cluster mass to galaxy-wide SFR ($M_{\rm ecl,max}$–$\bar{\psi}_{10^7{\rm yr}}$) relation. The optimally sampled results for different β are shown as a red solid curve for β following Eq. 1.10, blue dotted curve for $\beta = 2$, and green dashed curve for $\beta = 2.4$. Observational data (gray dots) adopted from Weidner et al. (2004) have a typical uncertainty of 0.3 dex. The $\beta = 2$ and 2.4 curves are almost identical with Fig. 6 in Weidner et al. (2004) (middle dotted and middle dashed curves, respectively), in which $\delta t = 10^7$ yr is also adopted. See also Randriamanakoto et al. (2013).

1.4.4 The gwIMF

$\alpha_3^{\rm gal}$–$\bar{\psi}_{10^7{\rm yr}}$

The gwIMF, which is an integration of power-law IMFs, is no longer a power law. Therefore, the slope and the "power-law index" of the gwIMF is different for each stellar mass range. We compare the IGIMF calculation with observationally estimated power-law indices of the gwIMF for the massive stars over different stellar mass ranges and galaxy-wide SFRs. For this purpose, the short IGIMF segments in each mass range are approximated by a power-law with index $\alpha_3^{\rm gal}$. The resulting $\alpha_3^{\rm gal}$–$\bar{\psi}_{10^7{\rm yr}}$ relation is shown in Fig. 1.5. The calculation given by the IGIMF theory matches the observations nicely. The gwIMF becomes top-heavy in high-SFR galaxies and top-light in low-SFR galaxies.

By applying the presumed star cluster scale IMF variation given by Marks et al. (2012), the observed ECMF, and the IGIMF theory that links this small scale IMF variation to the gwIMF, we find the calculated gwIMF agrees well with the observations. This is a consistency success of the IGIMF theory.

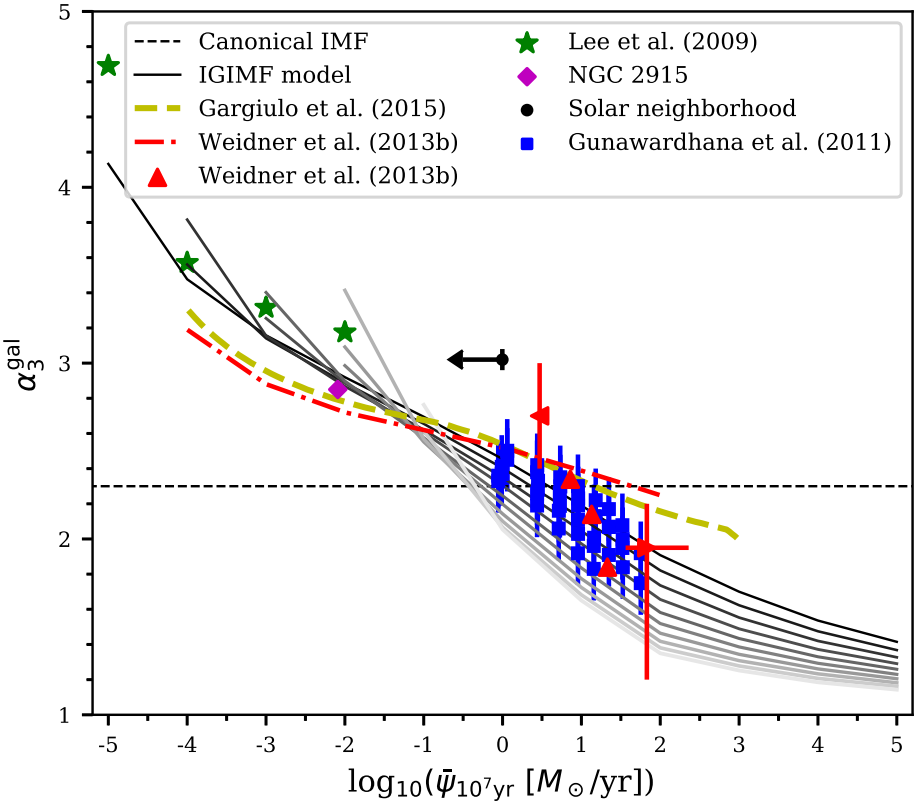

Figure 1.5: Figure taken from Yan et al. 2017. Observed high mass end power-law index of the gwIMF resulting from the calculated IGIMF, $\alpha_3^{\rm gal}$ (i.e. $\alpha^{\rm gal}$ for stars with mass $m > 1\ M_\odot$) as a function of the galaxy-wide SFR. $\alpha_3^{\rm gal}$ values diverge for different SFRs and also vary for different stellar masses. Because at each stellar mass value there exists a different $\alpha_3^{\rm gal}$–$\bar{\psi}_{10^7{\rm yr}}$ relation, we plot solid lines for $\log_{10}(m/M_\odot) = 0.2, 0.4, ..., 2$, that is, $1.58, 2.51, ..., 100\ M_\odot$ from black to gray (top to bottom) for the IGIMF calculated results. The blue squares are data from the GAMA galaxy survey (Gunawardhana et al., 2011). The red triangles and red dash-dotted line are data from Weidner et al. (2013c); the left triangle is for the MW field, the middle three triangles are galaxy studies, the right triangle is for the bulges of the MW and M31, and the dash-dotted line is their IGIMF model assuming $\beta = 2$. A recent study has suggested that the $2\ M_\odot$/yr SFR for MW is overestimated (Chomiuk and Povich, 2011), but we leave this data point the same as in Weidner et al. (2013c). Gargiulo et al. (2015) report consistency between their IGIMF model assuming $\beta = 2$ (thick orange dashed line) and the $[\alpha/Fe]$ abundance ratios of elliptical galaxies. The purple diamond is an individual analysis for the dwarf galaxy NGC 2915 (Bruzzese et al., 2015). Green stars are based on the Lee et al. (2009) 11HUGS observations of dwarf galaxies. The black circle is an observation for the solar neighbourhood from Rybizki and Just (2015) with adopted MW SFR from Robitaille and Whitney (2010) as an upper limit of the solar neighbourhood SFR because the Sun is located in an inter-arm region where the relevant SFR is significantly smaller. The thin horizontal dashed line represents the canonical IMF slope, $\alpha_3 = 2.3$.

The galaxy-wide most massive star mass–SFR relation

The most massive star in a galaxy also depends on the galaxy-wide SFR according to the IGIMF formulation. The calculation results shown in Fig. 1.6 are a testable prediction that requires further investigation. Galaxy NGC 2915 appears to fit perfectly with this relation (Bruzzese et al., 2015) but a large number of galaxies need to be studied to give a statistically significant result. See the discussion in Section 1.5 above.

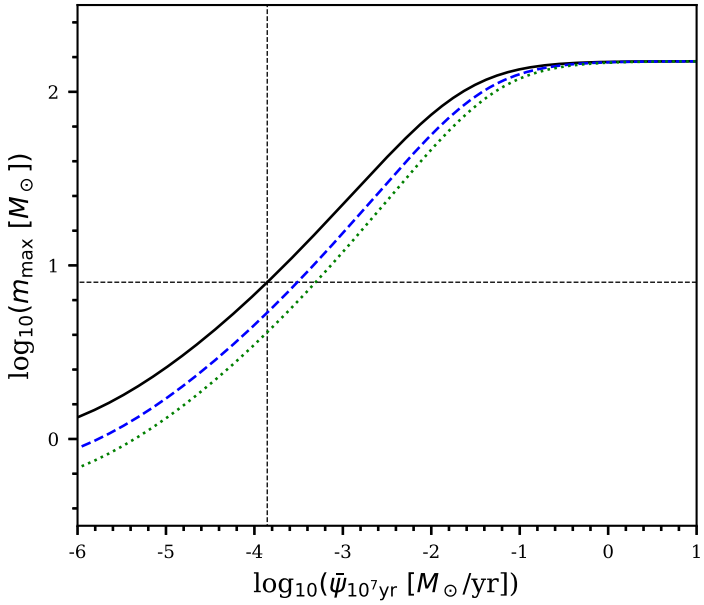

Figure 1.6: Optimally sampled most-, second-, and third-massive stars to be found in a galaxy as a function of the galaxy-wide SFR. These stars are shown as a solid curve, blue dashed curve, and green dotted curve, respectively. The thin horizontal dashed line indicates the mass limit below which CCSN explosions are not likely (8 $M_{\odot}$), and the vertical thin dashed line shows the SFR below which galaxies are not expected to host CCSN events, subject to the axioms adopted in the present study. We note that $\bar{\psi}_{10^7\mathrm{yr}}$ here is the true SFR, not an estimation assuming a universal IMF.

1.4.5 The TIgwIMF

The old stellar populations of ETGs have their most massive star weighing about 1 $M_{\odot}$. Observations of these galaxies can constrain the IMF of low-mass stars. For instance, the IMF-sensitive features of the old galaxies as well as their dynamical mass-to-light ratios can be compared with the theory.

The canonical galaxy model assuming an invariant IMF and considering old stellar populations simplifies the calculation by assuming a simple stellar population (SSP) for the galaxy that all stars have the same age and metallicity (e.g., Thomas et al. 2005). Such a simplification cannot be applied when the gwIMF evolves as a function of the star formation and metal enrichment history. The integrated IMF for all stars formed over the entire SFH, that is, the time-integrated gwIMF (TIgwIMF) also changes (see e.g. Fig. 2.7 below). To study the TIgwIMF, we must apply a self-consistent galaxy chemical evolution model which we developed as is introduced in the next Chapter.

1.5 Summary and caveats

In this section, we compare the IGIMF theory with the observed IMF variation from star cluster to galaxy scales. The IGIMF theory provides a mathematical framework that is able to reproduce a variety of extragalactic observations and is consistent with the local star cluster scale IMF measurements in so far as tests have been made, see, for example, the summaries and references in Pflamm-Altenburg and Kroupa (2008); Weidner et al. (2013c); Yan et al. (2017); Fontanot et al. (2017); Jeřábková et al. (2018); Yan et al. (2020, 2021). It is impressive and convincing to find many independent pieces of evidence that converge to the same trend of a systematically varying gwIMF and also to find that the IMF variation on the embedded cluster scale and on the galactic scale fit the same picture consistently.

However, the application of the IGIMF formulation has its limits. The empirical high-mass IMF variation given by Marks et al. (2012) is for clusters below a certain mass and metallicity. Extrapolation of their formulation may or may not be physically valid and one needs to be cautious when applying the formulation to extreme cases. Yan et al. (2017) show that galaxies with SFRs up to $100 M_\odot$/yr are still consistent with the calculation of the IGIMF theory but higher-SFR galaxies forming more extremely massive star clusters may start to deviate from the expectation of the present formulation. The ECMF formulation is also suggested by limited observations. When the SFR of a galaxy is too low (e.g. $\bar{\psi}_{10^7\mathrm{yr}} < 10^{-6} M_\odot$/yr), the ECMF is not well-defined because a temporarily and spatially correlated galactic star cluster population does not exist. This is clear since only $10 M_\odot$ of stars are formed in 10 Myr. For example, Yan et al. (2020) apply a SFH cut off (their Fig. 1) and a fluctuated SFH (their Fig. 9) to simulate a dwarf galaxy.

> The IGIMF theory is a mathematical framework that links the IMF on different spatial scales. By improving the description of the small embedded star cluster scale IMF variation, the large galactic scale IMF variation calculated according to the IGIMF theory will become more accurate. A disclaimer is made for galaxies with extremely high and low SFRs or super-solar metallicity.

In addition, we still lack a more direct constraint on the IMF. All the evidence that has been collected so far is indirect evidence coming from dynamical simulations, galactic abundance ratios and luminosity ratios, etc. These constraints on the IMF variation have a large uncertainty, which makes the calculation of the gwIMF not really accurate and conclusive. For the situations where the IGIMF does apply, a test of the IGIMF theory is not trivial to perform. For example, a calculation made in (Yan et al., 2017) applying the IGIMF theory gives a relation between the mass of the most massive star in a galaxy and the true galactic SFR. There are galaxies that agree perfectly with this calculation, such as with the compact dwarf galaxy NGC 2915 (Bruzzese et al., 2015). But there are also massive stars reported in low-SFR galaxies, such as Leo P (McQuinn et al., 2015), apparently being inconsistent with the IGIMF calculation.

It is discussed in Jeřábková et al. (2018) that Leo P actually fits perfectly with the IGIMF theory because the observationally deduced SFR changes when the gwIMF of Leo P is not the canonical IMF. There are some other galaxies that do not appear to agree with the IGIMF theory, e.g., Bruzzese et al. (2020, their table 9). Considering that the estimation of the IMF and the observed highest stellar mass are affected by the SFH assumed and the region being observed, it is not yet possible to tell whether these galaxies are outliers with the small number of galaxies being tested. Further work is required to fully examine these cases and the observation of more galaxies with a homogeneous study is required to test the IGIMF formulation.

A relatively clean method that avoids the difficult estimation of the stellar mass could be to statistically test whether low-SFR galaxies are lacking CCSN. The number of SNe detected are much lower than the number of galaxies we may explore, therefore, may not be able to result in a strong conclusion. But as a first step, such tests of the theory would allow us to achieve a better constraint on how the IMF varies in the embedded clusters. By improving the IGIMF formulation of the embedded cluster scale, the theory will provide a more accurate description for the gwIMF.

It is possible that the IMF variation depends on additional physical parameters. Currently, we apply the formulation given by Marks et al. (2012) where the IMF is affected by star formation intensity and metallicity. There are also other IMF variation considerations. For example, the formulation applied in Fontanot et al. (2018) relates the IMF variation to cosmic-ray intensity mostly produced by type II supernovae that exploded in the same star-forming region (Papadopoulos, 2010). Sharda and Krumholz (2021) studied how the characteristic stellar mass (i.e. the peak of the IMF) might vary as a function of metallicity due to the different physical processes dominating the cooling including molecular hydrogen cooling, metal line cooling, and dust-gas collisions. In comparison with varying the IMF power-law index, varying (in addition) the characteristic stellar mass has the advantage of being theoretically supported/derived. But it also introduces more free parameters to describe the IMF variation, therefore, being more difficult to validate. Such a modification of the IGIMF formulation in the GalIMF code is plausible as long as the proposed formulation is well calibrated with observations.

The above discussions are only for the high stellar mass part of the IMF. The IMF variation for the low-mass stars is more difficult to determine. Considering that the low-mass stars affect galactic metal enrichment by locking up mass, it is possible to constrain the IMF of low-mass stars by study the abundance and enrichment history of the galaxies. In the following Chapters, we combine the IGIMF theory with a newly developed GCE model. A GCE constrained low-mass IMF variation formulation is provided in Chapter 3.1.

For more details, we refer the reader to Yan et al. (2017) which is attached at the end of this dissertation.

2. Chemical evolution of the galaxies

This chapter is partially based on the publication Yan, Jeřábková, and Kroupa (2019) with the title "Chemical evolution of elliptical galaxies with a variable IMF. A publicly available code" and Yan, Jeřábková, and Kroupa (2021) with the title "Downsizing revised: Longer star formation timescales for elliptical galaxies with an environment-dependent IMF and number of SNIa". Modifications were made in order to present it as a chapter in the thesis.

2.1 Introduction

2.1.1 Motivation

Growing evidence suggests a systematic variation of the IMF as is successfully described by the IGIMF theory. While our understanding of the IMF has changed rapidly in the past decade, this has not been applied to related astrophysical studies. For example, the observed stellar abundance ratios in galaxies with different masses, SFRs, and metallicities has not been well explained by previous galaxy chemical evolution (GCE) models assuming the invariant canonical IMF. The evolution of galaxies sensitively depends on the IMF. GCE studies of massive elliptical galaxies have suggested a problem in simultaneously reproducing the total metallicity and α-enhancement of them (De Lucia et al., 2017; Okamoto et al., 2017) indicate the necessity of introducing at least one new degree of freedom, for example, a varying and top-heavy gwIMF (Arrigoni et al., 2010; Martín-Navarro et al., 2018).

The IGIMF theory is likely to be the missing link of the problem and needs to be explored. When the gwIMF varies, GCE will differ from the canonical estimate. However, the publicly available GCE codes (e.g. NuPyCEE, Ritter and Côté 2016) all assume invariant IMFs. For this contribution, we developed an open-source code that is able to couple an environment-dependent IMF theory with the GCE. The instantaneous environment (e.g. metallicity) determines and constantly updates the gwIMF while the gwIMF of each stellar population ever formed determines the later metal enrichment process.

2.1.2 New open source code – GalIMF

A freely available Python3 code, GalIMF, is developed for this PhD project and future applications to calculate the gwIMF according to the IGIMF theory and galaxy chemical evolution under the framework of an environment-dependent IMF. GalIMF stands for the Galaxy-wide Initial Mass Function. GalIMF version 1.0 (with a companion paper Yan et al. 2017) is a Python 3 module that computes

gwIMFs based on the IGIMF theory. GalIMF version 1.1 (with a companion paper Yan et al. 2019b) is a Python 3 module that couples the IGIMF theory with galaxy chemical evolution.

> The GalIMF code, deployment manual, examples, as well as version update records, are available at GitHub:
> https://github.com/Azeret/galIMF

Before looking into the details and the application of the GalIMF code, we introduce the following classification and terminology for the GCE models.

2.1.3 Classification of GCE models

Hydrodynamical versus mixing-zone model

A hydrodynamical simulation provides 3D resolution and constraints on the local SFR. It self-consistently includes star formation, SNe feedback and metal enrichment from CCSN and SNIa.

The mixing-zone model assumes the gas in each zone is well (stochastically) mixed. It can be coupled to cosmological N-body simulations.

The mixing-zone model has the advantage of a far smaller computational cost, allowing an easier exploration of the variation of free parameters in the model.

The "semi-analytic model" or SAM is often referred to in publications. We note that analytical relations and look-up tables are involved, to a certain extent, in both mixing-zone and hydrodynamical models. The difference between mixing-zone and hydrodynamical models is whether the mass-particle/well-mixed zone (for stars or gas) has an evolvable 3D coordinate.

In reality, the ISM is not well mixed. Stochastic models can involve inhomogeneous mixing statistically. These more "realistic" models (and the intermediate approaches mentioned above), considering more physic processes, are not necessarily more realistic if the processes are not effectively constrained by independent observation but act as free parameters (e.g. Côté et al. 2016, 2017; Andrews et al. 2017). It is therefore important to compare the number of free parameters with the number of observational constraints. Keep in mind that although not all the free parameters have a significant effect on the GCE results, many seemingly independent measurements also degenerate (correlate) under a low resolution.

Single-zone closed-box approximation

Instead of the high-resolution 3D hydrodynamical simulation that captures all the details of gas movements and mixing, the discussions here apply the zero dimension approximation, that is, the closed-box approximation, which is useful to describe the bulk average and essential galactic properties while being much cheaper and, more importantly, working with much fewer model parameters, many of which still cannot be well constrained by observation. The closed-box approximation without hydrodynamical considerations is useful especially when the galaxy being studied forms in a short timescale such that gas flows are not

a dominant factor determining the chemical abundance of the stellar population. This is likely to be the case for the present-day quiescent elliptical galaxies which I focused on.

Instantaneous recycling approximation

Many models before about the year 2010 assume the instantaneous recycling approximation (IRA), i.e. they neglect the dependence of stellar lifetimes on stellar mass, and assume that gas recycling and chemical enrichment occur "instantaneously". Modern models track the yield of CCSN, SNIa, and asymptotic giant branch (AGB) stars where the latter two cannot apply IRA.

2.1.4 Summary

Our GalIMF code is a single-zone GCE model with the possibility to include galactic gas inflow and outflow. The element yield of a star depends on its initial mass and metallicity. Precise stellar ages coupled with a short evolution time step (10 Myr) is implemented to result in accurate abundance evolution histories (i.e. no IRA). Other than applying different star formation laws (e.g. the Kennicutt–Schmidt law), it is also possible to specify the star formation activity for each 10 Myr time step. This mode has the advantage to compare different IMF formulations for identical SFHs. The number of SNIa is re-calibrated to account for the IMF variation and potential environmental effects.

In the following sections, we explain the code routine, demonstrate the mechanism and the impact caused by the variable IMF by the case study of a closed-box GCE simulation. It is shown that GCE can be significantly affected when the IGIMF theory is applied.

2.2 Ingredients of the GalIMF code

2.2.1 Star formation history

The SFH of a galaxy in a cosmological model assuming standard cosmology is determined by the merging history of dark matter halos (merger tree). The baryon density is correlated with the dark matter density which determines the SFR following the Kennicutt–Schmidt law.

On the other hand, galactic simulations assume an empirical SFH. This is performed either by assuming the SFH directly or by assuming a baryonic infall history along with the Kennicutt–Schmidt law. These two methods have essentially the same amount of input information to constrain the SFH but the adopted gas-mass related star formation law, in addition, affects the chemical evolution of the galaxy. GCE studies of a specific galaxy can apply the SFH determined by observation (e.g. SPS).

For this Chapter, we demonstrate our GCE model with a directly specified SFH. The SFH is set up before the simulation starts where the SFR per 10 Myr time, $\bar{\psi}_{10^7\mathrm{yr}}$, is given according to a log-normal distribution, as is shown in Fig. 2.1. The timescale over which 80% of the stellar population forms is called the star formation timescale (SFT). The SFT for the example galaxy shown in Fig. 2.1

is about 1 Gyr. Alternative SFH distributions can be applied with the GalIMF code, for example, a constant SFR over certain time, exponential or a skew-normal distribution, or a double burst SFH that models the bulk of the stellar formation with an earlier burst and the latest episode of star formation with a recent burst (Ciesla et al., 2016, 2017).

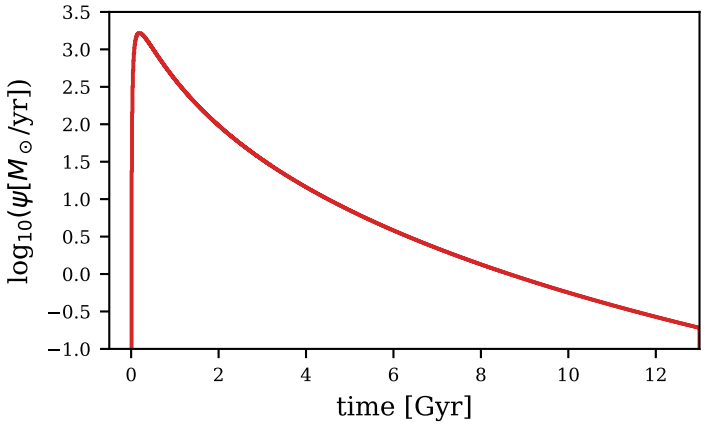

Figure 2.1: Figure taken from Yan et al. 2019b. Adopted SFH. The SFH given by a log-normal function finishes its 50%, 75%, and 90% star formation (in mass fraction) in 0.5, 0.98, and 1.8 Gyr, respectively.

2.2.2 Time structure

GCE is all about time. Stars with different masses return different amounts of elements to the galactic gas at different times due to the mass-dependent stellar evolution and stellar lifetimes. The returned elements then affect the following stellar populations because the star formation and the stellar evolution also depend on the stellar initial metal abundance. Therefore, the time structure of a GCE code is of crucial importance and a critical property of the code. It is not only the theoretical formalism a code intends to simulate but also the actual implication of the formalism in the code that matters.

There is a fundamental difference between the GCE codes that assume an invariant IMF and an environment-dependent IMF. The invariant IMF models apply a continuum star formation and use an iteration process to calculate the integrated mass and abundance evolution between two simulation time steps. That is, the star formation activity at each instant depends on the gas mass while the gas mass changes continually due to star formation and stellar back ejection, (Talbot and Arnett, 1971, their eq. 7).

On the other hand, the environment-dependent gwIMF needs to be calculated at a given time. The IMF evolution can only be calculated discretely. Therefore, the gas mass cannot be smoothly integrated when the IMF is different. For this reason, our code assumes that stars form in time steps. Stars formed in the same 10 Myr time step all have the same age and metallicity. The code simulates the evolution of the galaxy by adding the effects of all the previous stellar populations between two neighbouring time steps (Section 2.2.2).

The IMF evolution is not differentiable but discrete at each time step. The GalIMF code adds the effects of all the previous stellar populations between two neighbouring time steps.

Canonical GCE models assuming an invariant IMF also apply or can apply a 10 Myr or even shorter time steps. But that is only an integration boundary point for the continuous star formation activity. The finer time step results in a higher accuracy but a different time step would not significantly affect the results. On the other hand, for our code, the stars only form at time steps. A longer time step would significantly reduce the accuracy of our calculation of the stellar population. A shorter time step is also not appliable in the current IGIMF formulation because the formation of a galaxy-wide stellar population requires a minimum time. Under 10 Myr, too few star clusters have been formed to properly populate the ECMF (see Weidner et al. 2004, Yan et al. 2017).

At a new time step, the gas-phase element abundances are calculated given the values at the nearest previous time step and the ejections from all the stellar populations formed between these two simulation time steps. If there is star formation at the new time step, the amount of mass transformed into stars is deducted from the gas phase.

2.2.3 Gas-, star-, and remnant-mass evolution

In our GCE model, the mass of different elements in gas and stars are updated at each time step. Stars return a portion of their mass to the gas phase and turn into stellar remnants when exhausting their lifetimes. The stellar lifetime and the mass of stellar remnant are adopted from Portinari et al. (1998) and Marigo (2001) as a function of stellar initial mass and metallicity. Smoothing spline fits on the logarithmic scale of the stellar models are applied (Ritter et al., 2018) as is shown in our Figs. 2.2. We note that the spline fitted remnant mass is only for demonstration while the actual amount of gas ejection from the dying stars is given by a two-dimensional (metallicity and mass) interpolation of the stellar yield table. All SNIa are assumed to eject 1.15 $M_\odot$ of gas (Thielemann et al., 1993; Gibson et al., 1997).

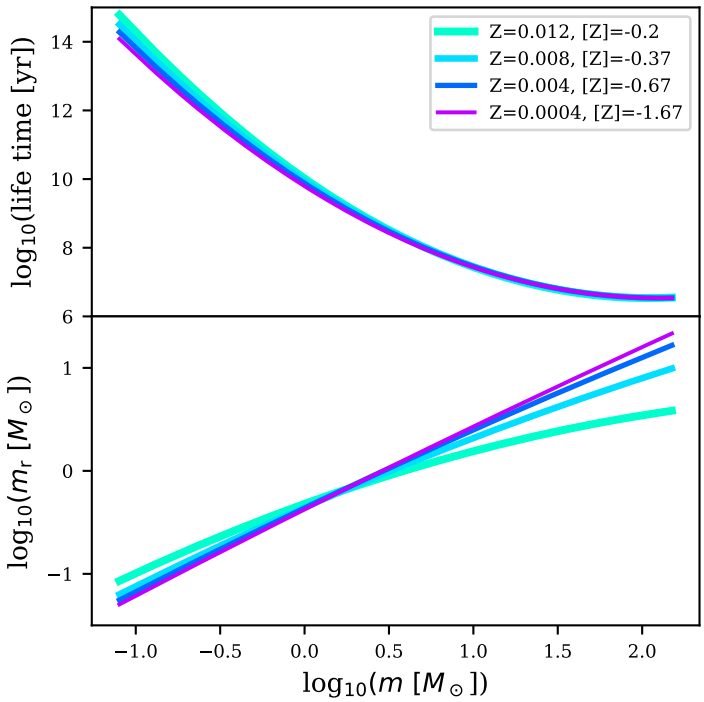

Figure 2.2: Figure taken from Yan et al. 2019b. Lifetime (upper panel) and remnant mass, $m_{\rm r}$ (lower panel), of a star as a function of its initial mass, m, and metal mass fraction, Z. The shown relations are one-dimensional smoothing spline fits to the stellar evolution tables given by Marigo (2001) and Portinari et al. (1998) for AGB and massive stars, respectively.

2.2.4 The definition of the metallicity

The values of $[Z]$ and $[Z/X]$ (or $[Z/H]$) are not the same, especially for helium-rich stars. Therefore, it is important to define "metallicity" in publications, which however is often omitted.

For each element i, we adopted the classical notations

$$A_i = \log_{10}(N_i/N_{\rm H}) + 12, \tag{2.1}$$

where N denotes the number of atoms and $N_{\rm H}$ is the number of the hydrogen atom. The abundance ratio of element i and hydrogen is defined as

$$[i/H] = A_{i,\star} - A_{i,\odot}, \tag{2.2}$$

where the subscripts $\star$ and $\odot$ denote the target value and the solar value, respectively. We note that the $[i/H]$ value is unaffected if we adopt the element mass ratio, $M_i/M_{\rm H}$, instead of the element number ratio, $N_i/N_{\rm H}$, in Eq. 2.1. This is the case for the calculation of the luminosity-weighted element ratio ($[Fe/H]_{\rm lw}$) introduced below.

Finally, the abundance ratio of two elements i and j is

$$[i/j] = [i/H] - [j/H]. \tag{2.3}$$

The mass fraction of hydrogen, helium, and all other elements (i.e. metals) in stars are denoted by X, Y, and Z, respectively. The "metallicity" in different publications is defined either as

$$[Z] = \log_{10}(Z/Z_{\odot}), \tag{2.4}$$

or $[Z/H]$. Our works apply a different symbol $[Z/X]$ which has the same value as $[Z/H]$ but is defined clearly as an element mass ratio instead of an element number ratio, although they have the same value in this case.

$$[Z/X] = \log_{10}(Z/X) - \log_{10}(Z_{\odot}/X_{\odot}). \tag{2.5}$$

$Z_{\odot}$ is the solar metal mass fraction. Our recent work adopts $Z_{\odot} = 0.0142$ estimated by Asplund et al. (2009). $X_{\odot} = 0.70683$ is the solar mass fraction of hydrogen adopted from Anders and Grevesse (1989).

We note that the values of $[Z]$ and $[Z/X]$ are similar but deviate from each other as stellar helium abundance increases to super-solar values. For example, if Y increases from the solar value of about 0.27 to 0.46 as is suggested by some observations of globular clusters (GCs) and early-type galaxies (ETGs, e.g. Yi et al. 2011, Karakas and Shingles 2017, and Ali et al. 2021), then $[Z]$ and $[Z/X]$ will differ by $\log_{10}(X/X_{\odot}) \approx 0.13$ dex, which is not negligible.

2.2.5 Metal enrichment

The gas-phase primordial element composition is adopted from Cyburt et al. (2016). The gas is enriched by stellar and SNIa ejections which then form a new generation of enriched stars. The masses of the elements H, He, C, N, O, Ne, Mg, Si, S, Ca, Fe are traced with the possibility to include more elements and isotopes. The total stellar yield for $[Z]$, Y, and $[Mg/Fe]$ values for stars with different initial mass and metallicity adopted from Portinari et al. (1998) and Marigo (2001) are shown in Fig. 2.3. The newest version of the code (version 1.1.10) updates the yield table for massive stars with the results given by Kobayashi et al. (2006). This Kobayashi's table is based on the theoretical modelling of Type II/Ibc supernovae and hypernovae. The yield for electron-capture supernova and rarer types of supernova (see relative number in Kobayashi et al. 2020, their table 2) and neutron star mergers are not included as they do not have a significant effect on the enrichment of elements lighter than iron. The SNIa yield is adopted from Gibson et al. (1997, their TNH93 dataset) and does not depend on the property of the SNIa progenitor. All elements in the gas reservoir are always well mixed, that is, there is only a single gas phase. More technical details are provided in Yan et al. (2019b).

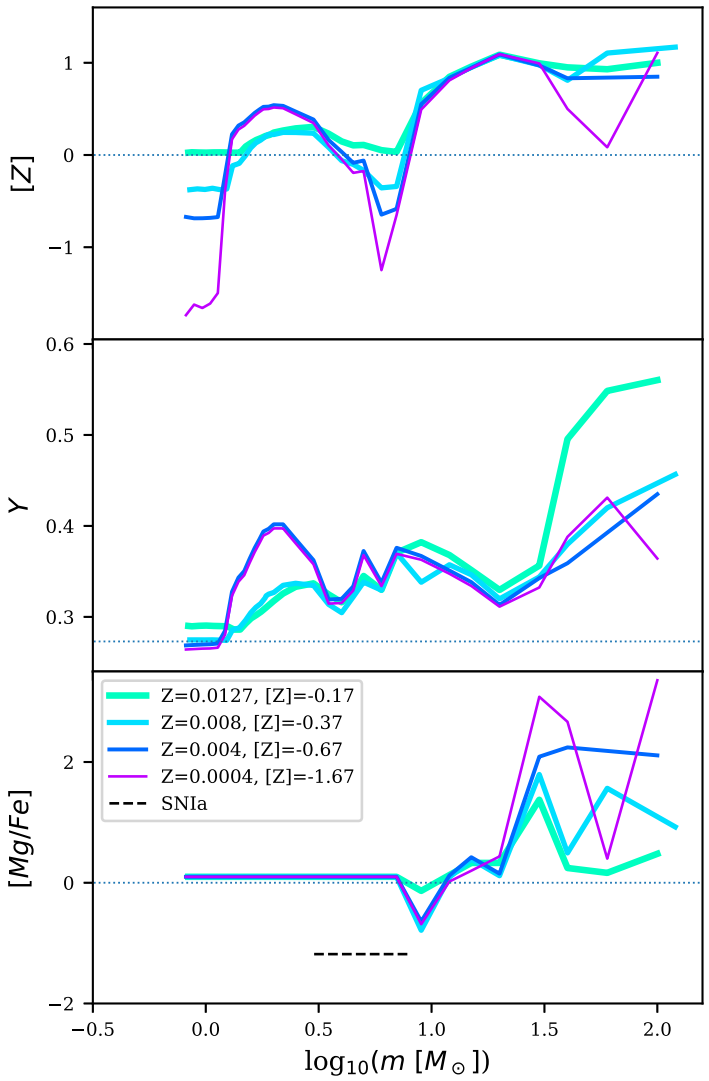

Figure 2.3: Figure taken from Yan et al. 2019b. Metallicity $[Z]$, helium mass fraction Y, and α-enhancement $[Mg/Fe]$ of the ejected gas from a dying star (or supernova event) as a function of the stellar initial metal mass fraction Z and the stellar initial mass m (or the initial mass of the possible SNIa progenitor, i.e. 3 to 8 $M_\odot$ shown by the horizontal dashed line). The horizontal thin dotted lines indicate the solar value (the solar value of $Y = 0.273$ is adopted from Serenelli and Basu 2010). The relation is interpolated from the stellar yield table given by Marigo (2001) and Portinari et al. (1998) where a solar value stellar initial helium abundance is assumed for the stellar evolution model.

In addition to the mass-weighted element abundance, our code also gives an estimation of the stellar luminosity-weighted abundance. A simple mass-luminosity relation for main-sequence stars is adopted (Duric 2004, their chapter 1.3.8 and Salaris and Cassisi (2006, their chapter 5.7)) while the AGB luminosity is not taken into consideration. The luminosity of a star of mass m is

$$\frac{L}{L_\odot} = \begin{cases} 0.23\left(\frac{m}{M_\odot}\right)^{2.3}, & \frac{m}{M_\odot} < 0.421; \\ \left(\frac{m}{M_\odot}\right)^{4}, & 0.421 \geqslant \frac{m}{M_\odot} < 1.96; \\ 1.4\left(\frac{m}{M_\odot}\right)^{3.5}, & 1.96 \geqslant \frac{m}{M_\odot} < 55.41; \\ 32000\frac{m}{M_\odot}, & 55.41 \geqslant \frac{m}{M_\odot}, \end{cases} \tag{2.6}$$

where m is the stellar initial mass. Then the luminosity-weighted metallicity, $Z_{\rm lw}$, of all the living stars at time t_n is calculated as

$$Z_{\rm lw}(t_n) = \frac{\sum_{t=t_1}^{t_n} \left[\int_{m=m_{\rm min}}^{m_{\rm max}(t_n-t)} \xi(t,m)L(m)dm \cdot Z(t)\right]}{\sum_{t=t_1}^{t_n} \left[\int_{m=m_{\rm min}}^{m_{\rm max}(t_n-t)} \xi(t,m)L(m)dm\right]}, \tag{2.7}$$

where $\xi(t)$ is the gwIMF for the stellar population formed at time t (see $\xi_{\rm IGIMF}$ in Yan et al. 2017 for definition), $m_{\rm max}$ is the mass of the most massive star that is still living at time t_n for the stellar population formed at time t, and $m_{\rm min} = 0.08\ M_\odot$ is the lowest possible stellar mass.

The luminosity-weighted element ratio ($[Fe/H]_{\rm lw}$) is calculated by a similar equation. It is not weighted with the $[Fe/H]$ value of each star, but with the element mass $M_{i,\rm mw}$ of the stars, where i is Fe or H and

$$M_{i,\rm mw}(t_n) = \frac{\sum_{t=t_1}^{t_n} \left[\int_{m=m_{\rm min}}^{m_{\rm max}(t_n-t)} \xi(t,m)L(m)dm \cdot M_i(t)\right]}{\sum_{t=t_1}^{t_n} \left[\int_{m=m_{\rm min}}^{m_{\rm max}(t_n-t)} \xi(t,m)L(m)dm\right]}. \tag{2.8}$$

Then, Eq. 2.1 to 2.3 are applied to calculate $[Fe/H]_{\rm lw}$ where N_i is substituted by $M_{i,\rm mw}$.

Finally, we note that some studies adjust the yields of metal elements (such as Mg and C) or the rate of SNIa in their model in order to fit certain observational constraints. The better approach (e.g. in Arrigoni et al. 2010) would be to (i) show straightforwardly that the model cannot fit the observation (cf. Kobayashi et al. 2020, their fig. 39) then (ii) suggest modifications on this fiducial model because the possible option includes, but is not restricted to, an adjustment of the metal yields. Different yield tables are compared by, e.g., Philcox et al. (2018).

2.2.6 Environment-dependent IMF

Recent developments of the GCE models have started to adopt non-canonical variable IMFs that depends on the local gas density, mentallicity and/or other properties. For example, Recchi et al. (2009); Haas and Anders (2010); Ploeckinger et al. (2014); Recchi et al. (2015); Gargiulo et al. (2015); Fontanot et al. (2017, 2018); Palla et al. (2020) and most recently Prgomet et al. (2021) applied a metallicity-dependent IMF in a hydrodynamical GCE model.

Most GCE models were developed initially assuming an invariant IMF and were then modified to adopt a variable IMF. It is not always the case that this paradigm shift is done or explained correctly. Many models assume the single degenerate SNIa scenario where the SNIa rate depends on the number and lifetime of the companion star and there with depends on the IMF shape. Therefore, the IMF dependence is encoded in this original formulation and the model can adopt different IMFs effortlessly. However, the calculation using the original single degenerate formulation is complicated and costly. The models usually apply an analytical fit of the SNIa rate result for a certain given IMF, thus assuming, not in the SNIa formulation or theory but in the implementation of the SNIa formulation in the code, that the IMF is invariant (e.g. Lia et al. 2002). Another

popular SNIa rate formulation is the power-law delay time distribution (DTD) formulation which does not depend on the IMF shape explicitly in the first place and requires recalibration on the total SNIa number for each new IMF shape as is described in Section 2.2.7 below. We urge the researchers to check and explain in more detail how their galaxy model assuming an invariant IMF is transformed into the variable IMF paradigm, if this information has not been covered in their previous publications.

Rather than introducing ad-hoc variations of the IMF, our calculation applies the IMF variation formulation that is consistent with previously established observational constraints, including dwarf galaxies (Lee et al., 2009; Dabringhausen et al., 2009, 2010, 2012), the young cluster R136 (Banerjee and Kroupa, 2012), globular clusters (Marks et al., 2012), dusty starburst galaxies (Zhang et al., 2018), and chemical-evolution constraints (Yan et al., 2020).

Our calculation applies a formulation of the IMF variation that is consistent with previously established observational constraints. No ad-hoc variation of the IMF is introduced.

A new code assuming not a continuum star formation activity but the formation of simple stellar populations (stars that have the same age and metallicity) for each 10 Myr star formation epoch is developed in particular for this PhD project to incorporate the environment-dependent gwIMF into the GCE model. The underlying notion is that the IMF is related to the embedded cluster mass and the embedded cluster mass distribution (ECMF) needs to be taken into consideration in the calculation of the gwIMF. That is, the IMFs of a population of star clusters need to be considered together. Since the typical time scale to form enough star clusters that properly populate the ECMF is about 10 Myr, it is difficult to consider shorter time steps in the one zone evolution model. That is why we only have 10 Myr steps. The hydrodynamical model can have a shorter time step which corresponds to the formation of single clusters instead of cluster population but there are other problems, such as resolving the vast number of very low-mass embedded clusters that form thoughout the galaxy.

To incorporate the environment-dependent gwIMF into the GCE model, the GCE module requires the gwIMF calculation module to calculate the gwIMF according to the IGIMF theory at each time step according to the instantaneous galaxy-wide SFR and gas-phase metallicity (Fig. 2.4). Different from the invariant IMF assumption where the star formation activity is assumed to be a continuum, the calculation of gwIMF with the IGIMF theory is done for 10 Myr time steps assuming that the gwIMF is invariant during each 10 Myr time.

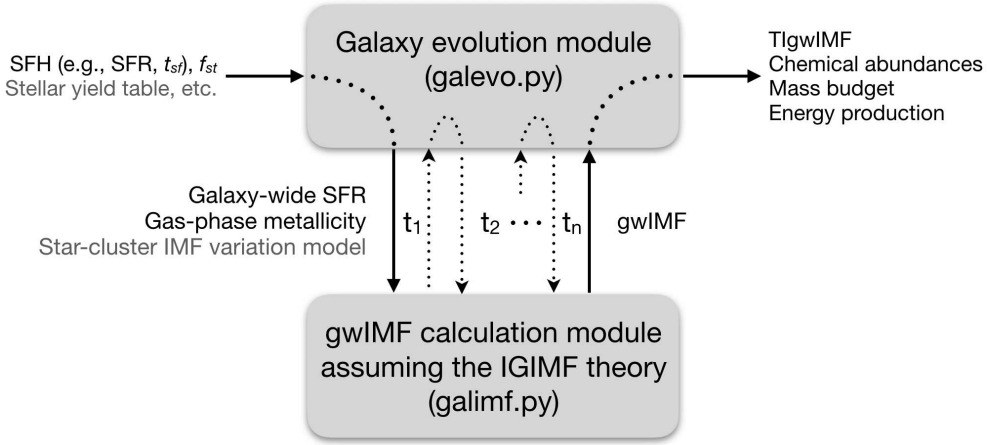

Figure 2.4: Figure taken from Yan et al. 2019b. Interaction between the GCE module and the IGIMF calculation module and the input/output.

2.2.7 The SNIa production efficiency

The number of SNIa depends on the number of possible SNIa progenitors, that is, on the number of stars with a mass between about 3 to $8 M_\odot$ (see below), therefore, on the gwIMF.

The total number of SNIa explosions for a simple stellar population (SSP, stars formed at the same time) after t years of the birth of the SSP per unit stellar mass of the SSP (i.e. the time-integrated number of SNIa per stellar mass formed until time t) is

$$n_{\rm Ia}(t, \xi, \bar{\psi}_{\delta t}) = N_{\rm Ia}(\xi, \bar{\psi}_{\delta t}) \int_0^t f_{\rm delay}(t) {\rm d}t \ , \tag{2.9}$$

where $N_{\rm Ia}$ is the SNIa production efficiency, that is, the total number of SNIa per unit mass of stars formed in the SSP, and $f_{\rm delay}$ is the delay time distribution (DTD) function, that is, the fraction of exploded SNIa for an SSP with age t. We adopt the empirical power-law DTD function from Maoz and Mannucci (2012),

$$f_{\rm delay}(t) = \begin{cases} 0, & t \leqslant 40 \text{ Myr}, \\ k \cdot t^{-1}, & t > 40 \text{ Myr}, \end{cases} \tag{2.10}$$

where the normalization factor k is determined by the condition $\int_{t=0}^{\infty} f_{\rm delay}(t) {\rm d}t = 1$. Therefore, $N_{\rm Ia} = n_{\rm Ia}(t = \infty) \approx n_{\rm Ia}(t = 10 \text{ Gyr})$.

A high fraction of multiple stellar systems and uncorrelated masses between the stars that form the multiple stellar systems is evident (Kroupa et al., 1993; Kroupa, 1995; Belloni et al., 2017, 2018). In the present work, we consider the simplest scenario that the mass of the primary and secondary star are independent concerning the formation of SNIa, that is, the probability of having a companion star of a certain mass is proportional to the number fraction of the stars having that mass and is independent of the accompanied SNIa progenitor star.

The SNIa production efficiency, $N_{\rm Ia}$, is calculated as

$$N_{\rm Ia}(\xi, \bar{\psi}_{\delta t}) = \frac{n_{3,8}(\xi)}{M_{0.08,150}(\xi)} \cdot B_{\rm bin}(\bar{\psi}_{\delta t}) \cdot \frac{n_{3,8}(\xi)}{n_{0.08,150}(\xi)} \cdot C_{\rm Ia}(\bar{\psi}_{\delta t}), \tag{2.11}$$

where $n_{3,8}$ and $n_{0.08,150}$ are the number of stars within the mass range given by their subscript (in the unit of $M_\odot$). Similarly, $M_{0.08,150}$ is the mass of stars in the mass range indicated by its subscript. Therefore the first and third terms on the r.h.s. depend on the IMF. $B_{\rm bin}$ denotes the binary fraction of stars within the mass range of 3 to 8 $M_\odot$ and $C_{\rm Ia}$ is the realisation probability of an SNIa explosion for the potential SNIa progenitor system. Both depend on environmental factors such as the stellar density and metallicity. The variation of the SNIa production efficiency has been suggested by, for example, Friedmann and Maoz (2018) and Freundlich and Maoz (2021) who find a significantly enhanced occurrence of SNIa in galaxy clusters (see Table 2.1). A more detailed interpretation and comprehensive discussion of the above equation is given in Yan et al. (2021), where this has been published for the first time.

Table 2.1: Observational estimations on the time-integrated number of SNIa per stellar mass formed. The estimations of the SNIa production efficiency are given in two groups, those targeted at galaxy clusters, and those obtained in volume-limited surveys and in field galaxies.

$N_{\rm Ia} \cdot 10^3$ $[M_\odot^{-1}]$	Reference
Volumetric and field galaxies	
2.3 ± 0.6	Maoz et al. (2011)
1.3 ± 0.15	Maoz et al. (2012)
0.485 ± 0.065	Perrett et al. (2012)
$0.43^{+0.04}_{-0.1}$	Graur and Maoz (2013)
$0.98^{+1.3}_{-0.76}$	Rodney et al. (2014)
1.3 ± 0.1	Maoz and Graur (2017)
1.6 ± 0.3	Maoz and Graur (2017)
2 ± 1	Heringer et al. (2019)
4^{+2}_{-1}	Heringer et al. (2019)
Galaxy clusters	
$4.4^{+1.5}_{-1}$	Maoz et al. (2010)
5.4 ± 2.3	Maoz and Graur (2017)
$3.1^{+1.1}_{-1.0}$	Freundlich and Maoz (2021)

Equation 2.11 is calibrated empirically. Assuming the average SFR of the local universe is $\psi_0 = 1 M_\odot/{\rm yr}$, which is a reasonable approximation. The value of $B_{\rm bin}(\psi_0) \cdot C_{\rm Ia}(\psi_0)$ is determined by the observed number of SNIa events in nearby stellar systems assuming they have the canonical gwIMF and a Galactic SFR of ψ_0. Following Maoz and Mannucci (2012), we set

$$n_{\rm Ia}(t = 10\ {\rm Gyr}, \xi_{\rm canonical}, \psi_0) = 0.0022/M_\odot, \tag{2.12}$$

where $\xi_{\rm canonical}$ denotes the canonical IMF (Kroupa 2001, i.e. Eq. 1.1 with $\alpha_1 = 1.3$ and $\alpha_2 = \alpha_3 = 2.3$).

In addition to the IMF variation effect, we define an SNIa realisation renormalisation parameter, $\kappa_{\rm Ia}(\bar{\psi}_{\delta t})$, to account for the environmental variation on

the SNIa production efficiency. $\kappa_{\rm Ia}$ represents the variation of the overall SNIa realisation parameter as a function of the galaxy-wide SFR,

$$\kappa_{\rm Ia}(\bar{\psi}_{\delta t}) = \frac{B_{\rm bin}(\bar{\psi}_{\delta t}) \cdot C_{\rm Ia}(\bar{\psi}_{\delta t})}{B_{\rm bin}(\psi_0) \cdot C_{\rm Ia}(\psi_0)}, \tag{2.13}$$

which allows the variable $B_{\rm bin}(\bar{\psi}_{\delta t}) \cdot C_{\rm Ia}(\bar{\psi}_{\delta t})$ to become larger in massive galaxies.

Through trial and error, we find that assuming

$$\kappa_{\rm Ia}(\bar{\psi}_{10^7{\rm yr}}) = 1.75 + 0.75 \cdot {\rm erf}[\log_{10}(\bar{\psi}_{10^7{\rm yr}}) \cdot 1.25 - 2], \tag{2.14}$$

where erf stands for the Gauss error function (Fig. 2.5), leads to a result that roughly fits the observed $\tau_{\rm SF,SPS}$–$M_{\rm dyn}$ relation suggested by McDermid et al. (2015).

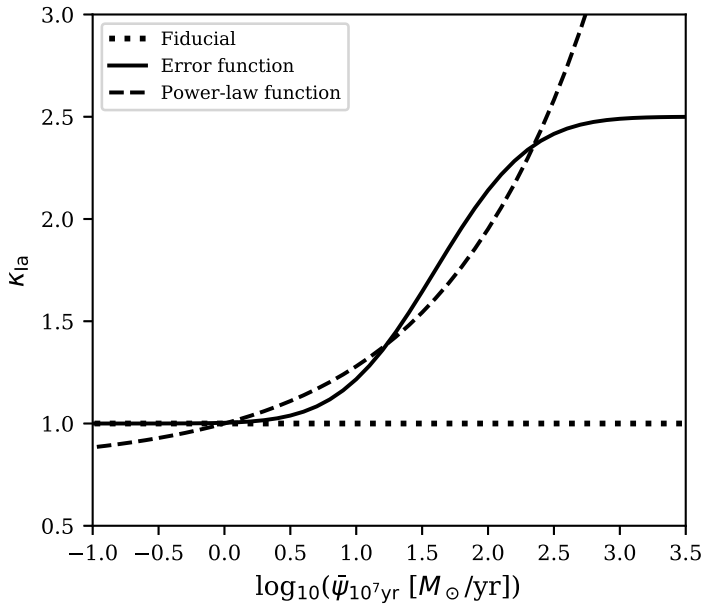

Figure 2.5: Figure taken from Yan et al. 2021. The SNIa realisation re-normalisation parameter, $\kappa_{\rm Ia}$ defined in Eq. 2.13, as a function of the galaxy-wide SFR, $\bar{\psi}_{10^7{\rm yr}}$. Different from the canonical assumption that the SNIa production efficiency is independent of the environment (the dotted line), we find that an increasing SNIa production efficiency for the higher-SFR galaxy described by Eq. 2.14 (solid line) best reproduces the observed ETGs. On the other hand, the dashed line, a power-law, has been excluded by our study (Yan et al., 2021).

Since the gwIMF predicted by the IGIMF theory is a function of the galaxy-wide SFR and metallicity (see Eq. 1.11), Fig. 2.6 shows how $n_{\rm Ia}(t = 10\ {\rm Gyr})$ changes as a function of these two parameters.

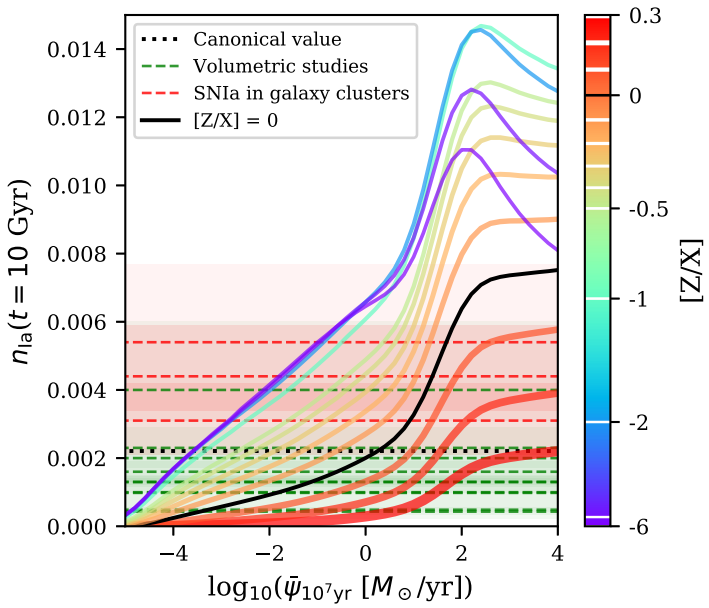

Figure 2.6: Figure taken from Yan et al. 2021. The number of SNIa per unit stellar mass integrated over 10 Gyr formed for the error function model (Eq. 2.14). The model assumes that the gwIMF is given by the IGIMF theory (Eq. 1.11) as a function of the galaxy-wide SFR, $\bar{\psi}_{10^7{\rm yr}}$, and metallicity, $[Z/X]$. The black line is the relation for $[Z/X] = 0$. Other lines with different colours represent different values of $[Z/X]$ as indicated by the white stripes on the colour map on the right: $[Z/X] = 0.3$, 0.2, 0.1, -0.1, -0.2, -0.3, -0.4, -0.5, -1, -2, -4, and -6. The black horizontal dotted line represents the canonical $n_{\rm Ia}(t = 10\ {\rm Gyr}, \xi_{\rm canonical})$ value of $0.0022/M_\odot$ (Maoz and Mannucci, 2012). The green and red horizontal dashed lines indicate observational constraints on $n_{\rm Ia}(t = 10\ {\rm Gyr})$ for SNIa surveys up to a certain redshift and in galaxy clusters, respectively. The shaded regions represent the uncertainty ranges of the horizontal dashed lines. Here we plot the observational values listed in Table 2.1, given $N_{\rm Ia} = n_{\rm Ia}(t = \infty) \approx n_{\rm Ia}(t = 10\ {\rm Gyr})$.

2.3 Galaxy evolution results

In this section, the calculation results of our GCE model applying the IGIMF theory, a log-normal SFH, and other assumptions described above are shown. The gwIMF is metallicity- and SFR-dependent. The initial gas mass is set to be the same as the sum of the initial stellar masses of all the stars ever formed throughout the galaxy formation history given in Fig. 2.1. The GCE is simulated for 13 Gyr.

2.3.1 Evolution of the TIgwIMF

Figure 2.7 shows the resulting time-integrated gwIMF (TIgwIMF) for the log-normal SFH shown in Fig. 2.1. The TIgwIMF changes gradually from top-heavy bottom-light (bottom lines) to top-light bottom-heavy (top lines).

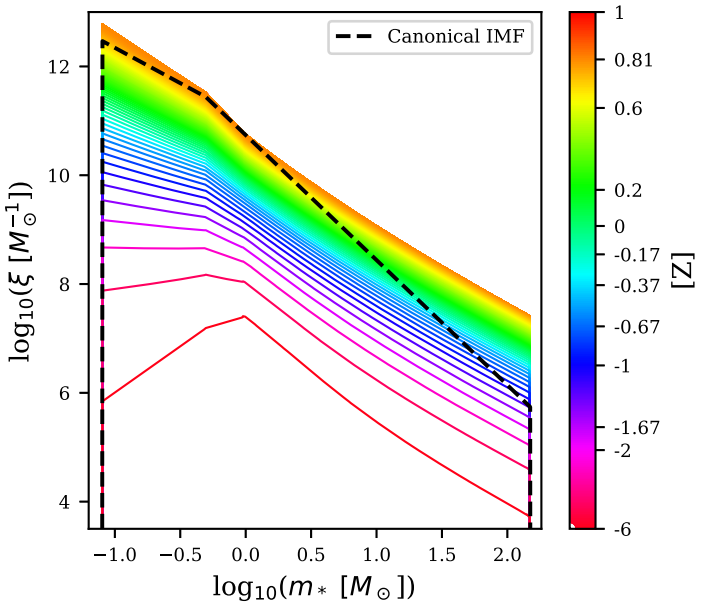

Figure 2.7: Figure taken from Yan et al. 2019b. Evolution of the TIgwIMF for a galaxy with the log-normal SFH shown in Fig. 2.1, where ξ is the total number of stars in the galaxy within a unit mass range. The assumed lowest and highest possible stellar mass is 0.08 $M_\odot$ and 150 $M_\odot$, respectively, following Yan et al. (2017). The solid lines represent the TIgwIMF after 10, 20, ..., and 1000 Myr since the beginning of the star formation (from bottom to top). The colour of the lines indicates the metallicity $[Z]$ in gas at the time. The colour-coding is the same as in Figs. 2.2 and 2.3. The dashed line is the canonical IMF given by Kroupa (2001), normalized to have the same ξ as the final TIgwIMF at $m = 1\ M_\odot$.

The gwIMF is top-heavy due to the high SFR during the early starburst (this being directly related to the rapid formation of supermassive black holes, Kroupa et al. 2020) and the gwIMF for the low-mass star evolves from bottom-light to bottom-heavy due to metal enrichment (according to Eq. 1.4). See a more in-depth discussion in Jeřábková et al. 2018).

For the old ETGs, the observations of the still living low-mass stars do not give information on the gwIMF slope for the massive stars. We demonstrated here that gwIMF can be both top-heavy and bottom-heavy. It would be incorrect to assume a single power-law IMF for such galaxies and to suggest a top-light gwIMF due to an observed bottom-heavy gwIMF.

2.3.2 Gas, living star, and stellar remnant mass evolution

The mass evolution of gas, stars, and stellar remnants are shown in Fig. 2.8. We assume no galactic outflow for this simulation which leads to a high gas-to-star mass ratio. This resembles the massive hot gas halo around the massive ETGs. For dwarf galaxies that do not have a deep galactic potential, gas outflow can be introduced which depletes the gas reservoir as we apply in Yan et al. (2020) (see Chapter 3.1 below).

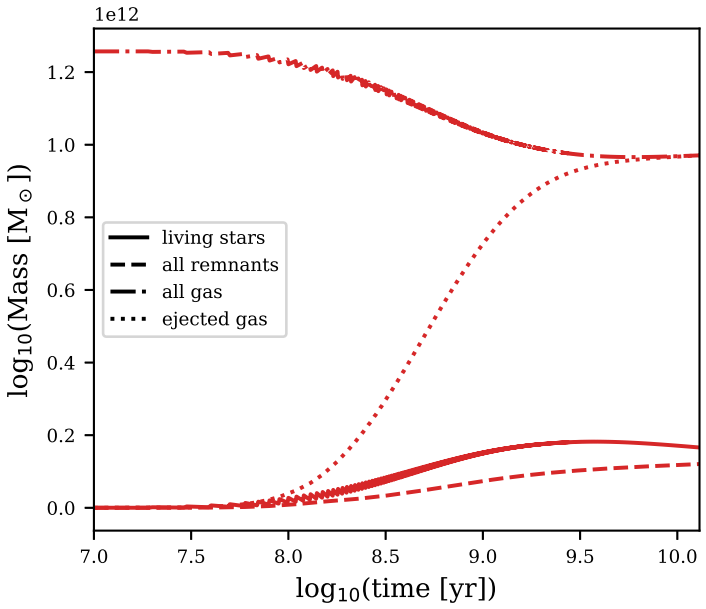

Figure 2.8: Mass evolution of gas, living stars, and stellar remnants as a function of time for the SFH shown in Fig. 2.1. The 'all gas' includes gas outside the galaxy that is constrained by the galactic potential. The final total gas mass at 13 Gyr equals the ejected gas mass only because the simulation is set such that the initial gas mass is the same value as the sum of the initial stellar masses of all the stars ever formed given by the assumed SFH (i.e. Fig. 2.1). Different from Fig. 2.7, here the mass values at 10, 19, 20, 29... Myr are also calculated and demonstrated in addition to the star formation times happen at 10, 20... Myr. The death of stars with a lifetime shorter than the star formation time step (10 Myr) causes the serrated shape of the lines (the serrated shape is more prominent in the logarithmic scale, e.g., Fig. 2.9 to 2.11). There is no colour code for the lines in this and the rest of the figures in this chapter.

The stellar remnant mass with the top-heavy gwIMF is significantly increased relative to a model assuming the canonical IMF. This leads to a higher dynamical mass-to-light ratio (cf. Cappellari et al. 2012, Li et al. 2017, and Oldham and Auger 2018) which we demonstrate in Chapter 3.2 below.

2.3.3 Number of supernovae

The time evolution of the number of SNIa and CCSN is plotted in Fig. 2.9. The high CCSN rate with about 1 CCSN event per day is a result of the assumed high SFR and top-heavy gwIMF, consistent with the observed CCSN rate for high-redshift galaxies (Labbé et al., 2013; Stark et al., 2015).

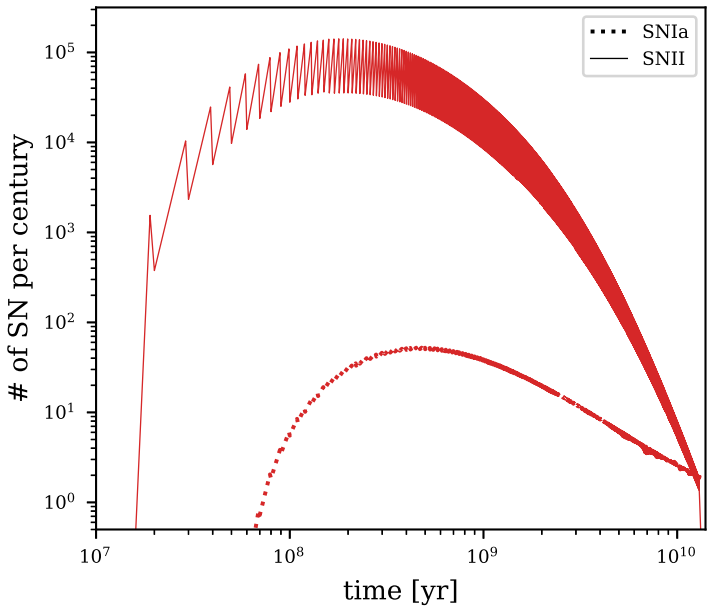

Figure 2.9: Figure taken from Yan et al. 2019b. Number of SNIa and CCSN per century as a function of time for the SFH shown in Fig. 2.1. The dotted line below and the solid line above are the rates for SNIa and CCSN, respectively. The serrated shape is caused by the simplification that all the stars formed in a 10 Myr star formation epoch have an identical age.

2.3.4 Element abundances

The mass- or luminosity-averaged $[Fe/H]$ and $[Mg/Fe]$ evolution for stars and gas are shown in Fig. 2.10 and 2.11, respectively. The stellar luminosity-weighted result approaches the gas-phase value during the star formation and then quickly falls back to the stellar mass-weighted value as the luminous massive stars die out on a hundred million year timescale.

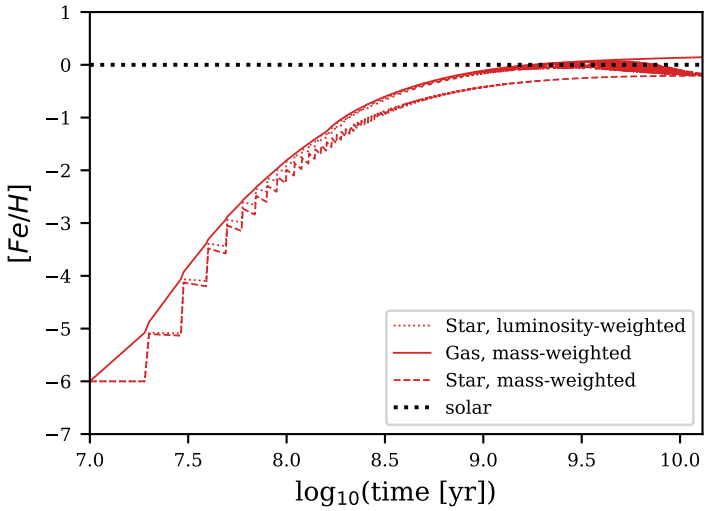

Figure 2.10: Figure taken from Yan et al. 2019b. Evolution of gas- and mass-averaged stellar $[Fe/H]$ for the SFH shown in Fig. 2.1. The solid, dashed, and dotted lines represent the value calculated for the gas phase, the mass averaged, and luminosity averaged (approximation, see text) values, respectively. The serrated shape is caused by our simplification that all the stars formed in a 10 Myr star formation epoch have an identical age.

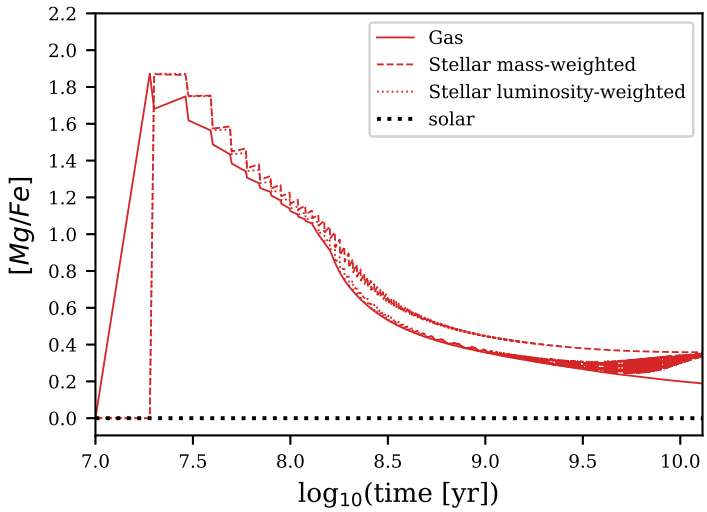

Figure 2.11: Same as Fig. 2.10, but for $[Mg/Fe]$.

Caveat: the calculation for the helium abundance here applies a simplified stellar total helium yield table that does not depend on the stellar initial helium abundance. This leads to a lower helium abundance than a more detailed calculation.

2.4 Outlook and Conclusion

GCE involves a large number of physical assumptions. Many of them are embodied implicitly in the GCE code. When applying the code to a new type of galaxy for the first time, it is likely that some of the implicit assumptions need to be adjusted. Such adjustments can only be done by someone who knows the code very well. In order to make the code easy to maintain and expandable, I plan to shift to a modular design of the code, with different physical assumptions easy to be exchanged. Currently, the GalIMF code is under further development under the following aspects:

1. The different parts of the code will be modulized to allow easier access and tailored modification. The star formation law is certainly more complicated than the current formulation assumed in the code and may depend on more environmental parameters other than local SFR and metallicity.

2. Allow more choices of the applied stellar yield table in order to allow tracing of more elements and isotopes. In particular, we would include the stellar yield table for better calculation of the helium abundance evolution and the yield of rotating stars. Theoretical studies suggest that stars with a high rotational speed (e.g. with an initial H-burning phase equatorial velocity of 300 km/s) may produce 10 or 100 times more metals for elements heavier than zinc (Limongi and Chieffi, 2018).

3. The code will be modified for faster and extensive calculations.

Our code will stay publicly available. It can be checked, questioned, and the results can be independently reproduced.

In this chapter, we describe the open-source GCE code, GalIMF. It is able to vary the gwIMF according to the star-forming environment at each time step, yielding the mass and chemical composition evolution of the galaxy. In particular, we considered the environmental and IMF variation effect on the SNIa production efficiency. This enables us to perform a comprehensive and detailed examination of the different IMF theories in GCE studies. Thus, results obtained for a high-mass starburst galaxy assuming the IGIMF theory demonstrates a strong modification of the element composition of the galaxy. We use the GalIMF code to explore the GCE of galaxies with different masses and SFHs in the following chapters.

For more details, we refer the reader to Yan et al. (2019b) and Yan et al. (2021) which are attached at the end of this dissertation.

3. Applications

3.1 Chemical evolution of dwarf galaxies

This section is based on the publication Yan, Jeřábková, and Kroupa (2021) with the title "Chemical evolution of ultra-faint dwarf galaxies in the self-consistently calculated integrated galactic IMF theory".

The nearby dwarf galaxies provide a unique opportunity to study their gwIMFs. Firstly, many of these low mass galaxies are formed with a short starburst, then the star formation stops due to a depletion of gas. This leaves a relatively simple stellar population with no recently formed younger stars. Not only the SPS is more reliable, but the SFH in the GCE model can also be greatly simplified. Secondly, there are a large number of them relative to massive galaxies, providing more close-by targets within which we can measure the abundances of single stars with high accuracy. This measurement is important as the abundances of stars formed at different times trace the gas abundance evolution of the galaxy. Fernández-Alvar et al. (2018) has suggested that the GCE model is able to deduce whether a difference in the abundance evolution is caused by a SFH or IMF variation. Indeed, the GCE of dwarf galaxies is different from the MW's. For instance, Theler et al. (2020) find that the stellar $[\alpha/Fe]$ values of Sextans, Sculptor, and Fornax dwarf galaxies bend and decrease at different $[Fe/H]$ values than in the MW. Minelli et al. (2021) find, in addition, that different α-elements behave differently as one would expect if the gwIMF varies because different elements are produced mainly by stars of different mass.

In Yan et al. (2020), we apply the IGIMF theory to the GCE modelling of one of the best-observed ultra-faint dwarf (UFD) satellite galaxies, Boötes I. We find that the $[\alpha/Fe]$–$[Fe/H]$ relation of Boötes I can be well reproduced if it has the average gas-depletion timescale of dwarf galaxies (Pflamm-Altenburg and Kroupa, 2009), challenging the idea that UFDs have a much longer gas-depletion timescale than dwarf galaxies. Remembering that when the galaxy stellar mass as an observable is known, the gas-depletion timescale determines the average SFR which then determines the gwIMF of the massive stars that affect the shape of the $[\alpha/Fe]$–$[Fe/H]$ relation. Therefore, the IGIMF theory suggesting a top-light IMF naturally accounts for the observed $[\alpha/Fe]$–$[Fe/H]$ relation of Boötes I.

The parameters applied in our GCE model are not fine-tuned to force a good fit. They are either inherited from previous studies or significantly constrained by independent sources or data. It is remarkable that the UFD Boötes I is so well described using the IGIMF theory. This confirms that the optimal sampling of ECMF and the IGIMF theory is most likely correct.

The gas-depletion timescales of galaxies are estimated by GCE studies and the conclusion depends on the assumed IMF. While the studies assuming the canonical IMF suggest a long gas-depletion timescale of the UFDs, our study assuming the IGIMF theory leads to a normal gas-depletion timescale which is, in fact, the same as the average gas-depletion timescale of dwarf galaxies (cf. Pflamm-Altenburg and Kroupa 2009).
When exploring a new IMF law, one must keep in mind that galactic properties such as the gas-depletion timescale determined previously from studies assuming the canonical IMF are no longer correct.

In addition, we find in Yan et al. (2020) that the GCE model can be used to constrain the IMF variation law of low-mass stars. Once the SFH and the gwIMF of the massive stars are determined by the $[\alpha/Fe]$–$[Fe/H]$ relation and, in addition, by an independent SPS study (Brown et al., 2014) of the galaxy, the mean stellar metallicity of the galaxy is affected by the gwIMF of the low-mass stars. Since the mean stellar metallicity is also deducible from SPS, the variation of the gwIMF of the low-mass stars can be constrained, that is, the parameter $\Delta\alpha$ in Eq. 1.4.

For more details, we refer the reader to Yan et al. (2020) which is attached at the end of this dissertation.

3.2 Evolution of ETGs with different masses

This section is based on the publication Yan, Jeřábková, and Kroupa (2019) with the title "The star formation timescale of elliptical galaxies - Fitting $[Mg/Fe]$ and total metallicity simultaneously" and Yan, Jeřábková, and Kroupa (2021) with the title "Downsizing revised: Longer star formation timescales for elliptical galaxies with an environment-dependent IMF and number of SNIa".

The SFH of a galaxy is not easy to determine when we can only look at the present-day snapshot of it, in particular for the galaxies that cannot be resolved and examined with a CMD of its stars. In this Chapter, we run the GCE calculation for ETGs and study how the newly implemented IGIMF theory affects our understanding of the formation history of ETGs.

The standard way to estimate the SFH, given the integrated galactic light, is to fit an artificially synthesized stellar population with a realistic age, metallicity, and mass distribution to the observed spectrum. This is the so-called stellar population synthesis (SPS) method. One problem of the SPS method is that the solution is not unique. The distribution of all three properties of the stellar population can be adjusted to fit the data. For example, a more fluctuating SFH instead of a smooth SFH (Furlanetto and Mirocha, 2021), a stellar population with some elements more abundant than usual, and a different IMF such as the one given by the IGIMF theory. All these factors affect the final estimation.

One of the important requirements, for the synthesized stellar population to be realistic, is that the age and metallicity distribution can be naturally reproduced by the GCE model. That is, the stellar population becomes more enriched as time passes.

A combination of SPS and GCE models to fulfil this requirement has been demonstrated recently by Bellstedt et al. (2020). Historically, the SPS method does not consider GCE and only estimates the average age and metal abundance of the stars. The formation time scale of the stars, SFT, is estimated on top of that using the α elements-to-iron peak elements ratio. This ratio is sensitive to the SFT because most of the two groups of elements are produced by different types of supernovae. α-elements are almost exclusively produced by CCSN over a short timescale, while about half of the iron-peak elements are continuously produced by thermonuclear supernovae long after the formation of the stellar population. With this method, the most famous "downsizing" relation of ETG formation is established by Thomas et al. (2005) and Thomas et al. (2010) with the result that more massive ETGs form at an earlier time with a shorter SFT. This conclusion revolutionized our understanding of how these galaxies form at the time when the standard cosmology model (LCDM) expected that more massive galaxies formed at the centre of massive dark matter halos (DMHs) as a result of the hierarchical merging of smaller DMHs and therefore should have formed later over longer timescales.

With the intention to introduce the IGIMF theory into the previous calculation done by Thomas, we first reproduced the previous "downsizing" relation in Yan et al. (2019a). We also improved the SFT estimation of the GCE method by considering the constraints of mean stellar metallicity in addition to the α elements-to-iron peak elements ratio. This is because the element ratio yields are different for stars with different metallicity.

We point out a few difficulties of the canonical "downsizing" scenario. Namely, the idea of shorting the SFT to reproduce the observed α-element enhancement only works in a simple GCE model where stellar ejections mix with environmental gas instantaneously, but does not work in a more realistic hydrodynamical model of galaxies. When considering the cooling and mixing of the gas, a non-negligible time is required for the stellar ejection to participate in the formation of a new generation of stars and increase the mean stellar metallicity. It happens that when the SFT is too short, the mean stellar metallicity of the galaxy does not have time to enrich to the observed value. Therefore, people struggle to fit both the α-element enhancement and mean stellar metallicity simultaneously as is demonstrated and explained in De Lucia et al. (2017) and Okamoto et al. (2017). The same intrinsic problem persists in Barber et al. (2018) and Pantoni et al. (2019). In addition, gravitational lensing observations of high-redshift quiescent galaxies find that the metal abundance and α-elements are enriched early on and that this cannot be explained by simple GCE models that vary only the SFT (Jafariyazani et al., 2020). We suggested that the IGIMF theory constitutes a natural solution to these difficulties.

In the follow-up paper, Yan et al. (2021, hereinafter Yan21), we perform the same SFT calculations but by introducing the environment-dependent IMF to this problem for the first time. We noted that there is no surprise if one manages to fit the same observational constraints with an arbitrarily adjusted IMF.

The point of our work is to test the independently and empirically constrained IGIMF theory to get a reliable insight into how the ETGs form. By doing this, we found out that the α-element production in the massive ETGs outperforms the iron-peak elements to a great extend, altering the SFT estimation significantly (Yan21, their Fig. 4). For the result to be consistent with other SFT constraints, such as using SPS methods (Yan21, their Fig. 7), it necessarily follows that the iron-element production is also elevated in these massive ETGs, most likely due to a higher production efficiency of SNIa in the high stellar density region of the high-SFR massive galaxies. We estimated how much the production efficiency of SNIa needs to rise as a function of galaxy mass (Yan21, their Fig. 5) and compared our estimation with the observational constraints given by direct SNIa number counts in field galaxies and in galaxy clusters (Yan21, their Table 1 and Fig. 6). As mentioned in Section 2.2.7, we find that our model nicely agrees with the theoretical expectation from the N-body simulations and the observational suggestion that the production efficiency of SNIa in higher density regions appears to be higher. This is exactly why the canonical IMF model cannot work as it would require a lower SNIa production efficiency for massive galaxies to better fit with the stellar abundance ratios, being inconsistent with the observations. Finally, we calculated the dynamical mass-to-light ratios (M/L) of the ETGs in our best-fit model and found them to naturally reproduce the observed M/L–galactic-mass relation (Yan21, their Fig. 10). The bottom-heavy gwIMF of massive ETGs in our model also agrees with recent observational suggestions (Yan21, their Fig. 9). Therefore, many observed ETG properties come together naturally and are straightforwardly explained, all are consequences of the application of the IGIMF theory to the monolithic collapse of post-Big Bang gas clouds.

For more details, we refer the reader to Yan et al. (2019a) and Yan et al. (2021) which are attached at the end of this dissertation.

Summary and conclusion

A systematic IMF variation is currently the simplest explanation to consistently account for the vast variety of anomalies observed for stellar populations on different scales and at different redshifts (Section 1.2). With the empirically calibrated IGIMF theory describing how the IMF varies (Yan et al., 2017) and the computational tool developed specifically for this study (Yan et al., 2019b), we are able to explore the effect of a realistic IMF variation scenario on the chemical evolution of different types of galaxies. From the dwarf galaxy with a stellar mass of only a few times 10^4 $M_\odot$ to the most massive monster galaxies with a dynamical mass of 10^{12} $M_\odot$, our GCE model adopting the IGIMF theory is able to explain the individual stellar chemical abundances inside the galaxy better than models that assume the IMF is invariant.

In Yan et al. (2020), it is shown that the IGIMF theory is able to naturally explain the element ratio of the dwarf galaxy Boötes I. According to our best-fit solution, we find that Boötes I is not unusual but follows the same gas-consumption process as other galaxies. This practice also allows us to put constraints on the low-mass IMF dependence on the metallicity for the first time. This is an important result because the IMF variation law of low-mass stars outside our Galaxy is difficult to constrain because the observed relation from old quiescent galaxies, where massive stars do not outshine the low-masses, is for the time-integrated present-day stellar mass function that is different from the varying IMF.

In Yan et al. (2019a) and Yan et al. (2021), we explain the scaling relation between the abundance ratios and galaxy mass which has not been understood in canonical models. Yan et al. (2019a) demonstrated the importance of considering stellar metallicity and α-element enhancement together when estimating the star formation timescale of a galaxy. The results show that the model adopting the canonical IMF does not give formation timescales that are consistent with independent constraints even if one allows a tuning of the stellar element yield table. Either the formation timescales for massive galaxies are too short or the formation timescales for the low-mass galaxies are too long. Following this work, Yan et al. (2021) shows that the IGIMF theory provides a natural solution to this problem. The more top-heavy galactic IMF of the massive and high-SFR galaxies produces a lot more α-elements at early times, modifying the estimated stellar formation timescales of these massive galaxies to longer values. In fact, the empirically calibrated IGIMF formulation predicts that too many α-elements should have been produced such that more iron-peak elements should also have been produced to result in the observed α element-to-iron peak element ratio. Therefore, we are able to use this constraint to estimate how the production efficiency of SNIa should change in a different environment.

We conclude that the realistic IMF variation can have a strong impact on the modelled GCE and our interpretation of galaxy observations. The estimated galaxy mass and formation timescales are different from the canonical model, which affects our understanding of how the universe evolves. The abnormal element abundances, if accounted by the IMF difference, no longer requires an adjustment of the stellar evolution model or the introduction of exotic stellar explosion scenarios. Therefore, the IMF variation, being the missing link between

the stars and the universe in many of today's astronomical studies, needs to be taken into consideration.

The future development of the field will require a significant amount of effort to further test and constrain the IMF variation formulation empirically in order to give an accurate and reliable description of how the IMF varies. Usage of different GCE codes with different advantages that make possible cross-checking are highly encouraged. Open-source codes or, at least, an extensively detailed description of the GCE method, should become the standard. Communication and collaborative effort are most valuable.

Bibliography

Fred C. Adams and Marco Fatuzzo. A Theory of the Initial Mass Function for Star Formation in Molecular Clouds. *ApJ*, 464:256, June 1996. doi: 10.1086/177318.

Fred C. Adams and Gregory Laughlin. Implications of White Dwarf Galactic Halos. *ApJ*, 468:586, September 1996. doi: 10.1086/177717.

S. S. Ali, R. De Propris, C. Chung, Steven Phillipps, and Malcolm Bremer. Evolution of the Ultraviolet Upturn at $0.3 < z < 1$: exploring helium rich stellar populations. *arXiv e-prints*, art. arXiv:2109.13935, September 2021.

E. Anders and N. Grevesse. Abundances of the elements - Meteoritic and solar. *Geochim. Cosmochim. Acta*, 53:197–214, January 1989. doi: 10.1016/0016-7037(89)90286-X.

Brett H. Andrews, David H. Weinberg, Ralph Schönrich, and Jennifer A. Johnson. Inflow, Outflow, Yields, and Stellar Population Mixing in Chemical Evolution Models. *ApJ*, 835(2):224, February 2017. doi: 10.3847/1538-4357/835/2/224.

Elaad Applebaum, Alyson M. Brooks, Thomas R. Quinn, and Charlotte R. Christensen. A stochastically sampled IMF alters the stellar content of simulated dwarf galaxies. *MNRAS*, 492(1):8–21, February 2020. doi: 10.1093/mnras/stz3331.

Matías Arrigoni, Scott C. Trager, Rachel S. Somerville, and Brad K. Gibson. Galactic chemical evolution in hierarchical formation models - I. Early-type galaxies in the local Universe. *MNRAS*, 402(1):173–190, February 2010. doi: 10.1111/j.1365-2966.2009.15924.x.

M. Asplund, N. Grevesse, A. J. Sauval, and P. Scott. The Chemical Composition of the Sun. *ARA&A*, 47:481–522, September 2009. doi: 10.1146/annurev.astro.46.060407.145222.

M. W. Auger, T. Treu, R. Gavazzi, A. S. Bolton, L. V. E. Koopmans, and P. J. Marshall. Dark Matter Contraction and the Stellar Content of Massive Early-type Galaxies: Disfavoring "Light" Initial Mass Functions. *ApJ*, 721:L163–L167, October 2010. doi: 10.1088/2041-8205/721/2/L163.

S. Banerjee and P. Kroupa. On the true shape of the upper end of the stellar initial mass function. The case of R136. *A&A*, 547:A23, November 2012. doi: 10.1051/0004-6361/201218972.

Sambaran Banerjee and Pavel Kroupa. Formation of Very Young Massive Clusters and Implications for Globular Clusters. In Steven Stahler, editor, *The Birth of Star Clusters*, volume 424, page 143, January 2018. doi: 10.1007/978-3-319-22801-3_6.

Christopher Barber, Robert A. Crain, and Joop Schaye. Calibrated, cosmological hydrodynamical simulations with variable IMFs I: method and effect on global galaxy scaling relations. *MNRAS*, 479(4):5448–5473, Oct 2018. doi: 10.1093/mnras/sty1826.

Matteo Barnabè, Chiara Spiniello, Léon V. E. Koopmans, Scott C. Trager, Oliver Czoske, and Tommaso Treu. A low-mass cut-off near the hydrogen burning limit for Salpeter-like initial mass functions in early-type galaxies. *MNRAS*, 436(1):253–258, November 2013. doi: 10.1093/mnras/stt1727.

Nate Bastian, Kevin R. Covey, and Michael R. Meyer. A Universal Stellar Initial Mass Function? A Critical Look at Variations. *ARA&A*, 48:339–389, September 2010. doi: 10.1146/annurev-astro-082708-101642.

Matthew R. Bate. The statistical properties of stars and their dependence on metallicity. *MNRAS*, 484(2):2341–2361, April 2019. doi: 10.1093/mnras/stz103.

H. Baumgardt and P. Kroupa. A comprehensive set of simulations studying the influence of gas expulsion on star cluster evolution. *MNRAS*, 380(4):1589–1598, October 2007. doi: 10.1111/j.1365-2966.2007.12209.x.

Holger Baumgardt and Junichiro Makino. Dynamical evolution of star clusters in tidal fields. *MNRAS*, 340(1):227–246, March 2003. doi: 10.1046/j.1365-8711.2003.06286.x.

Diogo Belloni, Abbas Askar, Mirek Giersz, Pavel Kroupa, and Helio J. Rocha-Pinto. On the initial binary population for star cluster simulations. *MNRAS*, 471(3):2812–2828, November 2017. doi: 10.1093/mnras/stx1763.

Diogo Belloni, Pavel Kroupa, Helio J. Rocha-Pinto, and Mirek Giersz. Dynamical equivalence, the origin of the Galactic field stellar and binary population, and the initial radius-mass relation of embedded clusters. *MNRAS*, 474(3):3740–3745, March 2018. doi: 10.1093/mnras/stx3034.

Sabine Bellstedt, Aaron S. G. Robotham, Simon P. Driver, Jessica E. Thorne, Luke J. M. Davies, Claudia del P. Lagos, Adam R. H. Stevens, Edward N. Taylor, Ivan K. Baldry, Amanda J. Moffett, Andrew M. Hopkins, and Steven Phillipps. Galaxy And Mass Assembly (GAMA): a forensic SED reconstruction of the cosmic star formation history and metallicity evolution by galaxy type. *MNRAS*, 498(4):5581–5603, November 2020. doi: 10.1093/mnras/staa2620.

Thomas M. Brown, Jason Tumlinson, Marla Geha, Joshua D. Simon, Luis C. Vargas, Don A. VandenBerg, Evan N. Kirby, Jason S. Kalirai, Roberto J. Avila, Mario Gennaro, Henry C. Ferguson, Ricardo R. Muñoz, Puragra Guhathakurta, and Alvio Renzini. The Quenching of the Ultra-faint Dwarf Galaxies in the Reionization Era. *ApJ*, 796(2):91, December 2014. doi: 10.1088/0004-637X/796/2/91.

S. M. Bruzzese, G. R. Meurer, C. D. P. Lagos, E. C. Elson, J. K. Werk, John P. Blakeslee, and H. Ford. The initial mass function and star formation law in the outer disc of NGC 2915. *MNRAS*, 447(1):618–635, February 2015. doi: 10.1093/mnras/stu2461.

S. M. Bruzzese, David A. Thilker, G. R. Meurer, Luciana Bianchi, A. B. Watts, A. M. N. Ferguson, A. Gil de Paz, B. Madore, D. Christopher Martin, and

R. Michael Rich. The initial mass function in the extended ultraviolet disc of M83. *MNRAS*, 491(2):2366–2390, January 2020. doi: 10.1093/mnras/stz3151.

R. Cañameras, N. P. H. Nesvadba, R. Kneissl, M. Limousin, R. Gavazzi, D. Scott, H. Dole, B. Frye, S. Koenig, E. Le Floc'h, and I. Oteo. Planck's dusty GEMS. III. A massive lensing galaxy with a bottom-heavy stellar initial mass function at z = 1.5. *A&A*, 600:L3, April 2017. doi: 10.1051/0004-6361/201630359.

M. Cappellari, R. M. McDermid, K. Alatalo, L. Blitz, M. Bois, F. Bournaud, M. Bureau, A. F. Crocker, R. L. Davies, T. A. Davis, P. T. de Zeeuw, P.-A. Duc, E. Emsellem, S. Khochfar, D. Krajnović, H. Kuntschner, P.-Y. Lablanche, R. Morganti, T. Naab, T. Oosterloo, M. Sarzi, N. Scott, P. Serra, A.-M. Weijmans, and L. M. Young. Systematic variation of the stellar initial mass function in early-type galaxies. *Nature*, 484:485–488, April 2012. doi: 10.1038/nature10972.

Michele Cappellari, Eric Emsellem, Davor Krajnović, Richard M. McDermid, Nicholas Scott, G. A. Verdoes Kleijn, Lisa M. Young, Katherine Alatalo, R. Bacon, Leo Blitz, Maxime Bois, Frédéric Bournaud, M. Bureau, Roger L. Davies, Timothy A. Davis, P. T. de Zeeuw, Pierre-Alain Duc, Sadegh Khochfar, Harald Kuntschner, Pierre-Yves Lablanche, Raffaella Morganti, Thorsten Naab, Tom Oosterloo, Marc Sarzi, Paolo Serra, and Anne-Marie Weijmans. The ATLAS^{3D} project - I. A volume-limited sample of 260 nearby early-type galaxies: science goals and selection criteria. *MNRAS*, 413(2):813–836, May 2011. doi: 10.1111/j.1365-2966.2010.18174.x.

L. Carigi and X. Hernandez. Chemical consequences of low star formation rates: stochastically sampling the initial mass function. *MNRAS*, 390(2):582–594, October 2008. doi: 10.1111/j.1365-2966.2008.13743.x.

M. Cerviño, C. Román-Zúñiga, V. Luridiana, A. Bayo, N. Sánchez, and E. Pérez. Crucial aspects of the initial mass function. I. The statistical correlation between the total mass of an ensemble of stars and its most massive star. *A&A*, 553:A31, May 2013. doi: 10.1051/0004-6361/201219504.

Gilles Chabrier. Galactic Stellar and Substellar Initial Mass Function. *PASP*, 115(809):763–795, July 2003. doi: 10.1086/376392.

Gilles Chabrier, Patrick Hennebelle, and Stéphane Charlot. Variations of the Stellar Initial Mass Function in the Progenitors of Massive Early-type Galaxies and in Extreme Starburst Environments. *ApJ*, 796(2):75, December 2014. doi: 10.1088/0004-637X/796/2/75.

Laura Chomiuk and Matthew S. Povich. Toward a Unification of Star Formation Rate Determinations in the Milky Way and Other Galaxies. *AJ*, 142(6):197, December 2011. doi: 10.1088/0004-6256/142/6/197.

L. Ciesla, A. Boselli, D. Elbaz, S. Boissier, V. Buat, V. Charmandaris, C. Schreiber, M. Béthermin, M. Baes, M. Boquien, I. De Looze, J. A. Fernández-Ontiveros, C. Pappalardo, L. Spinoglio, and S. Viaene. The imprint of rapid star formation quenching on the spectral energy distributions of galaxies. *A&A*, 585:A43, January 2016. doi: 10.1051/0004-6361/201527107.

L. Ciesla, D. Elbaz, and J. Fensch. The SFR-M_* main sequence archetypal star-formation history and analytical models. *A&A*, 608:A41, December 2017. doi: 10.1051/0004-6361/201731036.

Bart Clauwens, Joop Schaye, and Marijn Franx. Implications of a variable IMF for the interpretation of observations of galaxy populations. *MNRAS*, 462(3): 2832–2846, November 2016. doi: 10.1093/mnras/stw1808.

C. Conroy and P. G. van Dokkum. The Stellar Initial Mass Function in Early-type Galaxies From Absorption Line Spectroscopy. II. Results. *ApJ*, 760:71, November 2012. doi: 10.1088/0004-637X/760/1/71.

C. Conroy, G. J. Graves, and P. G. van Dokkum. Early-type Galaxy Archeology: Ages, Abundance Ratios, and Effective Temperatures from Full-spectrum Fitting. *ApJ*, 780:33, January 2014. doi: 10.1088/0004-637X/780/1/33.

Benoit Côté, Christian Ritter, Brian W. O'Shea, Falk Herwig, Marco Pignatari, Samuel Jones, and Chris L. Fryer. Uncertainties in Galactic Chemical Evolution Models. *ApJ*, 824(2):82, June 2016. doi: 10.3847/0004-637X/824/2/82.

Benoit Côté, Brian W. O'Shea, Christian Ritter, Falk Herwig, and Kim A. Venn. The Impact of Modeling Assumptions in Galactic Chemical Evolution Models. *ApJ*, 835(2):128, February 2017. doi: 10.3847/1538-4357/835/2/128.

D. A. Coulter, B. D. Lehmer, R. T. Eufrasio, A. Kundu, T. Maccarone, M. Peacock, A. E. Hornschemeier, A. Basu-Zych, A. H. Gonzalez, C. Maraston, and S. E. Zepf. Testing the Universality of the Stellar IMF with Chandra and HST. *ApJ*, 835(2):183, February 2017. doi: 10.3847/1538-4357/835/2/183.

R. H. Cyburt, B. D. Fields, K. A. Olive, and T.-H. Yeh. Big bang nucleosynthesis: Present status. *Reviews of Modern Physics*, 88(1):015004, January 2016. doi: 10.1103/RevModPhys.88.015004.

R. L. da Silva, M. Fumagalli, and M. Krumholz. SLUG – Stochastically Lighting Up Galaxies. I. Methods and Validating Tests. *ApJ*, 745:145, February 2012. doi: 10.1088/0004-637X/745/2/145.

J. Dabringhausen. Simple interpolation functions for the galaxy-wide stellar initial mass function and its effects in early-type galaxies. *MNRAS*, 490(1):848–867, Nov 2019. doi: 10.1093/mnras/stz2562.

J. Dabringhausen, M. Hilker, and P. Kroupa. From star clusters to dwarf galaxies: the properties of dynamically hot stellar systems. *MNRAS*, 386:864–886, May 2008. doi: 10.1111/j.1365-2966.2008.13065.x.

J. Dabringhausen, P. Kroupa, and H. Baumgardt. A top-heavy stellar initial mass function in starbursts as an explanation for the high mass-to-light ratios of ultra-compact dwarf galaxies. *MNRAS*, 394:1529–1543, April 2009. doi: 10.1111/j.1365-2966.2009.14425.x.

J. Dabringhausen, M. Fellhauer, and P. Kroupa. Mass loss and expansion of ultra compact dwarf galaxies through gas expulsion and stellar evolution for

top-heavy stellar initial mass functions. *MNRAS*, 403:1054–1071, April 2010. doi: 10.1111/j.1365-2966.2009.16189.x.

J. Dabringhausen, P. Kroupa, J. Pflamm-Altenburg, and S. Mieske. Low-mass X-Ray Binaries Indicate a Top-heavy Stellar Initial Mass Function in Ultra-compact Dwarf Galaxies. *ApJ*, 747:72, March 2012. doi: 10.1088/0004-637X/747/1/72.

G. De Lucia, F. Fontanot, and M. Hirschmann. AGN feedback and the origin of the α enhancement in early-type galaxies - insights from the GAEA model. *MNRAS*, 466:L88–L92, March 2017. doi: 10.1093/mnrasl/slw242.

S. Dib, J. Kim, and M. Shadmehri. The origin of the Arches stellar cluster mass function. *MNRAS*, 381:L40–L44, October 2007. doi: 10.1111/j.1745-3933.2007.00362.x.

K. Duncan, C. J. Conselice, A. Mortlock, W. G. Hartley, Y. Guo, H. C. Ferguson, R. Davé, Y. Lu, J. Ownsworth, M. L. N. Ashby, A. Dekel, M. Dickinson, S. Faber, M. Giavalisco, N. Grogin, D. Kocevski, A. Koekemoer, R. S. Somerville, and C. E. White. The mass evolution of the first galaxies: stellar mass functions and star formation rates at 4 ¡ z ¡ 7 in the CANDELS GOODS-South field. *MNRAS*, 444(3):2960–2984, November 2014. doi: 10.1093/mnras/stu1622.

N. Duric. *Advanced astrophysics*. Cambridge University Press, 2004.

B. G. Elmegreen. Variability in the stellar initial mass function at low and high mass: three-component IMF models. *MNRAS*, 354:367–374, October 2004. doi: 10.1111/j.1365-2966.2004.08187.x.

Andrew Emerick, Greg L. Bryan, and Mordecai-Mark Mac Low. Simulating an isolated dwarf galaxy with multichannel feedback and chemical yields from individual stars. *MNRAS*, 482(1):1304–1329, January 2019. doi: 10.1093/mnras/sty2689.

Eric Emsellem, Remco F. J. van der Burg, Jérémy Fensch, Tereza Jeřábková, Anita Zanella, Adriano Agnello, Michael Hilker, Oliver Müller, Marina Rejkuba, Pierre-Alain Duc, Patrick Durrell, Rebecca Habas, Federico Lelli, Sungsoon Lim, Francine R. Marleau, Eric Peng, and Rubén Sánchez-Janssen. The ultra-diffuse galaxy NGC 1052-DF2 with MUSE. I. Kinematics of the stellar body. *A&A*, 625:A76, May 2019. doi: 10.1051/0004-6361/201834909.

Christoph Federrath. On the universality of interstellar filaments: theory meets simulations and observations. *MNRAS*, 457(1):375–388, March 2016. doi: 10.1093/mnras/stv2880.

Jérémy Fensch, Remco F. J. van der Burg, Tereza Jeřábková, Eric Emsellem, Anita Zanella, Adriano Agnello, Michael Hilker, Oliver Müller, Marina Rejkuba, Pierre-Alain Duc, Patrick Durrell, Rebecca Habas, Sungsoon Lim, Francine R. Marleau, Eric W. Peng, and Rubén Sánchez Janssen. The ultra-diffuse galaxy NGC 1052-DF2 with MUSE. II. The population of DF2:

stars, clusters, and planetary nebulae. *A&A*, 625:A77, May 2019. doi: 10.1051/0004-6361/201834911.

Emma Fernández-Alvar, Leticia Carigi, William J. Schuster, Christian R. Hayes, Nancy Ávila-Vergara, Steve R. Majewski, Carlos Allende Prieto, Timothy C. Beers, Sebastián F. Sánchez, Olga Zamora, Domingo Aníbal García-Hernández, Baitian Tang, José G. Fernández-Trincado, Patricia Tissera, Douglas Geisler, and Sandro Villanova. Disentangling the Galactic Halo with APOGEE. II. Chemical and Star Formation Histories for the Two Distinct Populations. *ApJ*, 852(1):50, January 2018. doi: 10.3847/1538-4357/aa9ced.

I. Ferreras, F. La Barbera, I. G. de la Rosa, A. Vazdekis, R. R. de Carvalho, J. Falcón-Barroso, and E. Ricciardelli. Systematic variation of the stellar initial mass function with velocity dispersion in early-type galaxies. *MNRAS*, 429: L15–L19, February 2013. doi: 10.1093/mnrasl/sls014.

I. Ferreras, C. Weidner, A. Vazdekis, and F. La Barbera. Further evidence for a time-dependent initial mass function in massive early-type galaxies. *MNRAS*, 448:L82–L86, March 2015. doi: 10.1093/mnrasl/slv003.

F. Fontanot, G. De Lucia, M. Hirschmann, G. Bruzual, S. Charlot, and S. Zibetti. Variations of the stellar initial mass function in semi-analytical models: implications for the mass assembly and the chemical enrichment of galaxies in the GAEA model. *MNRAS*, 464:3812–3824, February 2017. doi: 10.1093/mnras/stw2612.

Fabio Fontanot. Variations of the initial mass function in semi-analytical models. *MNRAS*, 442(4):3138–3146, Aug 2014. doi: 10.1093/mnras/stu1078.

Fabio Fontanot, Francesco La Barbera, Gabriella De Lucia, Anna Pasquali, and Alexandre Vazdekis. On the shape and evolution of a cosmic-ray-regulated galaxy-wide stellar initial mass function. *MNRAS*, 479(4):5678–5685, October 2018. doi: 10.1093/mnras/sty1768.

Jonathan Freundlich and Dan Maoz. The delay time distribution of Type-Ia supernovae in galaxy clusters: the impact of extended star-formation histories. *MNRAS*, 502(4):5882–5895, April 2021. doi: 10.1093/mnras/stab493.

Matan Friedmann and Dan Maoz. The rate of Type-Ia supernovae in galaxy clusters and the delay-time distribution out to redshift 1.75. *MNRAS*, 479(3): 3563–3581, September 2018. doi: 10.1093/mnras/sty1664.

Michele Fumagalli, Robert L. da Silva, and Mark R. Krumholz. Stochastic Star Formation and a (Nearly) Uniform Stellar Initial Mass Function. *ApJ*, 741(2): L26, November 2011. doi: 10.1088/2041-8205/741/2/L26.

Steven R. Furlanetto and Jordan Mirocha. Bursty star formation during the Cosmic Dawn driven by delayed stellar feedback. *arXiv e-prints*, art. arXiv:2109.04488, September 2021.

I. D. Gargiulo, S. A. Cora, N. D. Padilla, A. M. Muñoz Arancibia, A. N. Ruiz, A. A. Orsi, T. E. Tecce, C. Weidner, and G. Bruzual. Chemoarchaeological downsizing in a hierarchical universe: impact of a top-heavy IGIMF. *MNRAS*, 446:3820–3841, February 2015. doi: 10.1093/mnras/stu2272.

Simona Ghizzardi, Silvano Molendi, Remco van der Burg, Sabrina De Grandi, Iacopo Bartalucci, Fabio Gastaldello, Mariachiara Rossetti, Veronica Biffi, Stefano Borgani, Dominique Eckert, Stefano Ettori, Massimo Gaspari, Vittorio Ghirardini, and Elena Rasia. Iron in X-COP: Tracing enrichment in cluster outskirts with high accuracy abundance profiles. *A&A*, 646:A92, February 2021. doi: 10.1051/0004-6361/202038501.

B. K. Gibson, M. Loewenstein, and R. F. Mushotzky. Supernovae Types Ia/II and intracluster medium enrichment. *MNRAS*, 290:623–628, October 1997. doi: 10.1093/mnras/290.4.623.

M. Gieles, S. S. Larsen, N. Bastian, and I. T. Stein. The luminosity function of young star clusters: implications for the maximum mass and luminosity of clusters. *A&A*, 450(1):129–145, April 2006. doi: 10.1051/0004-6361:20053589.

Valentino González, Ivo Labbé, Rychard J. Bouwens, Garth Illingworth, Marijn Franx, and Mariska Kriek. Evolution of Galaxy Stellar Mass Functions, Mass Densities, and Mass-to-light Ratios from z ~7 to z ~4. *ApJ*, 735(2):L34, July 2011. doi: 10.1088/2041-8205/735/2/L34.

Or Graur and Dan Maoz. Discovery of 90 Type Ia supernovae among 700 000 Sloan spectra: the Type Ia supernova rate versus galaxy mass and star formation rate at redshift ∼0.1. *MNRAS*, 430(3):1746–1763, April 2013. doi: 10.1093/mnras/sts718.

M. L. P. Gunawardhana, A. M. Hopkins, R. G. Sharp, S. Brough, E. Taylor, J. Bland-Hawthorn, C. Maraston, R. J. Tuffs, C. C. Popescu, D. Wijesinghe, D. H. Jones, S. Croom, E. Sadler, S. Wilkins, S. P. Driver, J. Liske, P. Norberg, I. K. Baldry, S. P. Bamford, J. Loveday, J. A. Peacock, A. S. G. Robotham, D. B. Zucker, Q. A. Parker, C. J. Conselice, E. Cameron, C. S. Frenk, D. T. Hill, L. S. Kelvin, K. Kuijken, B. F. Madore, B. Nichol, H. R. Parkinson, K. A. Pimbblet, M. Prescott, W. J. Sutherland, D. Thomas, and E. van Kampen. Galaxy and Mass Assembly (GAMA): the star formation rate dependence of the stellar initial mass function. *MNRAS*, 415:1647–1662, August 2011. doi: 10.1111/j.1365-2966.2011.18800.x.

Dávid Guszejnov, Michael Y. Grudić, Philip F. Hopkins, Stella S. R. Offner, and Claude-André Faucher-Giguère. STARFORGE: the effects of protostellar outflows on the IMF. *MNRAS*, 502(3):3646–3663, April 2021. doi: 10.1093/mnras/stab278.

M. R. Haas and P. Anders. Variations in integrated galactic initial mass functions due to sampling method and cluster mass function. *A&A*, 512:A79, March 2010. doi: 10.1051/0004-6361/200912967.

A. Hacar, M. Tafalla, and J. Alves. Fibers in the NGC 1333 proto-cluster. *A&A*, 606:A123, October 2017. doi: 10.1051/0004-6361/201630348.

A. Hacar, M. Tafalla, J. Forbrich, J. Alves, S. Meingast, J. Grossschedl, and P. S. Teixeira. An ALMA study of the Orion Integral Filament. I. Evidence for narrow fibers in a massive cloud. *A&A*, 610:A77, March 2018. doi: 10.1051/0004-6361/201731894.

Hosein Haghi, Pouria Khalaj, Akram Hasani Zonoozi, and Pavel Kroupa. A Possible Solution for the M/L-[Fe/H] Relation of Globular Clusters in M31. II. The Age-Metallicity Relation. *ApJ*, 839(1):60, April 2017. doi: 10.3847/1538-4357/aa6719.

E. Heringer, C. Pritchet, and M. H. van Kerkwijk. The Delay Times of Type Ia Supernova. *ApJ*, 882(1):52, September 2019. doi: 10.3847/1538-4357/ab32dd.

A. M. Hopkins. The Dawes Review 8: Measuring the Stellar Initial Mass Function. *PASA*, 35, November 2018. doi: 10.1017/pasa.2018.29.

Philip F. Hopkins. Variations in the stellar CMF and IMF: from bottom to top. *MNRAS*, 433(1):170–177, July 2013. doi: 10.1093/mnras/stt713.

E. A. Hoversten and K. Glazebrook. Evidence for a Nonuniversal Stellar Initial Mass Function from the Integrated Properties of SDSS Galaxies. *ApJ*, 675: 163–187, March 2008. doi: 10.1086/524095.

Chia-Yu Hu, Thorsten Naab, Simon C. O. Glover, Stefanie Walch, and Paul C. Clark. Variable interstellar radiation fields in simulated dwarf galaxies: supernovae versus photoelectric heating. *MNRAS*, 471(2):2151–2173, October 2017. doi: 10.1093/mnras/stx1773.

Marziye Jafariyazani, Andrew B. Newman, Bahram Mobasher, Sirio Belli, Richard S. Ellis, and Shannon G. Patel. Resolved Multi-element Stellar Chemical Abundances in the Brightest Quiescent Galaxy at z $\sim$ 2. *ApJ*, 897(2):L42, July 2020. doi: 10.3847/2041-8213/aba11c.

T. Jeřábková, A. Hasani Zonoozi, P. Kroupa, G. Beccari, Z. Yan, A. Vazdekis, and Z.-Y. Zhang. Impact of metallicity and star formation rate on the time-dependent, galaxy-wide stellar initial mass function. *A&A*, 620:A39, November 2018. doi: 10.1051/0004-6361/201833055.

Amanda I. Karakas and Luke J. Shingles. The effect of enhanced helium abundances on the AGB-supernove mass transition. *Mem. Soc. Astron. Italiana*, 88:244, January 2017.

Jr. Kennicutt, Robert C. Overview: The Initial Mass Function in Galaxies. In Gary Gilmore and Debbie Howell, editors, *The Stellar Initial Mass Function (38th Herstmonceux Conference)*, volume 142 of *Astronomical Society of the Pacific Conference Series*, page 1, January 1998.

Helen Kirk and Philip C. Myers. Variations in the Mass Functions of Clustered and Isolated Young Stellar Objects. *ApJ*, 745(2):131, February 2012. doi: 10.1088/0004-637X/745/2/131.

R. S. Klessen and P. Hennebelle. Accretion-driven turbulence as universal process: galaxies, molecular clouds, and protostellar disks. *A&A*, 520:A17, September 2010. doi: 10.1051/0004-6361/200913780.

Chiaki Kobayashi, Hideyuki Umeda, Ken'ichi Nomoto, Nozomu Tominaga, and Takuya Ohkubo. Galactic Chemical Evolution: Carbon through Zinc. *ApJ*, 653(2):1145–1171, December 2006. doi: 10.1086/508914.

Chiaki Kobayashi, Amanda I. Karakas, and Maria Lugaro. The Origin of Elements from Carbon to Uranium. *ApJ*, 900(2):179, September 2020. doi: 10.3847/1538-4357/abae65.

P. Kroupa. On the variation of the initial mass function. *MNRAS*, 322:231–246, April 2001. doi: 10.1046/j.1365-8711.2001.04022.x.

P. Kroupa. The Initial Mass Function of Stars: Evidence for Uniformity in Variable Systems. *Science*, 295:82–91, January 2002. doi: 10.1126/science.1067524.

P. Kroupa. The Fundamental Building Blocks of Galaxies. In C. Turon, K. S. O'Flaherty, and M. A. C. Perryman, editors, *The Three-Dimensional Universe with Gaia*, volume 576 of *ESA Special Publication*, page 629, January 2005.

P. Kroupa. Galaxies as simple dynamical systems: observational data disfavor dark matter and stochastic star formation. *Canadian Journal of Physics*, 93:169–202, February 2015. doi: 10.1139/cjp-2014-0179.

P. Kroupa and C. Weidner. Galactic-Field Initial Mass Functions of Massive Stars. *ApJ*, 598:1076–1078, December 2003. doi: 10.1086/379105.

P. Kroupa, C. A. Tout, and G. Gilmore. The distribution of low-mass stars in the Galactic disc. *MNRAS*, 262:545–587, June 1993. doi: 10.1093/mnras/262.3.545.

P. Kroupa, C. Weidner, J. Pflamm-Altenburg, I. Thies, J. Dabringhausen, M. Marks, and T. Maschberger. *The Stellar and Sub-Stellar Initial Mass Function of Simple and Composite Populations*, page 115. Springer Science+Business Media Dordrecht, 2013. doi: 10.1007/978-94-007-5612-0_4.

Pavel Kroupa. The dynamical properties of stellar systems in the Galactic disc. *MNRAS*, 277:1507, December 1995. doi: 10.1093/mnras/277.4.1507.

Pavel Kroupa and Tereza Jerabkova. The Salpeter IMF and its descendants. *Nature Astronomy*, 3:482–484, June 2019. doi: 10.1038/s41550-019-0793-0.

Pavel Kroupa, Ladislav Subr, Tereza Jerabkova, and Long Wang. Very high redshift quasars and the rapid emergence of supermassive black holes. *MNRAS*, 498(4):5652–5683, November 2020. doi: 10.1093/mnras/staa2276.

F. La Barbera, I. Ferreras, A. Vazdekis, I. G. de la Rosa, R. R. de Carvalho, M. Trevisan, J. Falcón-Barroso, and E. Ricciardelli. SPIDER VIII - constraints on the stellar initial mass function of early-type galaxies from a variety of spectral features. *MNRAS*, 433(4):3017–3047, August 2013. doi: 10.1093/mnras/stt943.

F. La Barbera, I. Ferreras, and A. Vazdekis. The initial mass function of early-type galaxies: no correlation with [Mg/Fe]. *MNRAS*, 449:L137–L141, April 2015. doi: 10.1093/mnrasl/slv029.

F. La Barbera, A. Vazdekis, I. Ferreras, A. Pasquali, C. Allende Prieto, B. Röck, D. S. Aguado, and R. F. Peletier. IMF and [Na/Fe] abundance ratios from optical and NIR spectral features in early-type galaxies. *MNRAS*, 464:3597–3616, January 2017. doi: 10.1093/mnras/stw2407.

F. La Barbera, A. Vazdekis, I. Ferreras, A. Pasquali, C. Allende Prieto, I. Martín-Navarro, D. S. Aguado, R. R. de Carvalho, S. Rembold, J. Falcón-Barroso, and G. van de Ven. IMF radial gradients in most massive early-type galaxies. *MNRAS*, 489(3):4090–4110, November 2019. doi: 10.1093/mnras/stz2192.

I. Labbé, P. A. Oesch, R. J. Bouwens, G. D. Illingworth, D. Magee, V. González, C. M. Carollo, M. Franx, M. Trenti, P. G. van Dokkum, and M. Stiavelli. The Spectral Energy Distributions of z ˜ 8 Galaxies from the IRAC Ultra Deep Fields: Emission Lines, Stellar Masses, and Specific Star Formation Rates at 650 Myr. *ApJ*, 777:L19, November 2013. doi: 10.1088/2041-8205/777/2/L19.

Cedric G. Lacey, Carlton M. Baugh, Carlos S. Frenk, Andrew J. Benson, Richard G. Bower, Shaun Cole, Violeta Gonzalez-Perez, John C. Helly, Claudia D. P. Lagos, and Peter D. Mitchell. A unified multiwavelength model of galaxy formation. *MNRAS*, 462(4):3854–3911, November 2016. doi: 10.1093/mnras/stw1888.

Charles J. Lada and Elizabeth A. Lada. Embedded Clusters in Molecular Clouds. *ARA&A*, 41:57–115, January 2003. doi: 10.1146/annurev.astro.41.011802.094844.

David J. Lagattuta, Jeremy R. Mould, Duncan A. Forbes, Andrew J. Monson, Nicola Pastorello, and S. Eric Persson. Evidence of a Bottom-heavy Initial Mass Function in Massive Early-type Galaxies from Near-infrared Metal Lines. *ApJ*, 846(2):166, September 2017. doi: 10.3847/1538-4357/aa8563.

R. B. Larson. Early star formation and the evolution of the stellar initial mass function in galaxies. *MNRAS*, 301:569–581, December 1998. doi: 10.1046/j.1365-8711.1998.02045.x.

J. C. Lee, A. Gil de Paz, C. Tremonti, R. C. Kennicutt, Jr., S. Salim, M. Bothwell, D. Calzetti, J. Dalcanton, D. Dale, C. Engelbracht, S. J. J. G. Funes, B. Johnson, S. Sakai, E. Skillman, L. van Zee, F. Walter, and D. Weisz. Comparison of Hα and UV Star Formation Rates in the Local Volume: Systematic Discrepancies for Dwarf Galaxies. *ApJ*, 706:599–613, November 2009. doi: 10.1088/0004-637X/706/1/599.

Dominik Leier, Ignacio Ferreras, Prasenjit Saha, Stéphane Charlot, Gustavo Bruzual, and Francesco La Barbera. Strong gravitational lensing and the stellar IMF of early-type galaxies. *MNRAS*, 459(4):3677–3692, July 2016. doi: 10.1093/mnras/stw885.

H. Li, J. Ge, S. Mao, M. Cappellari, R. J. Long, R. Li, E. Emsellem, A. A. Dutton, C. Li, K. Bundy, D. Thomas, N. Drory, and A. R. Lopes. SDSS-IV MaNGA: Variation of the Stellar Initial Mass Function in Spiral and Early-type Galaxies. *ApJ*, 838:77, April 2017. doi: 10.3847/1538-4357/aa662a.

Hui Li, Mark Vogelsberger, Greg L. Bryan, Federico Marinacci, Laura V. Sales, and Paul Torrey. Formation and evolution of young massive clusters in galaxy mergers: a SMUGGLE view. *arXiv e-prints*, art. arXiv:2109.10356, September 2021.

Cesario Lia, Laura Portinari, and Giovanni Carraro. Star formation and chemical evolution in smoothed particle hydrodynamics simulations: a statistical approach. *MNRAS*, 330(4):821–836, March 2002. doi: 10.1046/j.1365-8711.2002.05118.x.

P. Lieberz and P. Kroupa. On the origin of the Schechter-like mass function of young star clusters in disc galaxies. *MNRAS*, 465:3775–3783, March 2017. doi: 10.1093/mnras/stw2953.

Marco Limongi and Alessandro Chieffi. Presupernova Evolution and Explosive Nucleosynthesis of Rotating Massive Stars in the Metallicity Range -3 $\leq$ [Fe/H] $\leq$ 0. *ApJS*, 237(1):13, July 2018. doi: 10.3847/1538-4365/aacb24.

D. Maoz and F. Mannucci. Type-Ia Supernova Rates and the Progenitor Problem: A Review. *PASA*, 29:447–465, January 2012. doi: 10.1071/AS11052.

D. Maoz, K. Sharon, and A. Gal-Yam. The Supernova Delay Time Distribution in Galaxy Clusters and Implications for Type-Ia Progenitors and Metal Enrichment. *ApJ*, 722:1879–1894, October 2010. doi: 10.1088/0004-637X/722/2/1879.

Dan Maoz and Or Graur. Star Formation, Supernovae, Iron, and α: Consistent Cosmic and Galactic Histories. *ApJ*, 848(1):25, October 2017. doi: 10.3847/1538-4357/aa8b6e.

Dan Maoz, Filippo Mannucci, Weidong Li, Alexei V. Filippenko, Massimo Della Valle, and Nino Panagia. Nearby supernova rates from the Lick Observatory Supernova Search - IV. A recovery method for the delay-time distribution. *MNRAS*, 412(3):1508–1521, April 2011. doi: 10.1111/j.1365-2966.2010.16808.x.

Dan Maoz, Filippo Mannucci, and Timothy D. Brandt. The delay-time distribution of Type Ia supernovae from Sloan II. *MNRAS*, 426(4):3282–3294, November 2012. doi: 10.1111/j.1365-2966.2012.21871.x.

P. Marigo. Chemical yields from low- and intermediate-mass stars: Model predictions and basic observational constraints. *A&A*, 370:194–217, April 2001. doi: 10.1051/0004-6361:20000247.

M. Marks, P. Kroupa, J. Dabringhausen, and M. S. Pawlowski. Evidence for top-heavy stellar initial mass functions with increasing density and decreasing metallicity. *MNRAS*, 422:2246–2254, May 2012. doi: 10.1111/j.1365-2966.2012.20767.x.

I. Martín-Navarro, A. Vazdekis, J. Falcón-Barroso, F. La Barbera, A. Yıldırım, and G. van de Ven. Timing the formation and assembly of early-type galaxies via spatially resolved stellar populations analysis. *MNRAS*, 475:3700–3729, April 2018. doi: 10.1093/mnras/stx3346.

I. Martín-Navarro, M. Lyubenova, G. van de Ven, J. Falcón-Barroso, L. Coccato, E. M. Corsini, D. A. Gadotti, E. Iodice, F. La Barbera, R. M. McDermid, F. Pinna, M. Sarzi, S. Viaene, P. T. de Zeeuw, and L. Zhu. Fornax 3D project: a two-dimensional view of the stellar initial mass function in the massive lenticular galaxy FCC 167. *A&A*, 626:A124, June 2019. doi: 10.1051/0004-6361/201935360.

I. Martín-Navarro, F. Pinna, L. Coccato, J. Falcón-Barroso, G. van de Ven, M. Lyubenova, E. M. Corsini, K. Fahrion, D. A. Gadotti, E. Iodice, R. M. McDermid, A. Poci, M. Sarzi, T. W. Spriggs, S. Viaene, P. T. de Zeeuw, and L. Zhu. Fornax 3D project: assessing the diversity of IMF and stellar population maps within the Fornax Cluster. *arXiv e-prints*, art. arXiv:2107.14243, July 2021.

Ignacio Martín-Navarro, Pablo G. Pérez-González, Ignacio Trujillo, Pilar Esquej, Alexandre Vazdekis, Helena Domínguez Sánchez, Guillermo Barro, Gustavo Bruzual, Stéphane Charlot, Antonio Cava, Ignacio Ferreras, Néstor Espino, Francesco La Barbera, Anton M. Koekemoer, and A. Javier Cenarro. The Stellar Initial Mass Function at 0.9 ¡ z ¡ 1.5. *ApJ*, 798(1):L4, January 2015. doi: 10.1088/2041-8205/798/1/L4.

F. Matteucci. Abundance ratios in ellipticals and galaxy formation. *A&A*, 288: 57–64, August 1994.

Francesca Matteucci and Enzo Brocato. Metallicity Distribution and Abundance Ratios in the Stars of the Galactic Bulge. *ApJ*, 365:539, December 1990. doi: 10.1086/169508.

Richard M. McDermid, Katherine Alatalo, Leo Blitz, Frédéric Bournaud, Martin Bureau, Michele Cappellari, Alison F. Crocker, Roger L. Davies, Timothy A. Davis, and P. T. de Zeeuw. The ATLAS^{3D} Project - XXX. Star formation histories and stellar population scaling relations of early-type galaxies. *MNRAS*, 448(4):3484–3513, Apr 2015. doi: 10.1093/mnras/stv105.

Kristen B. W. McQuinn, Evan D. Skillman, Andrew Dolphin, John M. Cannon, John J. Salzer, Katherine L. Rhode, Elizabeth A. K. Adams, Danielle Berg, Riccardo Giovanelli, Léo Girardi, and Martha P. Haynes. Leo P: An Unquenched Very Low-mass Galaxy. *ApJ*, 812(2):158, October 2015. doi: 10.1088/0004-637X/812/2/158.

S. T. Megeath, R. Gutermuth, J. Muzerolle, E. Kryukova, J. L. Hora, L. E. Allen, K. Flaherty, L. Hartmann, P. C. Myers, J. L. Pipher, J. Stauffer, E. T. Young, and G. G. Fazio. The Spitzer Space Telescope Survey of the Orion A and B Molecular Clouds. II. The Spatial Distribution and Demographics of Dusty Young Stellar Objects. *AJ*, 151(1):5, January 2016. doi: 10.3847/0004-6256/151/1/5.

G. R. Meurer, O. I. Wong, J. H. Kim, D. J. Hanish, T. M. Heckman, J. Werk, J. Bland-Hawthorn, M. A. Dopita, M. A. Zwaan, B. Koribalski, M. Seibert, D. A. Thilker, H. C. Ferguson, R. L. Webster, M. E. Putman, P. M. Knezek, M. T. Doyle, M. J. Drinkwater, C. G. Hoopes, V. A. Kilborn, M. Meyer, E. V. Ryan-Weber, R. C. Smith, and L. Staveley-Smith. Evidence for a Nonuniform Initial Mass Function in the Local Universe. *ApJ*, 695:765–780, April 2009. doi: 10.1088/0004-637X/695/1/765.

G. E. Miller and J. M. Scalo. The Initial Mass Function and Stellar Birthrate in the Solar Neighborhood. *ApJS*, 41:513, November 1979. doi: 10.1086/190629.

A. Minelli, A. Mucciarelli, D. Romano, M. Bellazzini, L. Origlia, and F. R. Ferraro. A Homogeneous Comparison between the Chemical Composition of the Large Magellanic Cloud and the Sagittarius Dwarf Galaxy. *ApJ*, 910(2):114, April 2021. doi: 10.3847/1538-4357/abe3f9.

A. M. Muñoz, F. P. Navarrete, C. Del P. Lagos, N. D. Padilla, S. A. Cora, and T. E. Tecce. A Variable IMF Slope To Fit The LCDM Picture To Observed High-z Submillimeter Sources. In *Revista Mexicana de Astronomia y Astrofisica Conference Series*, volume 40 of *Revista Mexicana de Astronomia y Astrofisica Conference Series*, pages 21–22, October 2011.

Desika Narayanan and Romeel Davé. The cosmic evolution of the IMF under the Jeans conjecture with implications for massive galaxies. *MNRAS*, 436(4): 2892–2906, December 2013. doi: 10.1093/mnras/stt1548.

Andrew B. Newman, Russell J. Smith, Charlie Conroy, Alexa Villaume, and Pieter van Dokkum. The Initial Mass Function in the Nearest Strong Lenses from SNELLS: Assessing the Consistency of Lensing, Dynamical, and Spectroscopic Constraints. *ApJ*, 845(2):157, August 2017. doi: 10.3847/1538-4357/aa816d.

Seungkyung Oh and Pavel Kroupa. Very massive stars in not so massive clusters. *MNRAS*, 481(1):153–163, November 2018. doi: 10.1093/mnras/sty2245.

T. Okamoto, M. Nagashima, C. G. Lacey, and C. S. Frenk. The metal enrichment of passive galaxies in cosmological simulations of galaxy formation. *MNRAS*, 464:4866–4874, February 2017. doi: 10.1093/mnras/stw2729.

L. J. Oldham and M. W. Auger. Dark matter contraction and stellar-mass-to-light ratio gradients in massive early-type galaxies. *MNRAS*, 476:133–150, May 2018. doi: 10.1093/mnras/sty065.

M. Palla, F. Calura, F. Matteucci, X. L. Fan, F. Vincenzo, and E. Lacchin. The influence of a top-heavy integrated galactic IMF and dust on the chemical evolution of high-redshift starbursts. *MNRAS*, 494(2):2355–2373, May 2020. doi: 10.1093/mnras/staa848.

L. Pantoni, A. Lapi, M. Massardi, S. Goswami, and L. Danese. New Analytic Solutions for Galaxy Evolution: Gas, Stars, Metals, and Dust in Local ETGs and Their High-z Star-forming Progenitors. *ApJ*, 880(2):129, Aug 2019. doi: 10.3847/1538-4357/ab2adc.

P. P. Papadopoulos. A Cosmic-ray-dominated Interstellar Medium in Ultra Luminous Infrared Galaxies: New Initial Conditions for Star Formation. *ApJ*, 720:226–232, September 2010. doi: 10.1088/0004-637X/720/1/226.

M. B. Peacock, S. E. Zepf, A. Kundu, T. J. Maccarone, B. D. Lehmer, C. Maraston, A. H. Gonzalez, R. T. Eufrasio, and D. A. Coulter. Further Constraints on Variations in the Initial Mass Function from Low-mass X-ray Binary Populations. *ApJ*, 841:28, May 2017. doi: 10.3847/1538-4357/aa70eb.

K. Perrett, M. Sullivan, A. Conley, S. González-Gaitán, R. Carlberg, D. Fouchez, P. Ripoche, J. D. Neill, P. Astier, D. Balam, C. Balland, S. Basa, J. Guy, D. Hardin, I. M. Hook, D. A. Howell, R. Pain, N. Palanque-Delabrouille, C. Pritchet, N. Regnault, J. Rich, V. Ruhlmann-Kleider, S. Baumont, C. Lidman, S. Perlmutter, and E. S. Walker. Evolution in the Volumetric Type Ia Supernova Rate from the Supernova Legacy Survey. *AJ*, 144(2):59, August 2012. doi: 10.1088/0004-6256/144/2/59.

J. Pflamm-Altenburg, C. Weidner, and P. Kroupa. Converting Hα Luminosities into Star Formation Rates. *ApJ*, 671:1550–1558, December 2007. doi: 10.1086/523033.

Jan Pflamm-Altenburg and Pavel Kroupa. Clustered star formation as a natural explanation for the Hα cut-off in disk galaxies. *Nature*, 455(7213):641–643, October 2008. doi: 10.1038/nature07266.

Jan Pflamm-Altenburg and Pavel Kroupa. The Fundamental Gas Depletion and Stellar-Mass Buildup Times of Star-Forming Galaxies. *ApJ*, 706(1):516–524, November 2009. doi: 10.1088/0004-637X/706/1/516.

Jan Pflamm-Altenburg, Carsten Weidner, and Pavel Kroupa. Diverging UV and Hα fluxes of star-forming galaxies predicted by the IGIMF theory. *MNRAS*, 395(1):394–400, May 2009. doi: 10.1111/j.1365-2966.2009.14522.x.

S. Ploeckinger, G. Hensler, S. Recchi, N. Mitchell, and P. Kroupa. Chemodynamical evolution of tidal dwarf galaxies. I. Method and IMF dependence. *MNRAS*, 437(4):3980–3993, February 2014. doi: 10.1093/mnras/stt2211.

A. Poci, R. M. McDermid, M. Lyubenova, L. Zhu, G. van de Ven, E. Iodice, L. Coccato, F. Pinna, E. M. Corsini, J. Falcón-Barroso, D. A. Gadotti, R. J. J. Grand, K. Fahrion, I. Martín-Navarro, M. Sarzi, S. Viaene, and P. T. de Zeeuw. The Fornax3D project: Assembly histories of lenticular galaxies from a combined dynamical and population orbital analysis. *A&A*, 647:A145, March 2021. doi: 10.1051/0004-6361/202039644.

Adriano Poci, Richard M. McDermid, Ling Zhu, and Glenn van de Ven. Combining stellar populations with orbit-superposition dynamical modelling: the formation history of the lenticular galaxy NGC 3115. *MNRAS*, 487(3):3776–3796, August 2019. doi: 10.1093/mnras/stz1154.

L. Portinari, C. Chiosi, and A. Bressan. Galactic chemical enrichment with new metallicity dependent stellar yields. *A&A*, 334:505–539, June 1998.

Mateo Prgomet, Martin P. Rey, Eric P. Andersson, Alvaro Segovia Otero, Oscar Agertz, Florent Renaud, Andrew Pontzen, and Justin I. Read. EDGE: The sensitivity of ultra-faint dwarfs to a metallicity-dependent initial mass function. *arXiv e-prints*, art. arXiv:2107.00663, July 2021.

S. Ramírez Alegría, J. Borissova, A. N. Chené, C. Bonatto, R. Kurtev, P. Amigo, M. Kuhn, M. Gromadzki, and J. A. Carballo-Bello. Massive open star clusters using the VVV survey. V. Young clusters with an OB stellar population. *A&A*, 588:A40, April 2016. doi: 10.1051/0004-6361/201526618.

Z. Randriamanakoto, A. Escala, P. Väisänen, E. Kankare, J. Kotilainen, S. Mattila, and S. Ryder. Near-infrared Adaptive Optics Imaging of Infrared Luminous Galaxies: The Brightest Cluster Magnitude-Star Formation Rate Relation. *ApJ*, 775(2):L38, October 2013. doi: 10.1088/2041-8205/775/2/L38.

S. Recchi, F. Calura, and P. Kroupa. The chemical evolution of galaxies within the IGIMF theory: the [α/Fe] ratios and downsizing. *A&A*, 499:711–722, June 2009. doi: 10.1051/0004-6361/200811472.

S. Recchi, P. Kroupa, and S. Ploeckinger. The mass-metallicity relation of tidal dwarf galaxies. *MNRAS*, 450(3):2367–2372, July 2015. doi: 10.1093/mnras/stv798.

A. Renzini and S. Andreon. Chemical evolution on the scale of clusters of galaxies: a conundrum? *MNRAS*, 444:3581–3591, November 2014. doi: 10.1093/mnras/stu1689.

Yves Revaz, Alexis Arnaudon, Matthew Nichols, Vivien Bonvin, and Pascale Jablonka. Computational issues in chemo-dynamical modelling of the formation and evolution of galaxies. *A&A*, 588:A21, April 2016. doi: 10.1051/0004-6361/201526438.

C. Ritter and B. Côté. NuPyCEE: NuGrid Python Chemical Evolution Environment. Astrophysics Source Code Library, October 2016.

C. Ritter, B. Côté, F. Herwig, J. F. Navarro, and C. L. Fryer. SYGMA: Stellar Yields for Galactic Modeling Applications. *ApJS*, 237:42, August 2018. doi: 10.3847/1538-4365/aad691.

Thomas P. Robitaille and Barbara A. Whitney. The Present-Day Star Formation Rate of the Milky Way Determined from Spitzer-Detected Young Stellar Objects. *ApJ*, 710(1):L11–L15, February 2010. doi: 10.1088/2041-8205/710/1/L11.

Steven A. Rodney, Adam G. Riess, Louis-Gregory Strolger, Tomas Dahlen, Or Graur, Stefano Casertano, Mark E. Dickinson, Henry C. Ferguson, Peter Garnavich, Brian Hayden, Saurabh W. Jha, David O. Jones, Robert P. Kirshner, Anton M. Koekemoer, Curtis McCully, Bahram Mobasher, Brandon Patel, Benjamin J. Weiner, S. Bradley Cenko, Kelsey I. Clubb, Michael Cooper, Alexei V. Filippenko, Teddy F. Frederiksen, Jens Hjorth, Bruno Leibundgut,

Thomas Matheson, Hooshang Nayyeri, Kyle Penner, Jonathan Trump, Jeffrey M. Silverman, Vivian U, K. Azalee Bostroem, Peter Challis, Abhijith Rajan, Schuyler Wolff, S. M. Faber, Norman A. Grogin, and Dale Kocevski. Type Ia Supernova Rate Measurements to Redshift 2.5 from CANDELS: Searching for Prompt Explosions in the Early Universe. *AJ*, 148(1):13, July 2014. doi: 10.1088/0004-6256/148/1/13.

D. Romano, F. Matteucci, Z.-Y. Zhang, P. P. Papadopoulos, and R. J. Ivison. The evolution of CNO isotopes: a new window on cosmic star formation history and the stellar IMF in the age of ALMA. *MNRAS*, 470:401–415, September 2017. doi: 10.1093/mnras/stx1197.

Donatella Romano, Michele Bellazzini, Else Starkenburg, and Ryan Leaman. Chemical enrichment in very low metallicity environments: Boötes I. *MNRAS*, 446(4):4220–4231, February 2015. doi: 10.1093/mnras/stu2427.

K. Rowlands, H. L. Gomez, L. Dunne, A. Aragón-Salamanca, S. Dye, S. Maddox, E. da Cunha, and P. van der Werf. The dust budget crisis in high-redshift submillimetre galaxies. *MNRAS*, 441(2):1040–1058, June 2014. doi: 10.1093/mnras/stu605.

J. Rybizki and A. Just. Towards a fully consistent Milky Way disc model - III. Constraining the initial mass function. *MNRAS*, 447(4):3880–3891, March 2015. doi: 10.1093/mnras/stu2734.

M. Salaris and S. Cassisi. *Evolution of Stars and Stellar Populations*. Wiley, 2006.

Edwin E. Salpeter. The Luminosity Function and Stellar Evolution. *ApJ*, 121: 161, January 1955. doi: 10.1086/145971.

J. M. Scalo. The Stellar Initial Mass Function. *Fund. Cosmic Phys.*, 11:1–278, May 1986.

C. Schulz, J. Pflamm-Altenburg, and P. Kroupa. Mass distributions of star clusters for different star formation histories in a galaxy cluster environment. *A&A*, 582:A93, October 2015. doi: 10.1051/0004-6361/201425296.

A. M. Serenelli and S. Basu. Determining the Initial Helium Abundance of the Sun. *ApJ*, 719:865–872, August 2010. doi: 10.1088/0004-637X/719/1/865.

Mohsen Shadmehri. Variability in the stellar initial mass function at high mass: coalescence models for starburst clusters. *MNRAS*, 354(2):375–377, October 2004. doi: 10.1111/j.1365-2966.2004.08188.x.

Piyush Sharda and Mark R. Krumholz. When did the initial mass function become bottom-heavy? *arXiv e-prints*, art. arXiv:2107.08634, July 2021.

Matthew C. Smith. The sensitivity of stellar feedback to IMF averaging versus IMF sampling in galaxy formation simulations. *MNRAS*, 502(4):5417–5437, April 2021. doi: 10.1093/mnras/stab291.

R. J. Smith and J. R. Lucey. A giant elliptical galaxy with a lightweight initial mass function. *MNRAS*, 434:1964–1977, September 2013. doi: 10.1093/mnras/stt1141.

Russell J. Smith, John R. Lucey, and David Carter. The stellar initial mass function in red-sequence galaxies: 1-μm spectroscopy of Coma cluster galaxies with Subaru/FMOS. *MNRAS*, 426(4):2994–3007, November 2012. doi: 10.1111/j.1365-2966.2012.21922.x.

Russell J. Smith, Padraig Alton, John R. Lucey, Charlie Conroy, and David Carter. The IMF-sensitive 1.14-μm Na I doublet in early-type galaxies. *MNRAS*, 454(1):L71–L75, November 2015a. doi: 10.1093/mnrasl/slv132.

Russell J. Smith, John R. Lucey, and Charlie Conroy. The SINFONI Nearby Elliptical Lens Locator Survey: discovery of two new low-redshift strong lenses and implications for the initial mass function in giant early-type galaxies. *MNRAS*, 449(4):3441–3457, June 2015b. doi: 10.1093/mnras/stv518.

C. Spiniello, S. C. Trager, L. V. E. Koopmans, and Y. P. Chen. Evidence for a Mild Steepening and Bottom-heavy Initial Mass Function in Massive Galaxies from Sodium and Titanium-oxide Indicators. *ApJ*, 753(2):L32, July 2012. doi: 10.1088/2041-8205/753/2/L32.

C. Spiniello, S. C. Trager, and L. V. E. Koopmans. The Non-universality of the Low-mass End of the IMF is Robust against the Choice of SSP Model. *ApJ*, 803(2):87, April 2015. doi: 10.1088/0004-637X/803/2/87.

Chiara Spiniello, Scott Trager, Léon V. E. Koopmans, and Charlie Conroy. The stellar IMF in early-type galaxies from a non-degenerate set of optical line indices. *MNRAS*, 438(2):1483–1499, February 2014. doi: 10.1093/mnras/stt2282.

D. P. Stark, G. Walth, S. Charlot, B. Clément, A. Feltre, J. Gutkin, J. Richard, R. Mainali, B. Robertson, B. Siana, M. Tang, and M. Schenker. Spectroscopic detection of C IV λ1548 in a galaxy at z = 7.045: implications for the ionizing spectra of reionization-era galaxies. *MNRAS*, 454:1393–1403, December 2015. doi: 10.1093/mnras/stv1907.

I. W. Stephens, D. Gouliermis, L. W. Looney, R. A. Gruendl, Y.-H. Chu, D. R. Weisz, J. P. Seale, C.-H. R. Chen, T. Wong, A. Hughes, J. L. Pineda, J. Ott, and E. Muller. Stellar Clusterings around "Isolated" Massive YSOs in the LMC. *ApJ*, 834:94, January 2017. doi: 10.3847/1538-4357/834/1/94.

Kung-Yi Su, Philip F. Hopkins, Christopher C. Hayward, Xiangcheng Ma, Michael Boylan-Kolchin, Daniel Kasen, Dušan Kereš, Claude-André Faucher-Giguère, Matthew E. Orr, and Coral Wheeler. Discrete effects in stellar feedback: Individual Supernovae, Hypernovae, and IMF Sampling in Dwarf Galaxies. *MNRAS*, 480(2):1666–1675, October 2018. doi: 10.1093/mnras/sty1928.

Jr. Talbot, Raymond J. and W. David Arnett. The Evolution of Galaxies. I. Formulation and Mathematical Behavior of the One-Zone Model. *ApJ*, 170:409, December 1971. doi: 10.1086/151228.

R. Theler, P. Jablonka, R. Lucchesi, C. Lardo, P. North, M. Irwin, G. Battaglia, V. Hill, E. Tolstoy, K. Venn, A. Helmi, A. Kaufer, F. Primas, and M. Shetrone. The chemical evolution of the dwarf spheroidal galaxy Sextans. *A&A*, 642: A176, October 2020. doi: 10.1051/0004-6361/201937146.

F.-K. Thielemann, K. Nomoto, and M. Hashimoto. Explosive nucleosynthesis in supernovae. In N. Prantzos, E. Vangioni-Flam, and M. Casse, editors, *Origin and Evolution of the Elements*, pages 297–309, January 1993.

D. Thomas, C. Maraston, R. Bender, and C. Mendes de Oliveira. The Epochs of Early-Type Galaxy Formation as a Function of Environment. *ApJ*, 621: 673–694, March 2005. doi: 10.1086/426932.

D. Thomas, C. Maraston, K. Schawinski, M. Sarzi, and J. Silk. Environment and self-regulation in galaxy formation. *MNRAS*, 404:1775–1789, June 2010. doi: 10.1111/j.1365-2966.2010.16427.x.

C. Tortora, A. J. Romanowsky, and N. R. Napolitano. An Inventory of the Stellar Initial Mass Function in Early-type Galaxies. *ApJ*, 765(1):8, March 2013. doi: 10.1088/0004-637X/765/1/8.

O. Urban, N. Werner, S. W. Allen, A. Simionescu, and A. Mantz. A uniform metallicity in the outskirts of massive, nearby galaxy clusters. *MNRAS*, 470: 4583–4599, October 2017. doi: 10.1093/mnras/stx1542.

P. G. van Dokkum and C. Conroy. A substantial population of low-mass stars in luminous elliptical galaxies. *Nature*, 468:940–942, December 2010. doi: 10.1038/nature09578.

A. Vazdekis, A. J. Cenarro, J. Gorgas, N. Cardiel, and R. F. Peletier. Empirical calibration of the near-infrared CaII triplet - IV. The stellar population synthesis models. *MNRAS*, 340:1317–1345, April 2003. doi: 10.1046/j.1365-8711.2003.06413.x.

Enrique Vázquez-Semadeni, Manuel Zamora-Avilés, Roberto Galván-Madrid, and Jan Forbrich. Molecular cloud evolution - VI. Measuring cloud ages. *MNRAS*, 479(3):3254–3263, September 2018. doi: 10.1093/mnras/sty1586.

Alexa Villaume, Jean Brodie, Charlie Conroy, Aaron J. Romanowsky, and Pieter van Dokkum. Initial Mass Function Variability (or Not) among Low-velocity Dispersion, Compact Stellar Systems. *ApJ*, 850(1):L14, November 2017. doi: 10.3847/2041-8213/aa970f.

F. Vincenzo, F. Matteucci, S. Vattakunnel, and G. A. Lanfranchi. Chemical evolution of classical and ultra-faint dwarf spheroidal galaxies. *MNRAS*, 441 (4):2815–2830, July 2014. doi: 10.1093/mnras/stu710.

C. Weidner, P. Kroupa, and S. S. Larsen. Implications for the formation of star clusters from extragalactic star formation rates. *MNRAS*, 350:1503–1510, June 2004. doi: 10.1111/j.1365-2966.2004.07758.x.

C. Weidner, P. Kroupa, and I. A. D. Bonnell. The relation between the most-massive star and its parental star cluster mass. *MNRAS*, 401:275–293, January 2010. doi: 10.1111/j.1365-2966.2009.15633.x.

C. Weidner, I. Ferreras, A. Vazdekis, and F. La Barbera. The (galaxy-wide) IMF in giant elliptical galaxies: from top to bottom. *MNRAS*, 435:2274–2280, November 2013a. doi: 10.1093/mnras/stt1445.

C. Weidner, P. Kroupa, and J. Pflamm-Altenburg. The m_{max}-M_{ecl} relation, the IMF and IGIMF: probabilistically sampled functions. *MNRAS*, 434:84–101, September 2013b. doi: 10.1093/mnras/stt1002.

C. Weidner, P. Kroupa, J. Pflamm-Altenburg, and A. Vazdekis. The galaxy-wide initial mass function of dwarf late-type to massive early-type galaxies. *MNRAS*, 436:3309–3320, December 2013c. doi: 10.1093/mnras/stt1806.

Z. Yan, T. Jerabkova, and P. Kroupa. The optimally sampled galaxy-wide stellar initial mass function. Observational tests and the publicly available GalIMF code. *A&A*, 607:A126, November 2017. doi: 10.1051/0004-6361/201730987.

Zhiqiang Yan, Tereza Jerabkova, and Pavel Kroupa. The star formation timescale of elliptical galaxies. Fitting [Mg/Fe] and total metallicity simultaneously. *A&A*, 632:A110, December 2019a. doi: 10.1051/0004-6361/201936636.

Zhiqiang Yan, Tereza Jerabkova, Pavel Kroupa, and Alejandro Vazdekis. Chemical evolution of elliptical galaxies with a variable IMF. A publicly available code. *A&A*, 629:A93, September 2019b. doi: 10.1051/0004-6361/201936029.

Zhiqiang Yan, Tereza Jerabkova, and Pavel Kroupa. Chemical evolution of ultra-faint dwarf galaxies in the self-consistently calculated integrated galactic IMF theory. *A&A*, 637:A68, May 2020. doi: 10.1051/0004-6361/202037567.

Zhiqiang Yan, Tereza Jerabkova, and Pavel Kroupa. Downsizing revised: Star formation timescales for elliptical galaxies with an environment-dependent IMF and number of SNIa. *arXiv e-prints*, art. arXiv:2107.03388, July 2021.

S. K. Yi, J. Lee, Y.-K. Sheen, H. Jeong, H. Suh, and K. Oh. The Ultraviolet Upturn in Elliptical Galaxies and Environmental Effects. *ApJS*, 195:22, August 2011. doi: 10.1088/0067-0049/195/2/22.

E. Zari, H. Hashemi, A. G. A. Brown, K. Jardine, and P. T. de Zeeuw. 3D mapping of young stars in the solar neighbourhood with Gaia DR2. *A&A*, 620: A172, December 2018. doi: 10.1051/0004-6361/201834150.

E. Zari, A. G. A. Brown, and P. T. de Zeeuw. Structure, kinematics, and ages of the young stellar populations in the Orion region. *A&A*, 628:A123, August 2019. doi: 10.1051/0004-6361/201935781.

Z.-Y. Zhang, D. Romano, R. J. Ivison, P. P. Papadopoulos, and F. Matteucci. Stellar populations dominated by massive stars in dusty starburst galaxies across cosmic time. *Nature*, 558:260–263, June 2018. doi: 10.1038/s41586-018-0196-x.

List of Figures

List of Tables

List of Abbreviations

AGB asymptotic giant branch

CCSN core collapse supernova

CMD colour-magnitude diagram

DMH dark matter halo

DTD delay-time distribution

ECMF embedded cluster mass function

ETG early-type galaxy

FUV far ultraviolet

GC globular star cluster

GCE galaxy chemical evolution

gwIMF galaxy-wide stellar initial mass function

ICM intracluster medium

IGIMF integrated galactic stellar initial mass function

IMF stellar initial mass function

MDF metallicity distribution function

MW Milky Way

SDSS Sloan Digital Sky Survey

SFH star formation history

SFR star formation rate

SFT star formation timescale

SMG sub-millimeter galaxies

SNIa type Ia supernova

SPS stellar population synthesis

TIgwIMF time-integrated gwIMF

UFD ultra-faint dwarf galaxy

WD white dwarf

YSO young stellar object

List of publications

This thesis is based on 5 of my first author publications (attachments A to E). There are another 4 co-authored publications during my PhD study. The full list of these publications is given below in chronological order.

1. **Yan**, Jeřábková, and Kroupa A&A (2021, in press)
   "Downsizing revised: Longer star formation timescales for elliptical galaxies with an environment-dependent IMF and number of SNIa"

2. Wirth, Jeřábková, **Yan**, Haas, Šubr, and Kroupa MNRAS, 506, 4131 (2021).
   "How many explosions does one need? - Quantifying supernovae in globular clusters from iron abundance spreads"

3. **Yan**, Jeřábková, and Kroupa A&A, 637, A68 (2020).
   "Chemical evolution of ultra-faint dwarf galaxies in the self-consistently calculated integrated galactic IMF theory"

4. Chruślińska, Jeřábková, Nelemans, and **Yan** A&A, 636, A10 (2020).
   "The effect of the environment-dependent IMF on the formation and metallicities of stars over the cosmic history"

5. **Yan**, Jeřábková, and Kroupa A&A, 632, A110 (2019).
   "The star formation timescale of elliptical galaxies. Fitting [Mg/Fe] and total metallicity simultaneously"

6. **Yan**, Jeřábková, Kroupa and Vazdekis A&A, 629, A93 (2019).
   "Chemical evolution of elliptical galaxies with a variable IMF. A publicly available code"

7. Jeřábková, Hasani Zonoozi, Kroupa, Beccari, **Yan**, Vazdekis, and Zhang A&A, 620, A39 (2018).
   "Impact of metallicity and star formation rate on the time-dependent, galaxy-wide stellar initial mass function"

8. Kroupa, Jeřábková, Dinnbier, Beccari, and **Yan** A&A, 612, A74 (2018).
   "Evidence for feedback and stellar-dynamically regulated bursty star cluster formation: the case of the Orion Nebula Cluster"

9. **Yan**, Jeřábková, and Kroupa A&A, 607, A126 (2017).
   "The optimally sampled galaxy-wide stellar initial mass function. Observational tests and the publicly available GalIMF code"